DIFFERENTIAL POLARISATION STUDIES OF THE DIFFUSE INTERSTELLAR BANDS AND Be STARS

by

NADINE DINSHAW

B.Sc., University of British Columbia, 1989

A THESIS SUBMITTED IN PARTIAL FULFILLMENT OF

THE REQUIREMENTS FOR THE DEGREE OF

MASTER OF SCIENCE

in

THE FACULTY OF GRADUATE STUDIES

Department of Geophysics and Astronomy

We accept this thesis as conforming

to the required standard

THE UNIVERSITY OF BRITISH COLUMBIA

December 1991

In presenting this thesis in partial fulfilment of the requirements for an advanced degree at the University of British Columbia, I agree that the Library shall make it freely available for reference and study. I further agree that permission for extensive copying of this thesis for scholarly purposes may be granted by the head of my department or by his or her representatives. It is understood that copying or publication of this thesis for financial gain shall not be allowed without my written permission.

(Signature) _____

Department of GEOPHYSICS AND ASTRONOMY

The University of British Columbia
Vancouver, Canada

Date DEC 10, 1991

Abstract

A microcomputer-controlled polarisation analyser has been designed and built at the Dominion Astrophysical Observatory specifically for the 1.83-m telescope. It is mounted before the Cassegrain spectrograph entrance, and is capable of providing spectropolarimetry at the full (~ 0.15 Å) resolution of the spectrograph-detector system. The device uses a polarising beamsplitter for selecting a plane of polarisation, and a quarter-wave plate to remove most ($\sim 90\%$) of the effects of instrumental polarisation. The throughput of the analyser is $\sim 40\%$. The analyser may be rotated at a rate of up to 12.5° s^{-1}; position angles of the analyser may be set to within $\pm 0.5°$.

We present the results of three studies carried out with the polarisation analyser: If the diffuse interstellar bands arise in the same grains which produce the optical continuum polarisation, whereby the bands represent spectral regions of enhanced extinction, then a corresponding enhancement in the polarisation is expected. Differential polarisation measurements in four of the strongest diffuse features in the spectra of HD 183143, 55 Cyg and ζ Per revealed no polarisation structure through any of the bands at levels significantly lower than those predicted. From our results, we have established upper limits to the variation of polarisation in the 5780, 5797, 6177 and 6284 Å bands of 0.01, 0.01, 0.02 and 0.03%, respectively. We conclude that the diffuse features are not associated with the grains responsible for the continuum polarisation. Intermediate-sized grains ($0.02 < a < 0.1\mu$m) which are poorly aligned or spherical are still consistent with our results as well as other observational properties of the bands. The absence of polarisation tends to favour a molecular origin for the diffuse bands.

Attempts to measure differential polarisation associated with the line profile variations of two OB stars are also described. Analysis of the travelling subfeatures in the Hβ line of ζ Oph and the Hβ and He I λ4921 lines of ϵ Per failed to reveal polarisation structure with upper limits of 0.08% and 0.1%, respectively.

Differential polarisation measurements in the Hβ emission line of three intrinsically polarised Be stars are described. The stars ϕ Per and γ Cas exhibit significant polarisation changes across the Hβ line. These changes are characterised by a decrease of polarisation toward the center of the line and an increase at the line center itself. Our observations also show strong evidence for variations in the plane of polarisation across the line. We argue that unpolarised line emission cannot completely account for the observed polarisation changes. Indeed, some of the polarisation structure especially in the line wings appears to be caused by absorption processes in a rotating circumstellar envelope. No significant change of polarisation was detected in the Hβ line of 28 Cyg.

Contents

List of Tables

List of Figures

Acknowledgements

I would like to thank my supervisor, Dr. Gordon Walker, for suggesting this study, providing many valuable insights during the course of the work, and for allowing me the freedom to pursue many of my own ideas. I am equally grateful to Dr. Anne Underhill for reviewing several drafts of the thesis and providing help with the interpretation of the results. Financial support through a grant to Dr. Underhill is gratefully acknowledged.

The polarisation analyser used for all the observations presented in this thesis could not have been made without the support and contributions of a number of people at the Dominion Astrophysical Observatory. Frank Younger kindly helped me with the drafting of the analyser mount and allowed me the use of his wonderful drafting table. Les Saddlemyer developed the control system for the analyser and wrote most of the control software. The mount was expertly built in the DAO instrumentation shop by Jim Cockrill. Doug Bond was always helpful during my observing runs and made up many of my data tapes. David Duncan took the photographs of the analyser shown in Figs. 2.2 and 2.3.

I have benefitted greatly from many discussions with various members of the astronomy department, in particular, Drs. Dave Bohlender, Phil Bennett, Gerry Grieve and Stephenson Yang. Thanks also go to Ted Kennelly for generating the synthetic spectra presented in Figs 4.24 and 4.25, and for being a "decent kind of guy". I am indebted to Jonathan Thornburg for reading several drafts of the thesis and providing many (!) useful suggestions.

Chapter 1

Introduction

1.1 Historical Background

Most of our knowledge of the universe comes from the analysis of starlight. Therefore it is to our advantage to exploit as many different properties of this radiation as possible. One property of light which has received attention only in the last 50 years is its polarisation.

> The probable reason can be found in the assumption that all stars are spherical. Any such object would be completely symmetric about the line of sight from the observer to the center of the apparent disk so if even local regions on the surface emitted 100 percent polarized light, the symmetric orientation of their planes would yield no net polarization to an observer viewing the integrated light of the disk. However, many astronomical processes produce polarized light, and numerous stars are not spherical. (Collins 1989, p. 440)

Early theoretical work by Chandrasekhar (1946a, 1946b) of the atmospheres of early-type stars (where the dominant opacity is electron scattering) implied that as much as 11% of light emanating from a point at the stellar limb may be linearly polarised. He suggested that this polarisation might be observed when the early-type component of an eclipsing binary is occulted by its companion.

Attempts to detect polarisation in the eclipsing binary CQ Cephei led instead to the independent discovery by Hall (1949) and Hiltner (1949) of interstellar polarisation. Subsequent polarimetric observations showed that the light from a significant number of stars in our galaxy is linearly polarised. The polarisation is now known to be caused by scattering of stellar light by elongated interstellar grains aligned by the galactic magnetic field.

Since then, many astrophysical processes have been found to produce polarisation (cf. Serkowski 1974a). For example:

- scattering of light by molecules (Rayleigh scattering) in the atmospheres of Jupiter and other outer planets, and in the photosperes and circumstellar matter of late-type stars;
- scattering of light by free electrons (Thomson scattering) in the solar corona and the circumstellar envelopes of early-type stars;
- scattering of light by grains in the interstellar medium of our galaxy and other galaxies, as well as active galactic nuclei.

Polarimetry, therefore, provides important additional information about the nature and geometry of the source, which cannot be obtained from brightness measurements alone (McLean 1989).

1.2 The Description and Measurement of Polarisation

According to Maxwell's classical theory of electromagnetism, light is a propagating transverse electromagnetic wave. Any collection of such waves travelling in the same direction whose electric-field[1] vector displays a preferred plane of vibration is said to be linearly polarised. More precisely, linearly polarised light is defined as light for which the electric field vector is confined (at all times) to a single plane which also contains the propagation vector. The angle of polarisation, ϕ_p, is a measure of the orientation of this plane. It is conventional to define ϕ_p as the angle from celestial North to the plane, measured in the direction from North through East (Walker 1987). Note that ϕ_p has a range of 0° to 180°, rather than 0° to 360°, because it is a measure of the orientation of a *plane* as opposed to that of a vector.

We can resolve any light beam into two orthogonal linearly polarised components and classify the light according to the components' relative amplitudes.[2] Unpolarised light

[1] It is conventional to discuss polarisation entirely in terms of the electric-field component of light (Clarke 1974).

[2] In this thesis, we always assume the case of incoherent superposition, so the question of the phase relationship between the components does not arise.

is defined as light in which the two (orthogonal) components are of equal intensity. In contrast, partially polarised light is defined as light in which the two components are of different intensities.

We can consider a beam of partially polarised light of total intensity I to consist of two components, one of intensity I_p which is completely polarised, and the other of intensity I_{up} which is unpolarised. The contribution of the polarised component to the total beam determines the "degree" of linear polarisation of the total beam, defined by the ratio

$$P \equiv \frac{I_p}{I}. \tag{1.1}$$

As we have seen in Section 1.1, the light from a variety astronomical sources is partially polarised and its measurement involves determining the quantities P and ϕ_p.

The measurement of P and ϕ_p entails passing the light through a *polarisation analyser*, an optical component which divides the incident beam into its two orthogonally (linearly) polarised components, and measuring the intensities of the components leaving the analyser. For the special case of linearly polarised incident light the transmission of the analyser is given by Malus' Law:

$$\frac{I_{out}}{I_{in}} = \cos^2\psi \tag{1.2}$$

where $\psi = \theta - \phi_p$ is the angle between the axis of the analyser (at an angle θ) and the plane of polarisation of the incident light (at an angle ϕ_p). In the general case of partially polarised light, it is useful to consider the transmission of the polarised and unpolarised components separately. Because the polarised and unpolarised components of the incident beam are incoherent, the total intensity of the beam after passing through the analyser is simply given by the sum of the component intensities

$$I(\theta) = \tfrac{1}{2}I_{up} + I_p\cos^2(\theta - \phi_p) \tag{1.3}$$

where we have averaged Eqn. 1.2 over all possible values of ϕ_p to obtain the transmission for the unpolarised component.

If the orientation, ϕ_p, of the source polarisation is already known, then it is easy to show from Eqn. 1.3 that the degree of polarisation is given by

$$P = \frac{I_{max} - I_{min}}{I_{max} + I_{min}} \tag{1.4}$$

where I_{max} and I_{min} are defined to be the maximum and minimum values of $I(\theta)$.

Alternatively, if the orientation is not known or if it varies, it is useful to write Eqn. 1.3 in terms of P

$$I(\theta) = I_{avg}\{1 + P\cos[2(\theta - \phi_p)]\} \tag{1.5}$$

where $I_{avg} = \frac{1}{2}(I_{max} + I_{min})$. The parameters P and ϕ_p may then be determined by a least-squares fit to I measured at a number of different orientations, θ, of the analyser.

1.3 An Outline of this Thesis

In this thesis we present differential spectropolarimetric studies at ~ 0.15 Å resolution of the diffuse interstellar bands and of features in Be star spectra. The data were obtained with a new polarisation analyser; a detailed description of the design and performance of the instrument is provided in Chapter 2. In Chapter 3, we describe a search for differential polarisation effects in four of the strongest diffuse interstellar bands and discuss the constraints imposed on their possible origin by our results. In Chapter 4, we describe an attempt to measure the differential polarisation associated with the line profile variations of two OB stars. In the same chapter, we describe the results of differential polarisation measurements of the Hβ emission line in three intrinsically polarised Be stars; these results are explained in terms of the dynamics of the stars' circumstellar envelopes. In these last two chapters, we also describe different techniques used to reduce and analyse our differential polarisation measurements.

Chapter 2

The UBC/DAO Polarisation Analyser

2.1 Introduction

Polarimetry has traditionally been carried out using single-channel detectors, such as photomultipliers, and many of the first polarimetric observations were restricted to broad-band continuum measurements. Polarisation measurements in spectral lines usually employ narrow-band interference filters which are either fixed or scanned in wavelength by tilting the filter to various discrete positions. Since both techniques exclude most of the incident light, the precision of the measurements are limited by low photon statistics. But the second method of observation, in particular, requires high accuracy because the measurements are made sequentially at various wavelength points across the spectral feature. Another drawback of the narrow-band measurements is that they are confined to spectral resolutions of the order of the full width at half maximum (FWHM) of the filter, at best ~ 2 Å.

In the past decade, the trend in polarimetry has been toward using multi-channel solid-state detectors. These detectors offer greater efficiency because data may be recorded simultaneously at many wavelengths. In addition, used with a spectrograph, they also allow very high resolution spectropolarimetry.

In this chapter, we describe the design and performance of a microcomputer-controlled polarisation analyser which, when incorporated into the DAO 1.83-m telescope, allows

differential spectropolarimetry at the full spectral resolution of the spectrograph-detector system.

2.2 Design of the Polarisation Analyser

The UBC/DAO polarisation analyser (hereinafter, analyser) was designed and built in 1990 at the Dominion Astrophysical Observatory specifically for the 1.83-m telescope. The instrument comprises four main components: the optics, the mount, the controller and the data analysis software. The hardware components are discussed in the following three sections; the data analysis software is discussed in Section 4.4. Technical specifications of the component parts are given in Appendix A.

2.2.1 The Optics

The analyser was designed for *linear* polarisation measurements. The optical design of the analyser is straightforward and is shown schematically in Fig. 2.1. It incorporates a polarising beamsplitter cube and a quarter-wave plate. The beamsplitter selects a plane of polarisation by separating unpolarised or partially-polarised light into two beams having opposite (or orthogonal) polarisations. The two beams emerge from adjacent faces of the beamsplitter cube with an angular separation of 90°. The component of the incident beam whose plane of polarisation is aligned with the transmission axis of the beamsplitter is transmitted straight through the cube and emerges linearly polarised from the opposite face (Fig. 2.1). The component whose plane of polarisation is oppositely oriented is reflected at right angles to the incident beam and is not used in our configuration. Thus the efficiency of the analyser is at best 50%.

For reasons that will become apparent in Section 2.4.1, the directly transmitted beam is then passed through a quarter-wave plate whose optical axis is oriented at a 45° angle to the beamsplitter axis. At this orientation, the linearly polarised light from the beamsplitter is transformed to circularly polarised light. The plate rotates with the beamsplitter so as to maintain this angle.

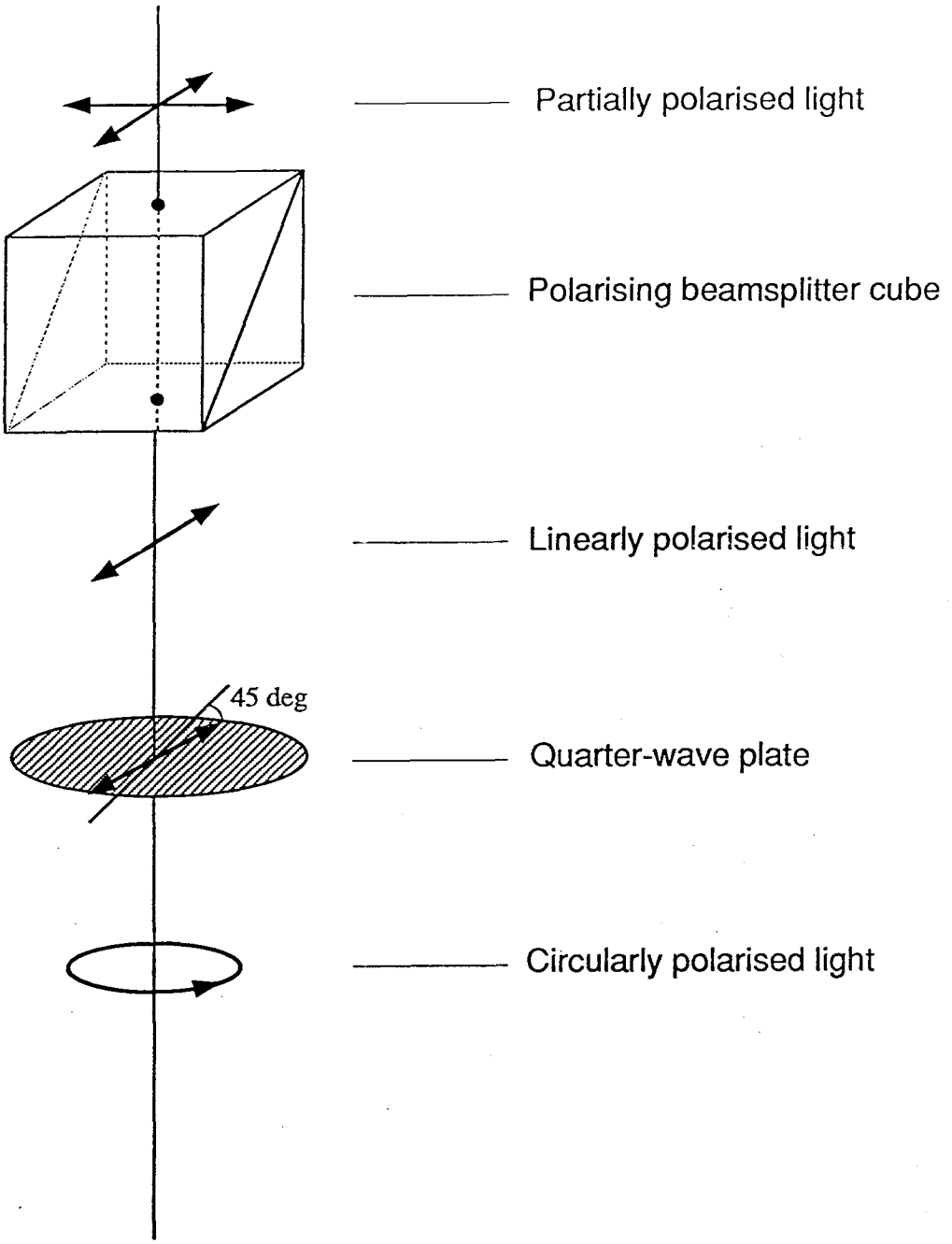

Figure 2.1: The optical design of the UBC/DAO polarisation analyser. The polarising beamsplitter cube selects the plane of polarisation. Linearly polarised light is then converted to circularly polarised light by the quarter-wave plate whose fast axis is always oriented at a 45° angle to the beamsplitter transmission axis.

2.2.1.1 Beamsplitter Cubes

The beamsplitter cubes are broad-band (~ 60 nm) devices with peak transmittance at the wavelengths 488 nm and 633 nm. The 25.4-mm cubes are constructed from two right-angle prisms cemented together with a multilayer dielectric film sandwiched in between. For unpolarised incident light of the specified wavelength, the emerging beams are linearly polarised to a purity of 98%. Each entrance and exit face has also been coated with a multilayer antireflection coating such that less than 0.25% of the light is lost to reflection. The specifications of the beamsplitters are listed in Table A.1 of Appendix A.

2.2.1.2 Quarter-Wave Plate

The quarter-wave plate is a broad-band device suitable for use in the visible spectrum from 400 nm to 700 nm. It is made of mica cemented between two protective glass discs. Unfortunately, mica retarders suffer from high absorption coefficients ($\sim 20\%$) and possible inhomogeneities in the mica. The latter should not seriously affect the uniformity of the telescope beam since, at the location of the analyser, the beam fills most ($\sim 60\%$) of the retarder disc's area. Those disadvantages, however, are compensated by the retarder's relatively low cost, typically, 5–6 times cheaper than their quartz counterparts. The specifications of the retarder are given in Table A.1 of Appendix A.

2.2.2 The Mount

The analyser mount was designed specifically for use on the DAO 1.83-m telescope. It is mounted in the telescope beam approximately 33 cm above the Cassegrain spectrograph entrance. The mount supports the optical components of the analyser as well as a stepper motor. It is held in place by a support arm which screws onto a mirror cell located beneath the primary mirror. [The mirror is free to move along an overhead track between two positions. When in the path of the telescope beam, it directs the light onto a TV camera allowing the observer to locate and set on a star within a wide field of view. Once the star has been found, the mirror can be moved back along the track (out of the path of the telescope beam) so that the beam can be focussed onto the spectrograph slit. In this position, the beam is automatically centered on the analyser.]

Photographs of the top and bottom of the assembled mount are shown, respectively, in

Figs. 2.2 and 2.3. The beamsplitter cube is housed in the cylindrical cell shown in Fig. 2.2, and the quarter-wave plate is held in place by the aluminum ring shown in Fig. 2.3. Both the beamsplitter cube and the wave plate rotate together.

The entire analyser housing is mounted onto the main plate, and is free to rotate on a flange fixed to the housing. Rotation of the analyser is acheived via a worm gear assembly and stepper motor. This type of gear allows very precise rotation of the analyser. The stepper motor sits in its own bracket which then mounts onto the main plate (Fig. 2.3). The position of the bracket may be adjusted to set the pressure between the worm and the gear.

The mount is slotted in two orthogonal directions so that it may be adjusted in both the North-South and East-West directions. This allows positioning of the telescope beam at the center of the beamsplitter cube. Once the analyser has been aligned in this way, the entire mount may be removed from the solid mirror and replaced without requiring further adjustments. The analyser was originally aligned using a laser beam to define the optical axis of the telescope. The laser was mounted at the location of the spectrograph collimator.

The main components of the mount, including the main mounting plate, were made at the DAO from 5 mm thick aluminum, except the cell bushing which was made 11 mm thick so that the analyser housing when rotating does not wobble or tilt from the stress applied by the gear assembly. Flexure of the mount at different positions of the telescope should similarly be neglible.

2.2.3 The Controller

Direct or low-level control of the analyser is provided by an Intel 80286-based single-board computer operating under an iRMX 86 environment. The controller is interfaced to a custom-made motor driver dubbed the "DAO Instrumentation Crate" which responds to signals from the CPU. In addition to controlling the power output to the stepper motor, the driver also returns status of a number of monitoring switches. Both the controller/CPU and motor-driver box are mounted on the spectrograph.

The control-system software was written in PL/M-286, a high-level programming language designed by the Intel Corporation for microcomputer applications. The routine which controls the analyser is incorporated into a larger software package that will even-

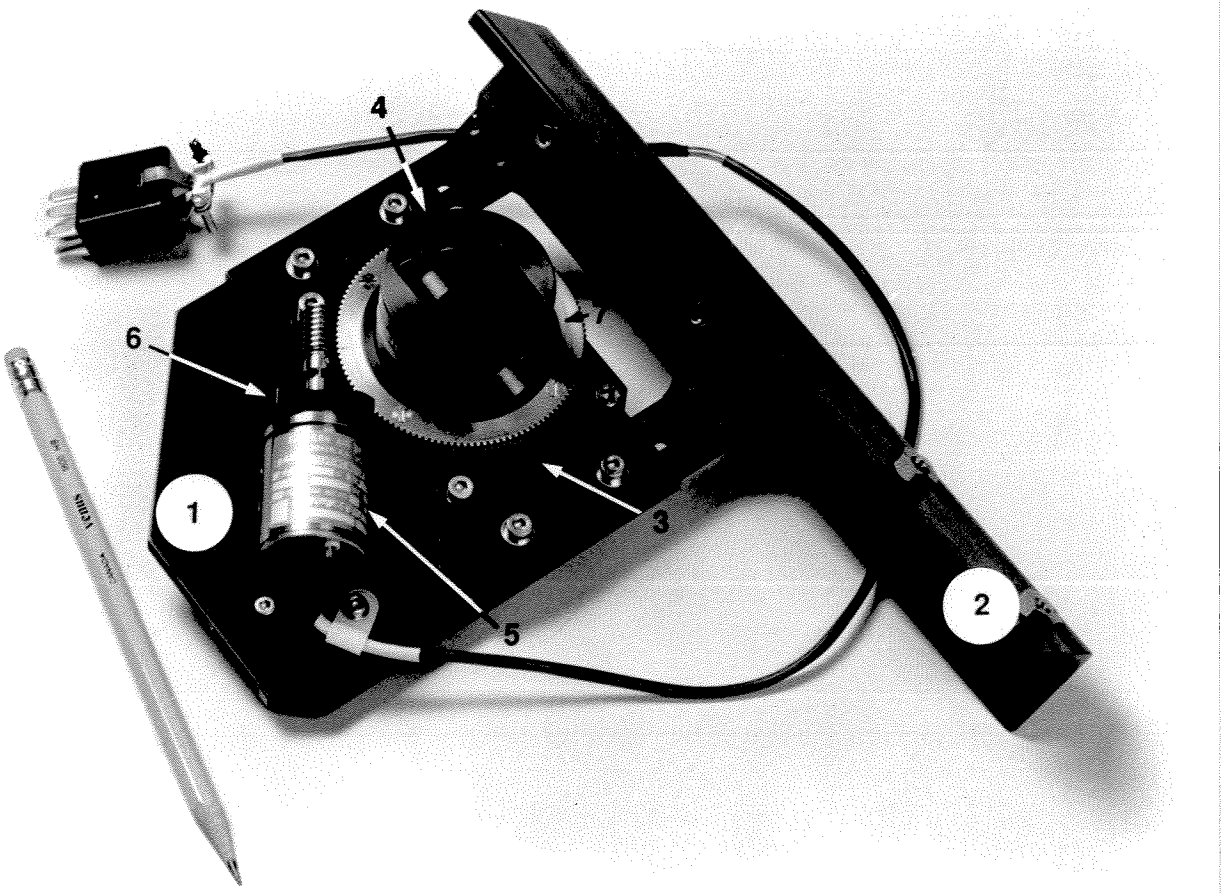

1. Main Plate
2. Support Arm
3. Cell Bushing
4. Beamsplitter Cube Cell
5. Stepper Motor
6. Stepper Motor Bracket
7. Worm Gear

Figure 2.2: Top view of analyser mount.

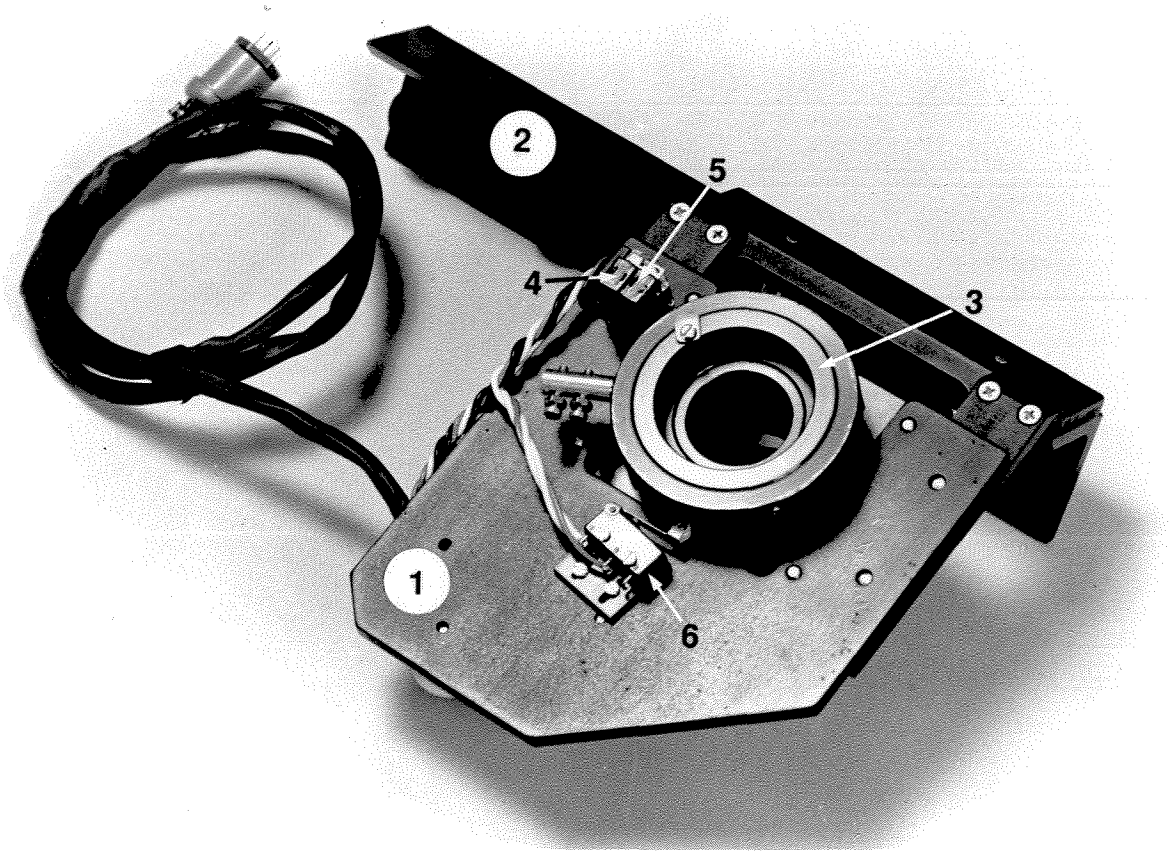

1. Main Plate
2. Support Arm
3. Quarter-Wave Plate Ring
4. Reference Switch
5. Limit Switch
6. Index Switch

Figure 2.3: Bottom view of analyser mount.

tually operate all the spectrograph and imaging devices using the same computer and driver as described above. When a call to the analyser-control routine is made, the position angle of the analyser is checked against the desired, or target, position. If the present position does not equal the target position, the analyser is rotated by the amount corresponding to one step of the stepper motor, i.e., one sixteenth of a degree. Each subsequent call to the routine causes another step of the motor until the target position is reached. The absolute position of the analyser is monitored by counting the number of steps of the stepper motor from a reference position (discussed below).

A call to the analyser-control routine is made every 5 ms. This effectively determines the rotation rate of the analyser, i.e., 200 step s^{-1}, or 12.5° s^{-1}. Ideally, the positioning precision should be limited by the step increment ($\frac{1}{16}$°); however, in practice, it is closer to 0.5° owing to slippage or imperfect meshing of the gears.

At the start of each run, the analyser is automatically initialised to the zero-degree position (the north-south direction) from which all subsequent positioning of the device is made. This is achieved by stepping "down" (to smaller position angles of the analyser) until a zero-degree reference switch (Fig. 2.3) is sensed (i.e., the switch is turned on). The device is then stepped "up" until the reference switch registers the off position. If the reference switch is not found after the number of steps (5760) corresponding to the full rotation of the device, an error is returned. The analyser may be initialised to the zero-degree reference position periodically throughout the night to ensure proper zero-point calibration of the analyser position angle.

To ensure that the analyser is rotating correctly, an index switch was mounted alongside a wheel which rotates with the analyser (Fig. 2.3) . The wheel has ridges every 20° at 0°, 20°, 40°, etc., and, as it rotates, a ridge depresses the switch to reveal the orientation of the analyser; the switch is released as the ridge moves away. While the analyser is rotating, the software checks that at every odd multiple of 10° (i.e. 10°, 30°, 50°, etc.) the index switch is off and at every even multiple of 10° (i.e. 0°, 20°, 40°, etc.) the index switch is turned on. If this switching sequence is not followed at the correct intervals, an error is returned.

As a further precaution, an electrical limit switch which will shut down the device was also installed to protect the device from damage due to power surges. The limit switch is mounted just behind the zero-degree reference switch and cannot be reached in normal

operation.

2.3 Data Acquisition and Analysis

Only a general overview of some of the ideas and principles behind polarisation measurements with the analyser is given here. The data acquisition and analysis techniques are discussed in greater detail in Sections 3.2, 3.3 and 4.2–4.4.

Observations with the analyser were made with either the DAO Reticon or the RCA CCD detector, employing standard spectroscopic techniques. For the measurement of P and ϕ_p, spectra were obtained at a minimum of four equally-spaced position angles of the analyser [as recommended by Serkowski (1962)] to ensure adequate sampling of the cosine function in Eqn. 1.5 (cf. Chapter 4). However, where the polarisation angle ϕ_p was known, measurements at only the two angles, corresponding to ϕ_p and $\phi_p + 90°$, were obtained (cf. Chapter 3). We found that measurements were best performed by alternating between clockwise and anticlockwise rotations of the analyser. In this way, it was possible to reduce the effects of systematic changes in the spectra [e.g., wavelength shifts due to spectrograph flexure (cf. Section 4.5.1) and variations in the strengths of telluric lines caused by variable air mass (cf. Sections 3.2 and 3.4)] that could lead to spurious detections of polarisation.

The procedure for processing the polarisation data departs from conventional techniques in one important way. Since the flat field lamps do not illuminate the detector in the same way as the light from the star,[1] we have generally found cancellation of the diode-to-diode variations in flat-fielded spectra to be unsatisfactory. But, in astronomical sources P is generally small (typically $\lesssim 1\%$), demanding high polarimetric accuracy. Therefore, no flat-flielding of the spectra was performed; instead, we analysed our data in terms of the ratios of two spectra. The spectral ratios were formed by dividing a spectrum obtained at a given position angle by either another spectrum taken at the orthogonal position angle or the mean of spectra taken over a range of angles. Besides normalising the different sensitivities of the diodes, this technique also revealed any polarisation effects in the line profiles. The residual spectra were then rectified by dividing by polynomial fits to selected continuum points.

[1] Proper facilities for dome flats were unavailable at DAO.

Following Fahlman and Walker (1975), if the polarisation in the line profile P_L is written

$$P_L = P_C + \Delta P \tag{2.1}$$

where P_C is the continuum polarisation, then the rectification procedure removes P_C as well as any instrumental polarisation.[2] Our analysis procedure is sensitive only to the *change* in polarisation ΔP in the line profile.

2.4 Performance

2.4.1 Design Evolution

The optical design of the analyser was tested at the focus of the 1.83-m telescope during two observing runs in late 1989. A temporary mount was built for this purpose and the position angles were set manually.

The original design incorporated a half-wave plate[3] (in place of the quarter-wave plate) after the beamsplitter cube which rotated the plane of polarisation of the transmitted beam such that the same (optimum) polarisation was delivered to the spectrograph regardless of the beamsplitter position angle. In this way, we had hoped to eliminate any polarisation effects caused by the different efficiencies of the spectrograph grating to the planes of polarisation parallel and perpendicular to the rulings (cf. Walker 1987; Fig. 5.5). At the same time, we thought we could to take advantage of the greater efficiency of the grating to the latter orientation of polarisation. We encountered, however, an unexpected problem.

Fig. 2.4 shows a polarised spectrum of the standard unpolarised star β Orionis (B8 Ia; V = 0.12). A third-order polynomial fit to selected continuum points has been divided into the spectrum to emphasise the obvious depression in the continuum. The size of the depression is large, nearly 20% of the continuum. Moreover, it was found to be highly variable, being largely a function of guiding and seeing quality. The problem was less severe for long-exposure data as the effects of guiding and seeing averaged out.

[2]Eqn. 2.1 assumes that the position angles ϕ_p of the continuum and line polarisations are the same.

[3]Linearly polarised light incident on a half-wave plate such that the plane of polarisation of the light makes an angle of θ with the axis of the plate emerges with its plane of polarisation at $-\theta$ to the axis of the plate. Thus the effect of the half-wave plate is to rotate the plane of polarisation by the amount 2θ.

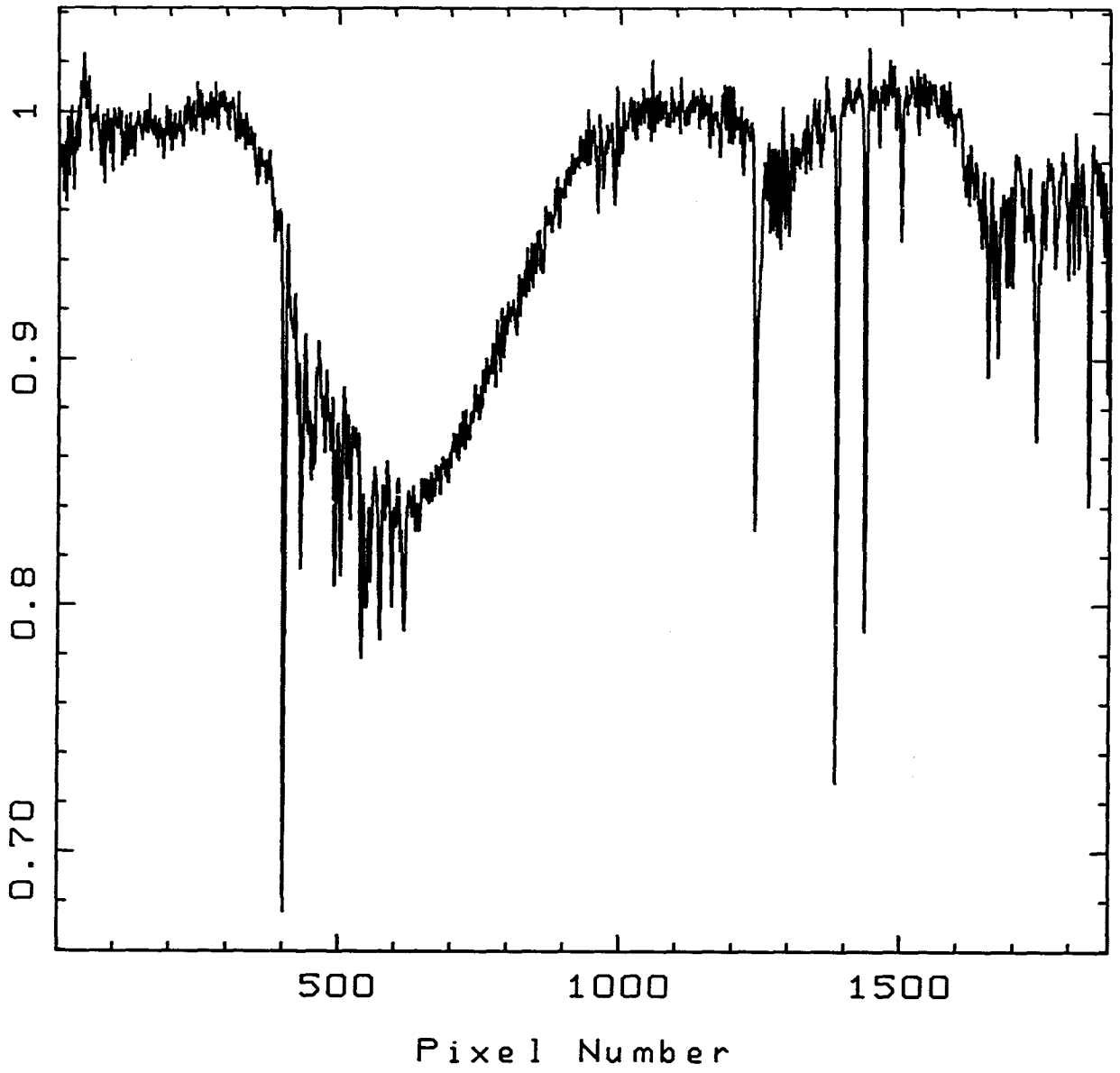

Figure 2.4: Polarised spectrum of the standard unpolarised star β Ori showing the effects of the different responses of the image slicer's aperture and slit mirrors to polarised light. The spectrum was obtained with only the beamsplitter in the path of the light. A third-order polynomial fit has been divided into the spectrum.

It is unlikely that this kind of structure could be caused by the differential response of the spectrograph grating to polarised light. That would tend to introduce only large-scale gradients in the slopes of the spectra and would not be expected cause such highly variable structure. Rather, the structure in Fig. 2.4 was almost certainly caused by the Richardson image slicer (cf. Walker 1987; p. 155) used during the observations. It is plausible that different responses of the aperture and slit mirrors of the slicer to polarised light could cause variations in the intensities of the individual slices, introducing large ripples into the continuum of each spectrum.

In order to minimise the undesirable polarisation effects from the image slicer, it was necessary to introduce a depolariser into the beam before the slicer. The simplest and least expensive approach was to use a quarter-wave plate, whose fast axis is oriented 45° to the beamsplitter axis. The light incident on the image slicer is therefore circularly polarised, which, as far as what the image slicer "sees", is indistinguishable from natural or unpolarised light.[4]

The effectiveness of the quarter-wave plate is demonstrated by the residual spectra in Fig. 2.5. The residuals were formed by dividing a spectrum of the standard polarised star HD 183143 (Serkowski 1974b) taken at the 179° orientation of the analyser by another at the 89° orientation. The integration times for all spectra were one hour. The spectra used to compute the residual spectrum in Fig. 2.5*a* were obtained with only the beamsplitter in the path of the light; those used to form the residual in Fig. 2.5*b* were obtained using both the beamsplitter and quarter-wave plate. In Figs. 2.5*a*′ and b′, we have plotted the residual spectra in Fig. 2.5*a* and *b*, divided by a straight-line fit.

The addition of the quarter-wave plate was effective in reducing two intrumental effects: (1) small-scale structure or ripples in the residuals and (2) large-scale gradients in their slopes. The small-scale structure, being of the order of a few percent ($\sim$3–4%) without the quarter-wave plate (Fig. 2.5*a*′) have been reduced to tenths of a percent ($\sim$0.8%) with the wave plate in place (Fig. 2.5*a*′). Similarly the reduction in the slopes of both residuals (from $\sim$25% in Fig. 2.5*a* to $\sim$4% in Fig. 2.5*b*) represents an order of magnitude improvement. The remaining variations are probably due to imperfect "depolarisation" of the light entering the spectrograph as well as unavoidable guiding errors. The quarter-

[4]Recall that unpolarised and circularly polarised light are both composed of equal amounts of two orthogonally-orientated linearly-polarised components of light.

wave plate was therefore $\sim 90\%$ effective in eliminating the sensitivity dependence of the image slicer and spectrograph to the plane of polarisation.

The residual spectrum in Fig. 2.5*b* also contains a real component since the continuum light from HD 183143 is highly polarised with $\phi_p = 179°$ (Hiltner 1956). Therefore, in order to estimate the level of instrumental polarisation, we have plotted the residual spectra of the standard unpolarised star α Cyg in Fig 2.6. The residuals were obtained on four different nights and were formed in an identical manner to the HD 183143 spectra of Fig 2.5. (In fact, they were obtained for the DIB polarisation study of Chapter 3 in order to monitor instrumental polarisation effects in those data.) The integration times of the spectra ranged from 60–120 s. From Fig 2.6, it is clear that instrumental polarisation is present in the residuals at the very low level of ~ 2–3%. But more importantly, the general shape of the residual spectra did not vary significantly from night-to-night.

2.4.2 Testing the Analyser

The efficiency of the analyser was estimated from observations of α Cyg obtained with and without the analyser. It was found that the analyser caused a reduction in the light from the star of ~ 1 mag. (Of course, this is in addition to the requirement that measurements be taken at multiple position angles in order to derive the polarisation parameters.)

In addition to observations of standard unpolarised stars, another important test of *any* polarisation analyser is its ability to accurately measure the degree and position angle of polarisation in standard stars of known polarisation. Unfortunately, since our analysis technique is not sensitive to continuum polarisation, there are few objects suitable for such a test. It is known that some emission-line stars exhibit reduced polarisation (from the continuum value) across their hydrogen Balmer lines. We have measured this change in the Hβ λ4861 line of two Be stars ϕ Per and γ Cas (cf. Figs 4.19 and 4.20*a, b*) for which reduced polarisation has previously been measured. Although most of these other measurements are of lower spectral resolution and therefore do not exhibit the level of detail of our data, our results compare favourably in both the degree and position angle of polarisation. Besides forming the basis of this test, these measurements are also of astrophysical interest; therefore, more detailed discussions may be found in Section 4.5.2.

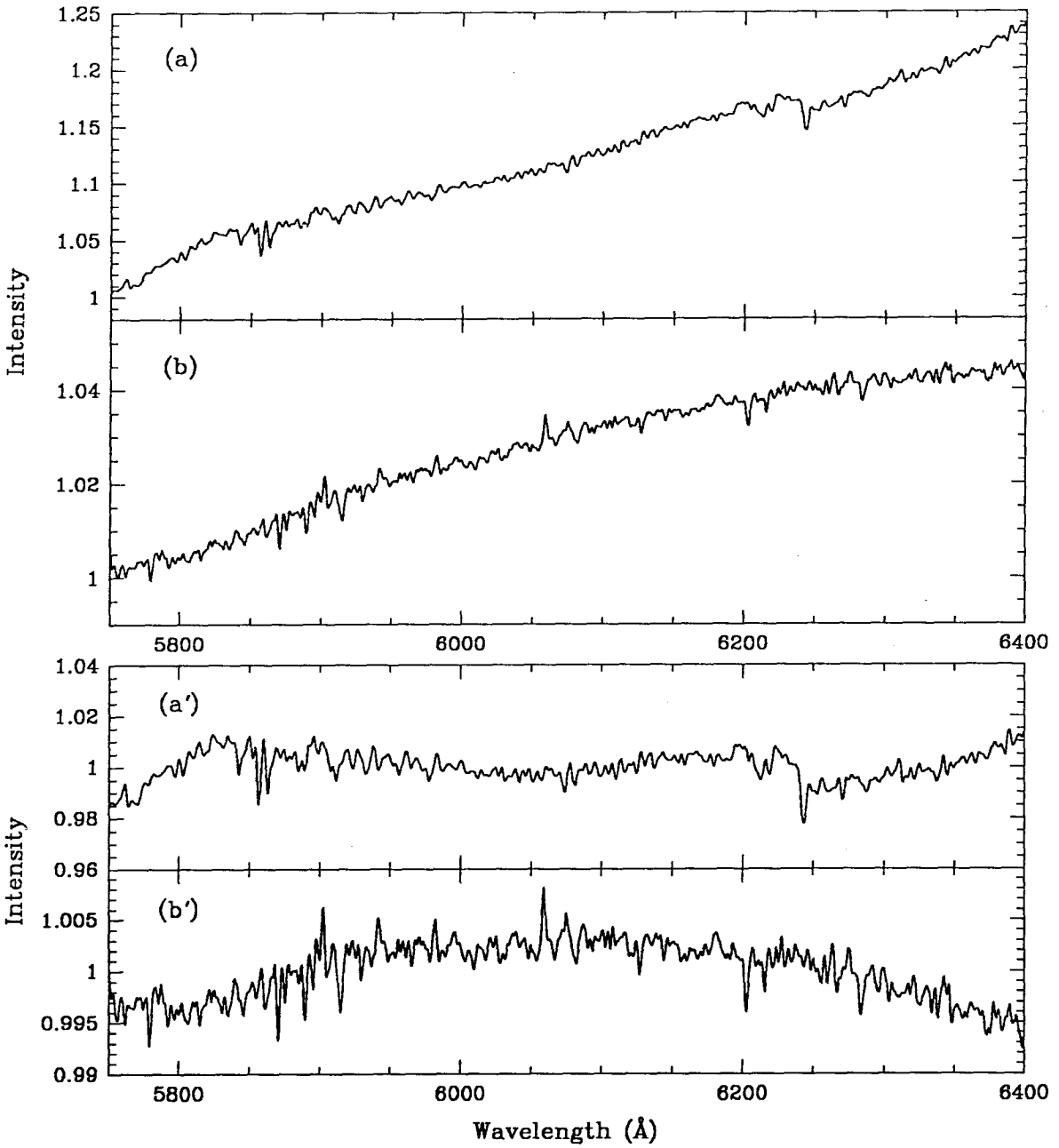

Figure 2.5: Polarisation curves of the standard polarised star HD 183143 showing the effectiveness of the quarter-wave plate in reducing instrumental polarisation. The curves were formed by dividing a spectrum of HD 183143 at the 179° orientation of the analyser by a similar spectrum at the 89° orientation.
(a) Residual spectrum obtained with only the beamsplitter in the path of the light.
(b) Residual spectrum obtained with the beamsplitter plus the quarterwave plate.
(a') As a, rectified by a straight line fit.
(b') As b, rectified by a straight line fit.

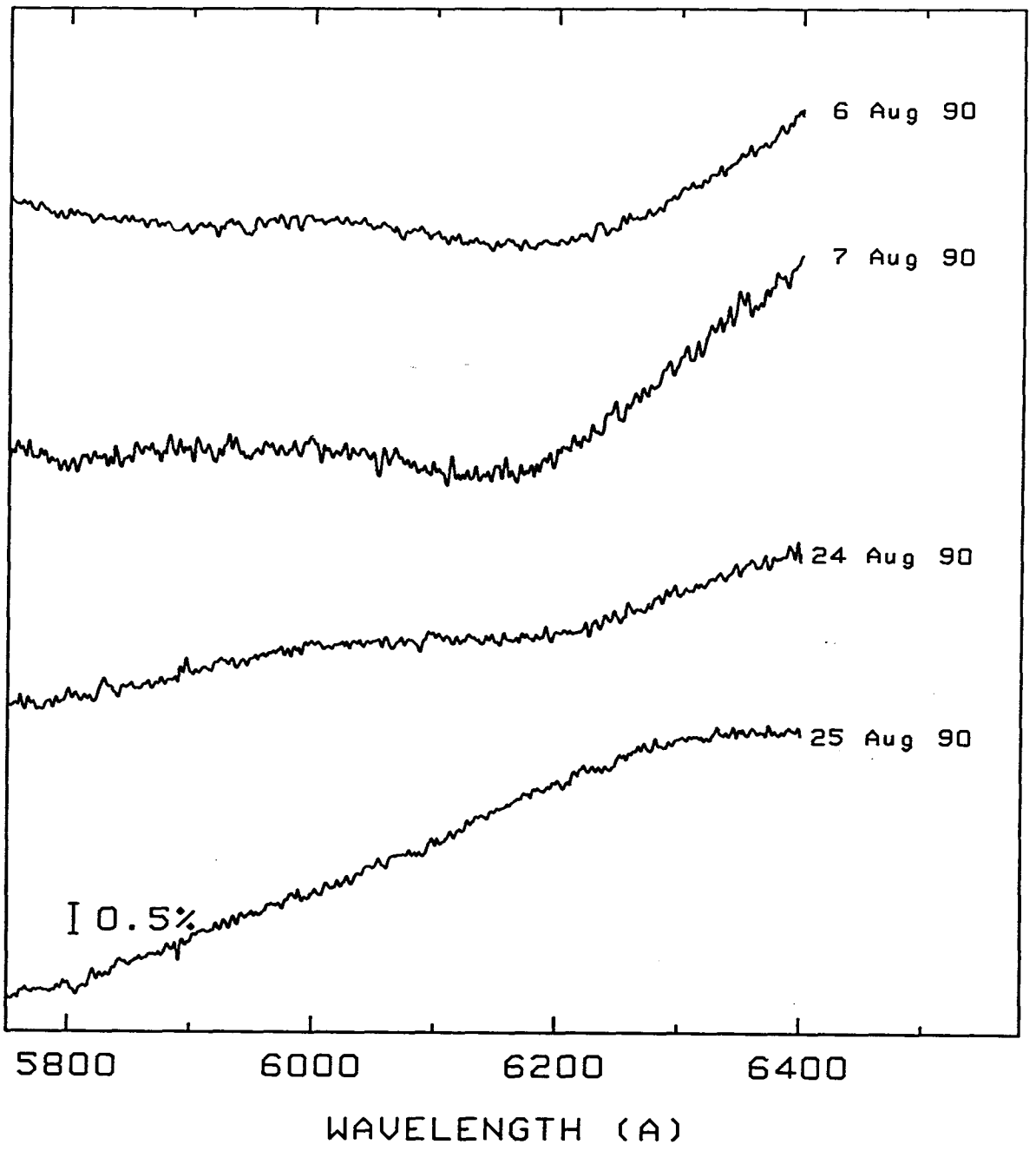

Figure 2.6: Polarisation curves of the standard unpolarised star α Cyg, formed by dividing a spectrum of α Cyg at the 179° orientation of the analyser by a similar spectrum at the 89° orientation. Instrumental polarisation is present in the residuals at the $\sim$2–3% level of the continuum.

Chapter 3

Differential Polarisation Studies of the Diffuse Interstellar Bands

3.1 Diffuse Interstellar Bands

3.1.1 Introduction

Besides producing the general extinction and reddening of the light from stars and certain atomic and molecular resonance lines in their spectra, the interstellar medium (ISM) is also responsible for a series of unexplained absorption features known as the diffuse interstellar bands (DIBs). There are more than 60 such features scattered over approximately 4000 Å of the visible spectrum, with no obvious pattern in wavelength (Herbig 1988). They display a range of full widths at half intensity from about 1 Å to 40 Å. The strongest bands are at 4430 Å and at 6177 Å, with equivalent widths of 3.4 Å and 2.0 Å, respectively, in the heavily reddened star HD 183143 (Greenberg 1978). The strengths of the bands depend largely on the amount of interstellar matter in the line-of-sight to the star. Despite their large numbers, the DIBs make only a small contribution to the total energy absorption of starlight (Puget and Léger 1989). However, they potentially harbour important information about the composition and physical nature of the ISM. Reviews of the observational aspects of DIBs may be found in Krelowski (1988).

Since their discovery by Merrill in 1934, the diffuse bands have inspired a great deal of speculation as to their origin. However, no definitive picture of the agents responsible for the DIBs has yet emerged. One fundamental question is whether the DIBs arise from the

grain or gas component of the ISM. Polarisation studies present an ideal opportunity to distinguish between the two possibilities. If the interstellar grains responsible for the optical continuum extinction and polarisation are also the cause of the DIBs, such that the bands represent spectral regions of enhanced extinction, then a corresponding enhancement in the polarisation might also be present (cf. Martin and Angel 1974; Fahlman and Walker 1975). On the other hand, no polarisation of the stellar light is expected if the DIBs are formed by the interstellar gases (atoms and/or molecules) [cf. Smith, Snow and York 1977; van der Zwet 1986].

3.1.2 Possible Carriers of the DIBs

Almost all current research on the diffuse interstellar bands is devoted to understanding the origins of these enigmatic features. Many carriers for the bands have been proposed; they may be grouped according to the two main components of the interstellar medium: solid grains and gas-phase molecules. At present, the arguments for molecular and grain origins of the DIBs are equally strong. Excellent reviews may be found in the articles by Herbig (1975), Smith *et al.* (1977), Chlewicki *et al.* (1986) and van der Zwet (1986).

Prior to the mid-1970's, the favoured explanation for the DIBs was that they arose from impurities embedded in the solid grains responsible for interstellar reddening [cf. Aannestad and Purcell (1973); Herbig (1975); Smith *et al.* (1977)]. This was motivated by the generally good correlation between the band strengths and $E(B-V)$ colour excess (Herbig 1975) and by the absence of detectable fine structure in the band profiles which might be expected if the DIBs are caused by free molecules (Smith *et al.* 1977; Josafatsson and Snow 1987).

The possible link between DIBs and interstellar grains was first suggested by Merrill and Wilson (1938) because of the strength-reddening correlation. Since then, further studies of the correlations between DIB strengths and various extinction parameters have been made in efforts to identify the particular grain population responsible for the bands. Some of the earliest studies by Greenstein and Aller (1950), Duke (1951) and Underhill (1955) showed correlations between the 4430 Å band and the then photometric index for extinction, E_1. Walker (1963) and Wampler (1966) found positive correlations between the 4430 Å band and $E(B-V)$. Their results were confirmed by Wu (1972) whose study also included DIBs at 5780 and 5797 Å. Herbig (1975) also conducted correlation studies

of all the stronger DIBs in his Table I and reported reasonable correlations between those DIBs and $E(B-V)$. Better correlations were found when the band strengths were compared with red and near-IR colour excesses (Herbig 1975; Sneden *et al.* 1978). Those observations would seem to suggest that the grains which produce the visible and IR extinction are also responsible for the diffuse interstellar bands.

As noted originally by van de Hulst (1949), extinction profiles produced by large grains ($\sim 0.1\mu$m, such as those responsible for the extinction in the visible) would be strongly asymmetric with steeper edges and obvious emission wings blueward of the absorption (see also Greenberg and Hong 1976; Chlewicki *et al.* 1986; van der Zwet 1986). Observations obtained with modern detectors provide no evidence for an emission component in any of the DIBs (cf. Chlewicki *et al.* 1986; Krelowski and Walker 1987; Krelowski 1988). Moreover, the intrinsic profiles of the DIBs show a high degree of symmetry (e.g. 4430, 5778, 6177, 6284 Å), although a number of the narrow DIBs do possess slight asymmetry (e.g. 5780, 5797 Å; Chlewicki *et al.* 1986; Krelowski and Walker 1987; Krelowski 1988). Using similar arguments, Herbig (1975) concluded that the DIBs probably arise from impurities in very small grains ($a \sim 0.01\mu$m), which are also required to explain the far-UV extinction (Greenberg and Chlewicki 1983).

If the small grains are responsible for the DIBs, then there might be a correlation between band strength and UV colour excess. Although a weak correlation exists between the 4430 Å band and the extinction bump at 2175 Å (Witt, Bohlin and Stecher 1983; Seab and Snow 1984; Josafatsson and Snow 1987), no correlations between the strengths of the 4430 Å band and $E(1500-1800)$ [Krelowski *et al.* 1987] and between the 4430, 5780, 6284 Å bands and $E(1800-V)$ [Wu, York and Snow 1981] have been found (see also Nandy, Morgan and Houziaux 1982; Witt *et al.* 1983; Seab and Snow 1984).[1] Nevertheless, it is worth noting that Savage (1976) and Welter and Savage (1977) were able to obtain good fits to the asymmetric profiles of 5780 and 6614 Å assuming the lines are caused by impurities in small ($a \simeq 0.075\,\mu$m) cold grains.

Another problem with the grain-based hypothesis, and perhaps the most serious, is that the bands do not show the significant variations in central wavelength expected if they arise from impurity sites in grains (Chlewicki *et al.* 1986). Laboratory studies indicate shifts in wavelength as large as 100 Å can occur depending on the chemical composition

[1]The 2175 Å bump does not appear to correlate with the far-UV extinction (Bless and Savage 1972).

and temperature of the grains (Smith *et al.* 1977; Chlewicki *et al.* 1986; van der Zwet 1986). The observed lack of variability in the band wavelengths would require the grains to have very similar formation histories and physical environments toward all lines-of-sight (Smith *et al.* 1977).

Partly because of such problems, there has been a definite shift, in the last decade, towards molecular theories of the diffuse interstellar bands. In fact, some of the earlier criticisms of the molecular hypothesis may not be entirely valid in light of new observational and theoretical evidence.

The presence of rotational fine structure within an interstellar band would be strong evidence that the bands are formed by free molecules (Smith *et al.* 1977). Attempts to resolve the narrowest of the diffuse interstellar bands into discrete structure have been made by several authors (e.g. Savage 1976; Danks and Lambert 1976; Welter and Savage 1977; Snell and Vanden Bout 1981; Herbig and Soderblom 1982). No structure at the level of 0.05 Å resolution was detected in any of the features studied. However, according to Danks and Lambert (1976), the absence of structure may be understood if the diffuse bands are the result of electronic transitions in large molecules. The rotational structure of the bands from such electronic transitions might be compressed below the observational resolution limit.

One of the major criticisms of a molecular origin for the bands has been the perception that gas-phase molecules would not be able to survive the harsh ultraviolet radiation field of the ISM in sufficient numbers to account for the DIBs. Recently, van der Zwet and Allamandola (1985), Léger and d'Hendecourt (1985) and Crawford, Tielens and Allamandola (1985) have proposed that polycyclic aromatic hydrocarbons (PAHs) [which are used to explain the unidentified infrared emission bands (UIB)] could also be the carriers of the DIBs. PAHs are attractive molecular candidates because they are thought to be extremely stable to UV radiation and their abundance, calculated from the UIBs, is sufficient to produce the observed equivalent widths of DIBs. Although they look promising, there remain a number of problems with PAHs as the carriers of the DIBs. Because of the large variety of PAH species, any model which tries to explain the DIBs using PAH molecules must account for the existence in the ISM of only those species which cause the DIBs (Puget and Léger 1989). Moreover, no laboratory spectra of PAHs in the visible are available to compare with the DIB spectra.

It is now becoming apparent that all DIBs may not even arise from the same carrier. Although Herbig (1975) reported that all the bands correlated well with each other and therefore must share a common origin, recent correlation studies do not bear this out (Chlewicki *et al.* 1986; Krewlowski and Walker 1987; Josafatsson and Snow 1987). By analysing the anomalous strengths of some DIBs and the absence of others in the lightly reddened star ζ Per whose diffuse bands are thought to be caused by a single cloud, Krelowski and Walker (1987) concluded that there are at least three DIB carriers. A similar conclusion was reached by Josafatsson and Snow (1987), based on the degree of correlation between individual DIBs.

3.1.3 Past Polarisation Studies of the DIBs

There have been numerous attempts to detect polarisation changes within the diffuse bands. Walker (1963) searched for polarisation excess associated with the 4430 Å band of HD 183143. His observations were made using a photoelectric photometer and polaroid filter at five position-angle settings. A narrow-band filter was used to isolate the band. He was not able to detect any polarisation to within the uncertainty of his measurements. Another null result was obtained two years later by Wampler (1966) using similar photoelectric techniques at considerably higher resolution.

A'Hearn (1972) also looked for excess polarisation in the 4430 Å feature of five stars including 55 Cyg and HD 183143. He employed a variety of photopolarimeters at three different observing sites and compared the intensity within a 20 Å bandpass centred on the feature with the intensities in two similar bandpasses in the neighbouring continuum. A'Hearn found no evidence of polarisation excess for any of the stars and established a low upper limit to the change in polarisation in the 4430 Å band of about 0.05–0.1%. His results represent the most accurate polarimetric measurements of the DIBs, prior to this thesis.

Later efforts by Martin and Angel (1974, 1975) and Fahlman and Walker (1974) confirmed the results of A'Hearn. Besides the 4430 Å band, Martin and Angel also investigated the 5780 Å feature in HD 183143 and the 6284 Å feature in HD 21389, using a scanning polarimeter. Their observations revealed no significant polarisation change exceeding the standard error (0.1%) of their measurements. Fahlman and Walker (1975) also looked for polarisation changes in one of the strongest features at 6284 Å in the spec-

trum of HD 183143. They employed a spectrograph and Isocon television camera in order to resolve the line; they set an upper limit of 0.4% to the polarisation change.

Amidst those null results, there have been two reports of positive detections. The first was made by Nandy and Seddon (1970) who claimed to have found polarisation structure in the 4430 Å band of 55 Cyg. Their photographic data suggested an incredible doubling of the polarisation from 2.7% in the continuum to 5% in the band. That report was never confirmed. This was followed by Gammelgaard and Rudkjobing's (1973) report (also unconfirmed) of differential polarisation within the broad 6177 Å band. An interesting point about their result is that the angle of polarisation they measured within the band does not match the continuum polarisation angle, but is nearly orthogonal to it.

The most recent polarimetric observations of DIBs were made roughly 15 years ago, before the introduction of solid-state detectors. These new detectors are ideally suited to investigating the polarisation structure in the diffuse bands given the small levels expected. For example, one of the most favourable cases, the 6284 Å feature in HD 183143, was predicted by Fahlman and Walker (1974) to have an excess polarisation no greater than 0.8%. Until now, only A'Hearn's work has had a precision capable of showing an effect of the predicted size. However, his broadband measurements were incapable of showing the change with wavelength of the polarisation within the profiles of the bands.

By using a Reticon detector and our polarisation analyser, we can acheive order-of-magnitude improvements in both precision and wavelength resolution over the earlier studies. In addition, spectropolarimetric measurements over a moderate wavelength band (840 Å) allow us to investigate the polarisation structure across a number of DIBs suspected of having different origins, to test the multiple carrier hypothesis.

3.2 Observations

Table 3.1 lists the stars observed for this program, their spectral type, visual magnitudes (V), $E(B-V)$ colour excess, wavelength λ_{max} at which their polarisation $P(\lambda_{max})$ is a maximum, and position angle ϕ_p of the continuum polarisation. The first two, HD 183143 and 55 Cyg, were the main focus of our observations, both having been the object of earlier searches for polarisation structure in their DIBs. Krelowski and Walker (1987) have argued that the last star in Table 3.1, ζ Per, lacks one family of DIBs and is probably obscured

by only one cloud. Thus, observations of ζ Per present the possibility of studying DIB polarisation effects from a single cloud.[2]

Spectropolarimetry of the three stars in Table 3.1 was carried out at the DAO 1.8 m telescope using the UBC/DAO polarisation analyser (described in Chapter 2) and 633 nm beamsplitter cube. The observations of ζ Per were made on one night in November 1989 and those of HD 183143 and 55 Cyg during two observing runs in August 1990. The detector was a liquid-nitrogen-cooled RL1872 F/30 EG&G Reticon, described in detail by Walker, Johnson and Yang (1985). All of the observations were taken with the 600 lines mm^{-1} grating blazed at 5000 Å which give a reciprocal dispersion of 30 Å mm^{-1}. On the Reticon array, this corresponds to a resolution of 0.45 Å $diode^{-1}$ and a spectral coverage of 840 Å.

The polarised spectra were taken in pairs with the beamsplitter transmission axis orientated in the two orthogonal positions corresponding to the position angle (ϕ_p) of the *continuum* polarisation and perpendicular to it ($\phi_p + 90°$). By sampling only these two position angles, it was assumed that the agent responsible for the enhanced extinction of the diffuse features is distributed in the same grains that produce the adjacent continuum polarisation.

Observations were confined to the yellow-red region of the spectrum where a significant number of prominent diffuse features are found, including one of the strongest at 6284 Å. They are identified along with some of the weaker DIBs in Fig. 3.1 which shows the rich interstellar spectrum of HD 183143. By convention, the DIBs are named according to their approximate central wavelengths listed in Herbig's (1975) Table I. The stellar He I λ5875 and Si II $\lambda\lambda$6347, 6371 lines and interstellar Na D lines are also indicated.

Representative spectra of 55 Cyg and ζ Per are also provided in Figs. 3.2*a* and *b* for comparison. Notice that the broad 6177 Å band is very weak in the spectrum of ζ Per.

The spectra are contaminated by the rotational bands of atmospheric H_2O in the wavelength interval from 5880–6000 Å. The 6284 Å feature is strongly affected by the α-band of O_2, which has its bandhead at 6276 Å. Since we intended to analyse the data in terms of the ratios between the spectra at the two angles of polarisation, if the individual spectra were obtained at different air masses, the absorption lines from water vapour and

[2]If the absorption bands arise from several clouds along the line-of-sight and the alignment of the grains varies from cloud-to-cloud, the net amount of polarisation is reduced. Studying polarisation effects in DIBs produced by a single cloud, however, ensures preferential grain alignment.

Table 3.1: Program Stars for DIB Polarisation Study

HD	Star	Spectral Type	V	$E(B-V)$	λ_{max} (μm)	$P(\lambda_{max})$ (%)	ϕ_p (degrees)
24398.....	ζ Per	B1 Ib[a]	2.83[a]	0.31[b]	0.54[b]	1.2[b]	145[c]
183143.....		B7 Ia	6.87	1.28	0.56	6.1	179
198478.....	55 Cyg	B3 Ia	4.83	0.52	0.53	2.8	2

a) Hoffleit and Jaschek 1982.

b) Serkowski, Matthewson and Ford 1973.

c) Hiltner 1956.

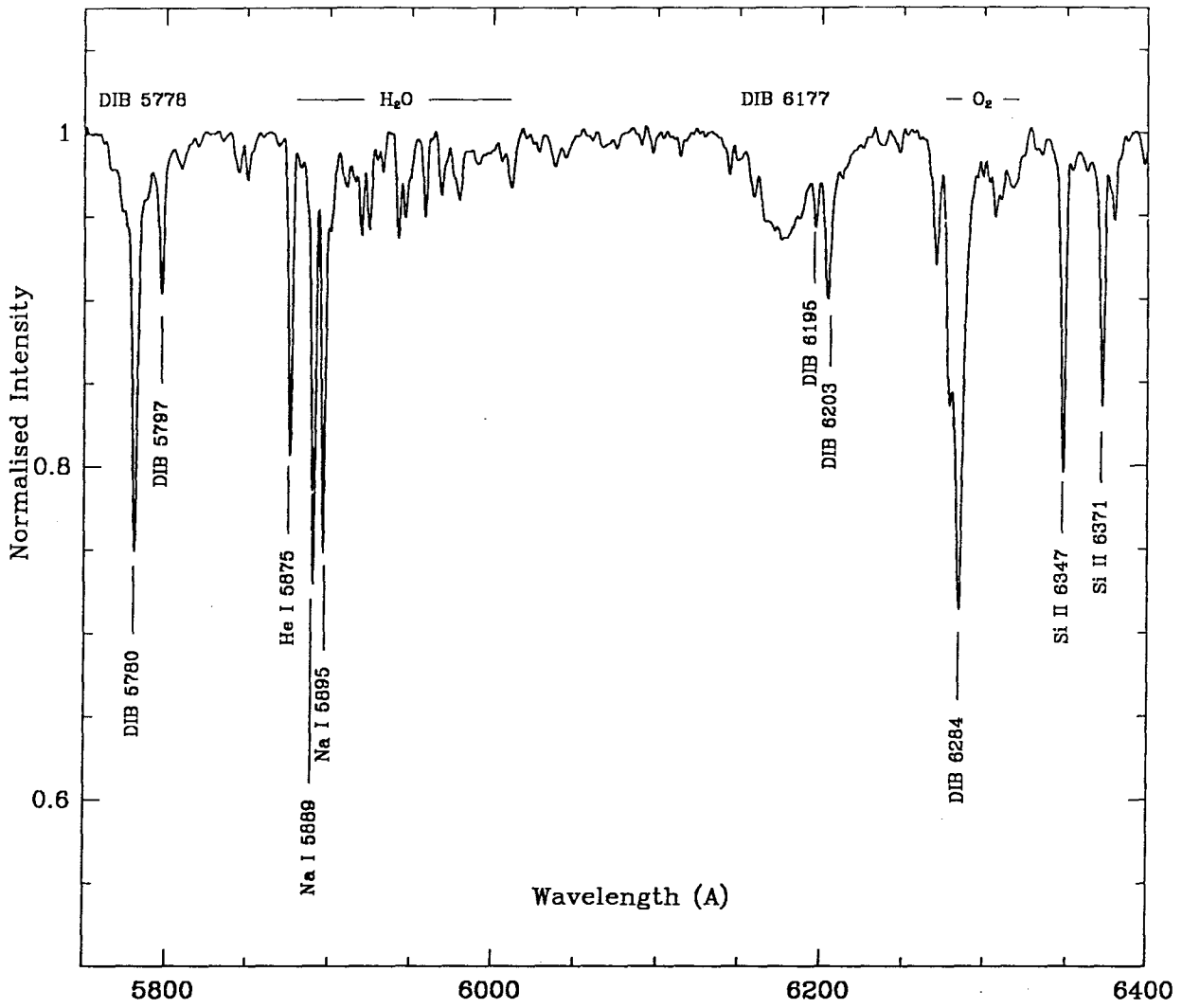

Figure 3.1: Representative spectrum of HD 183143. The strongest DIBs are identified along with the interstellar Na D and stellar lines. The telluric α-band of O_2 and the rotational bands of H_2O are also marked.

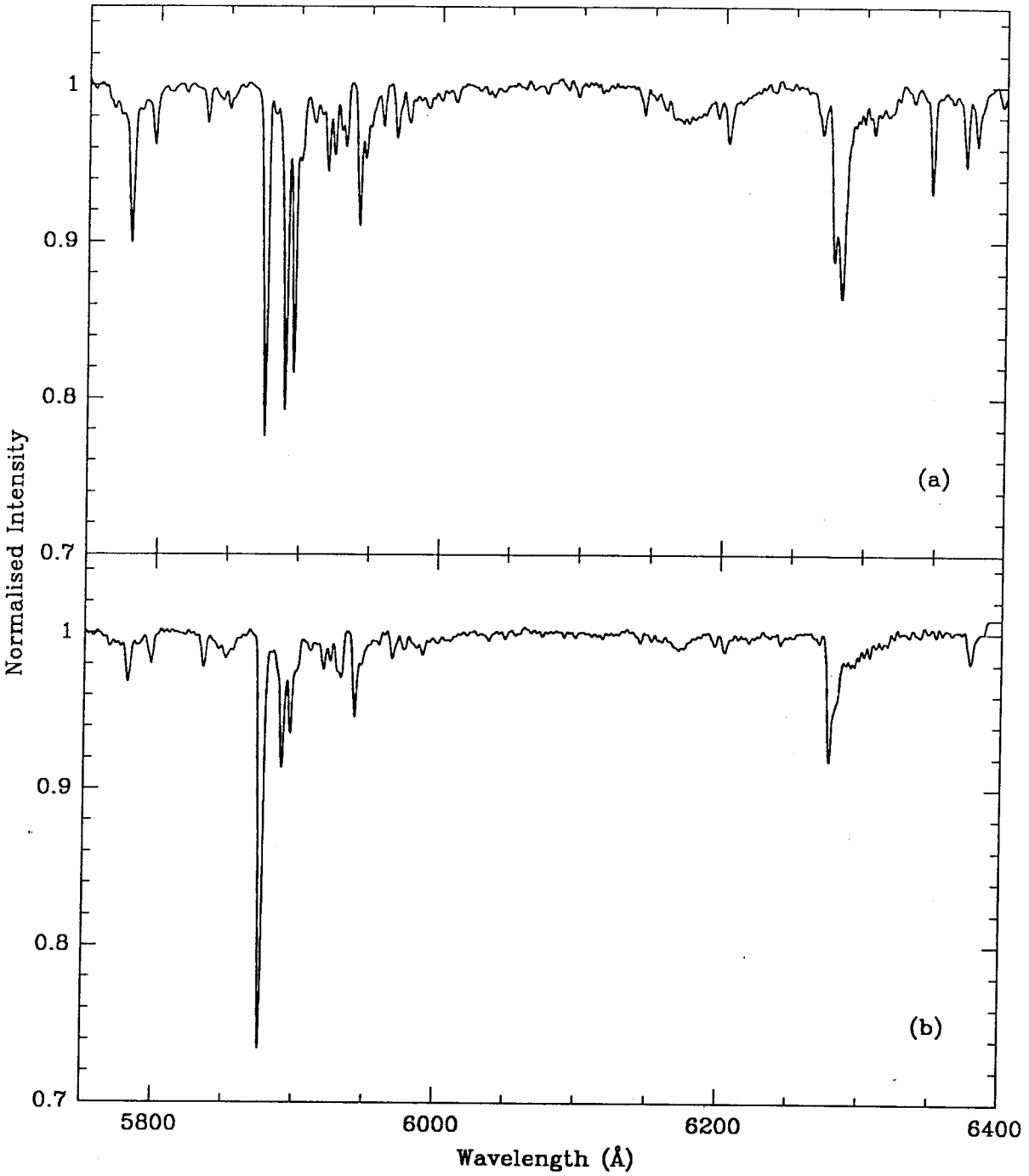

Figure 3.2: Representative spectra of (a) 55 Cyg and (b) ζ Per.

the α-band of oxygen would not completely cancel in the ratio. This was recognised as a possible source of confusion at the times of the observations. Therefore, when multiple pairs of spectra were obtained on a given night, they were taken in the sequence: I_{max} I_{min} I_{min} I_{max}. If the air mass varied monotonically over the sequence of observations, then the ratios I_{max}/I_{min} from the first and last pair in each sequence, should show residual effects within the telluric bands that are similar in strength but *opposite* in sense. That is, one should show residual emission and the other residual absorption. In the mean, the spurious structure is expected to cancel out. When only one pair of spectra could be obtained, especially in the case of HD 183143 which required long integration times, attempts were made to observe the star near the meridian.

Table 3.2 summarises of the observations, including the number of pairs of spectra taken per night, the mean exposure time of each pair and the average S/N per diode of each spectrum.

Polarised spectra of the relatively unreddened star, α Cyg, were obtained in the same way as the program star spectra to monitor possible instrumental polarisation effects.

3.3 Data Reduction

The data were reduced using the UBC version of the program RETICENT (Pritchet, Mochnacki and Yang 1982). The preprocessing techiques described by Walker *et al.* (1985) for extracting optimal S/N from Reticon data were employed. Each stellar spectrum was corrected for the fixed pattern in its baseline by subtracting the average of 10–12 ten-second dark exposures, taken immediately following readout of every stellar spectrum. The differential offsets between the four video-line amplifier zero-points were calibrated using the outputs of the pre- and post-scan diodes and the appropriate normalisations made to each spectrum.

Ratios of the spectra within each set (defined as two consecutive spectra taken at orthogonal orientations of the analyser) were then formed for all the program stars. Besides enhancing the visibility of any polarisation structure in the bands, this step effectively removed diode-to-diode variations in sensitivity, as well as the four-point fixed pattern arising from the differential gains of the amplifiers. Also, the small variations in the linearity of the amplifiers were automatically normalised in the ratio since the exposure

Table 3.2: Summary of DIB Observations

Star	Date (UT)	N^a	Exposure Time (s)	S/N
HD 183143.....	06 Aug 1990	1	7200	450
	07 Aug 1990	2	3600	600
	24 Aug 1990	2	3600	540
	25 Aug 1990	1	3600	550
55 Cyg.....	06 Aug 1990	1	1800	500
	07 Aug 1990	1	1340	950
	24 Aug 1990	2	1200	740
	25 Aug 1990	2	1800	850
ζ Per.....	07 Nov 1989	3	900	1400

a) Number of pairs of spectra.

levels between the spectra in a set are nearly equal. Finally, an eight-point multiplicative normalisation was applied to the ratios to remove any persistent fixed pattern.

Prior to forming the ratios, the spectra in each set were aligned with respect to each other. This was done in order to correct for shifts in the spectral line positions caused by spectrograph flexure which could, in the ratio, lead to spurious S-shape structure within the diffuse bands. To calculate the shifts, each spectrum was divided by a continuous lamp spectrum and rectified by a second-order cubic-spline fit to selected continuum points. The relative shifts between spectra were determined using the Fahlman-Glaspey difference-function technique (Fahlman and Glaspey 1973). This technique evaluates, for a range of trial shifts, the relative shift needed to minimise the difference between two spectra. Only the sharp interstellar Na D doublet at $\lambda\lambda$5890, 5896 and the stellar Si II lines at $\lambda\lambda$6371, 6347 were used in the calculations in order not to bias the results. The computed shifts amounted to no more than one-tenth of a pixel for HD 183143 and were much smaller for the other stars. Because the shifts were so small, effective cancellation of the diode-to-diode variations in the ratios was still acheived. In each set, the spectrum corresponding to I_{max} was chosen as the reference spectrum.

The calculated shifts were used to align the *original* spectra which had not been divided by a flat-field spectrum nor rectified, from which ratios were then formed.

The final step in the reductions involved aligning the ratios for each program star to allow later averaging of all the ratios of a given star. Since all the ratios were aligned with respect to the spectra at the ϕ_p orientation, the amount of shift required to align the ratios was evaluated from those same spectra relative to a mean spectrum for each star. The mean spectra for HD 183143 and 55 Cyg were formed from the average of their respective 24th Aug 1990 UT observations; for ζ Per the average of the 7th Nov 1989 UT observations was used.

3.4 Results

Spectral ratios in the sense I_{max}/I_{min} are plotted in Figs. 3.3*a*, *b* and *c* for all the program stars. In order to improve the S/N ratio, the ratios have been smoothed by a Gaussian transfer function with a σ value of 0.90 Å. (This assumes that no significant wavelength dependent change of polarisation occurs in the wavelength range $2\sigma = 1.80$ Å.)

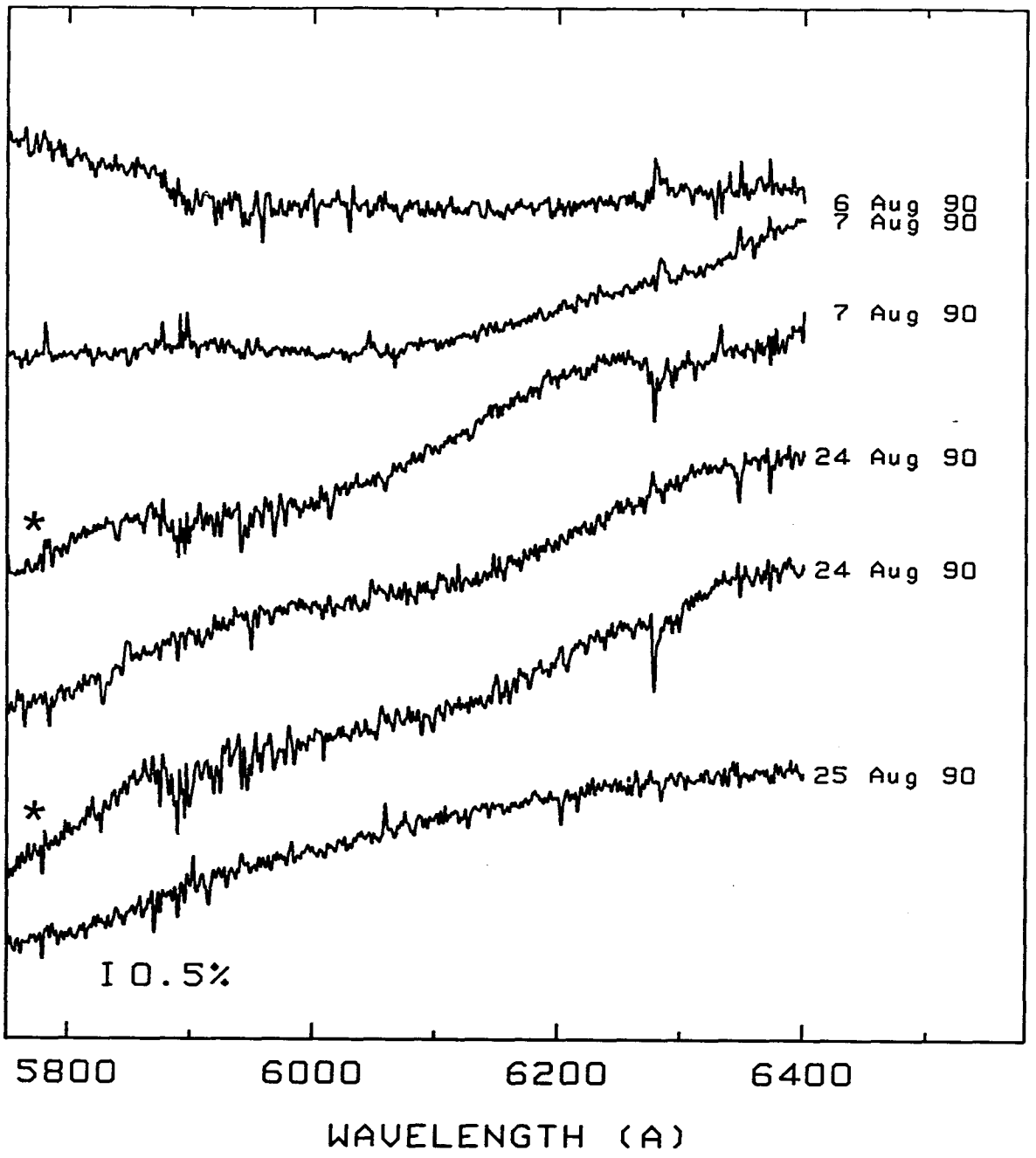

Figure 3.3: (*a*) The complete set of residual spectra of HD 183143. The residuals were formed by forming the spectral ratios in the sense: I_{max}/I_{min}.

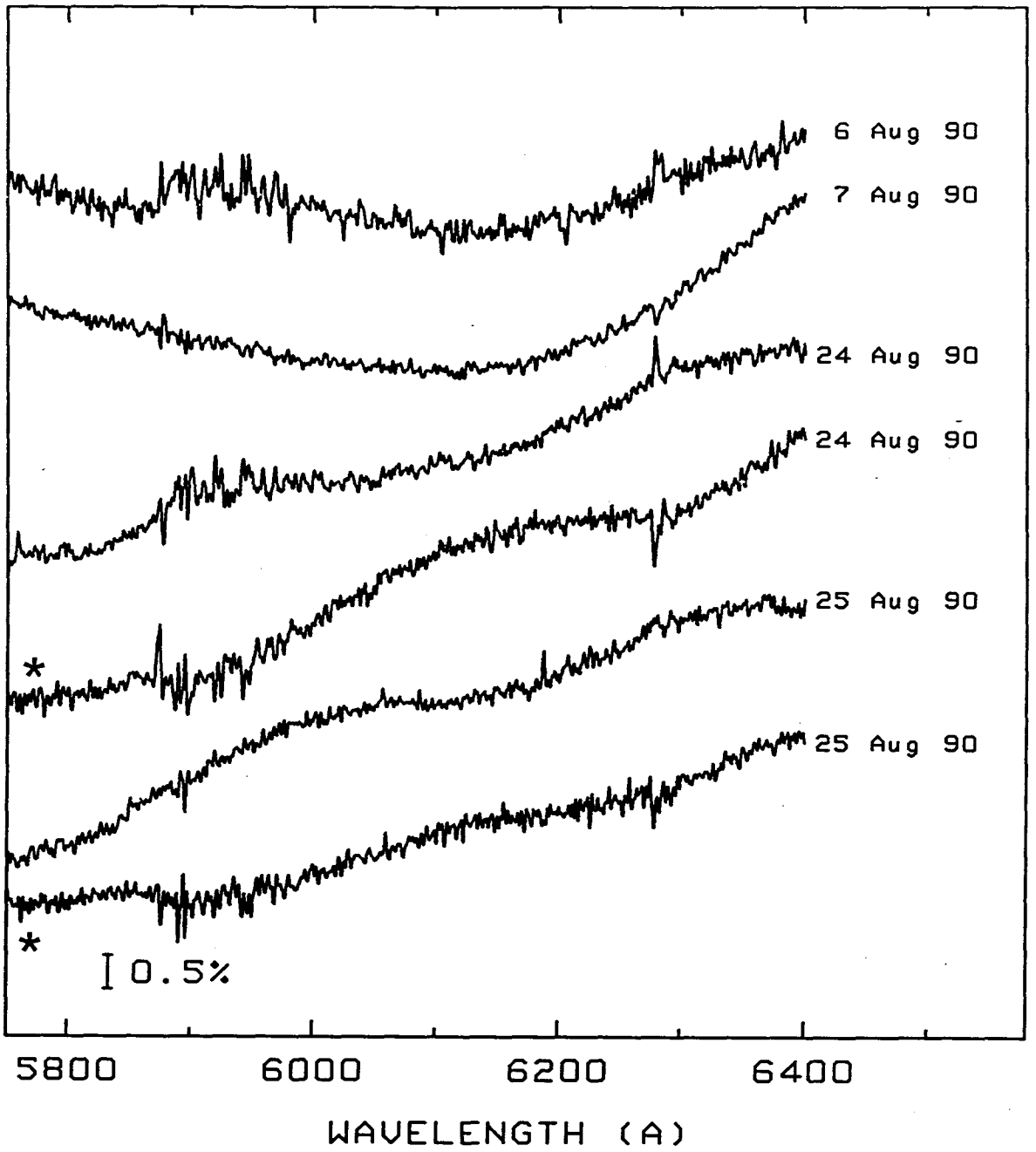

Figure 3.3: (*b*) As Fig. 3.3*a* for 55 Cyg.

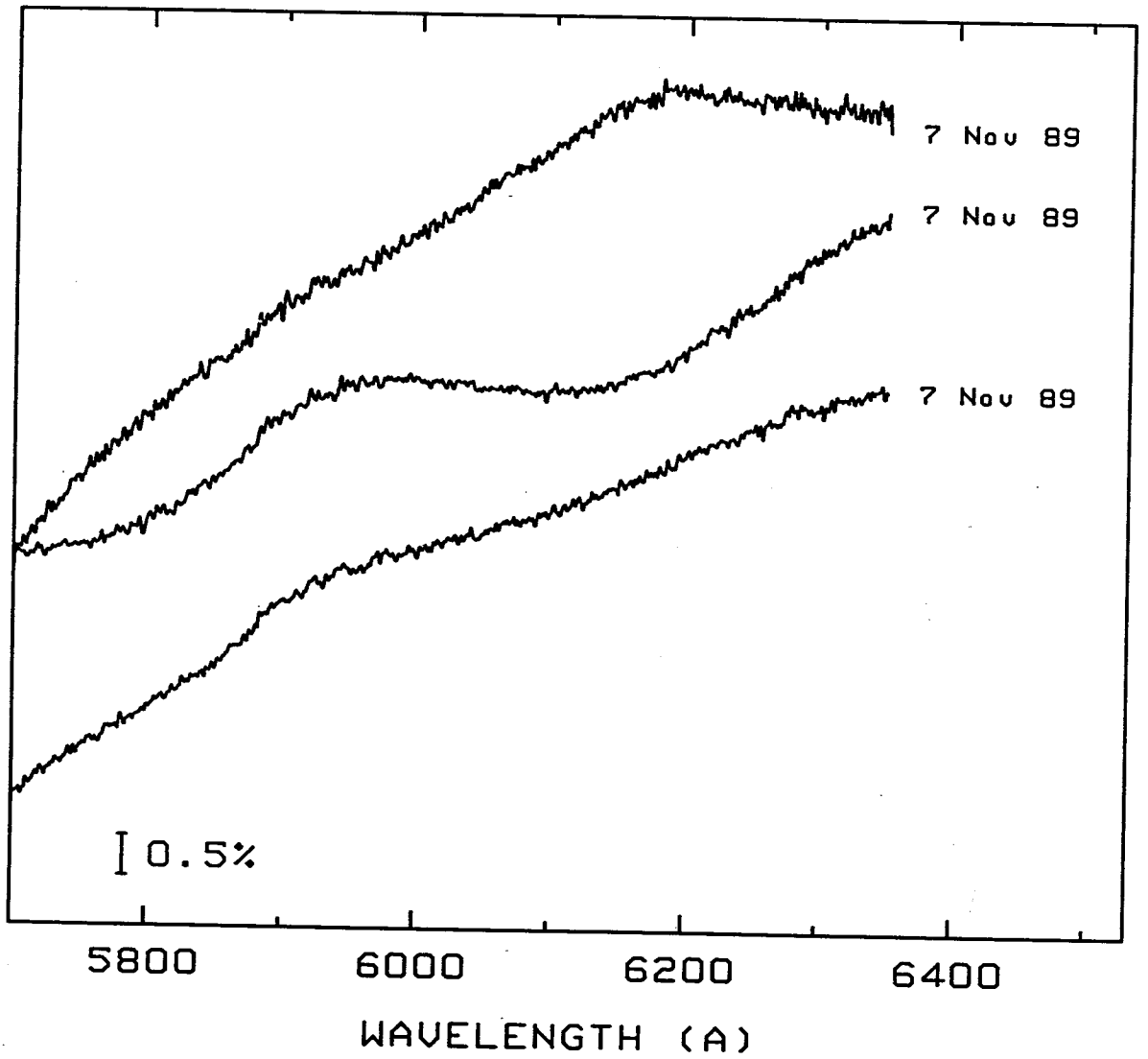

Figure 3.3: (c) As Fig. 3.3a for ζ Per.

Any polarisation effects within the diffuse bands should appear as enhancements in the continuum polarisation curve at the locations of the features (Martin and Angel 1974; Fahlman and Walker 1975). The curvature evident in some residuals near the broad 6177 Å band deserves comment since it could be misinterpreted as polarisation excess within the band. A gradual downturn in the residual intensities at the bandhead of the telluric α-band of oxygen appears in the ratios of HD 183143 and 55 Cyg indicated by the asterices in Figs. 3.3*a* and *b*. Those ratios all show significant residual absorption at the oxygen band since the spectra were taken at increasingly larger air masses. The depression is rather broad, spanning the extent of the band, ~ 60 Å, and tends to draw the intensity level of the residual spectrum downward, giving the appearance of enhanced polarisation shortward of the bandhead. Notice similar curvature on the short-wavelength side of the water-vapour and Na D lines. We therefore conclude that this effect is an artifact of imperfect cancellation of the telluric bands in the ratio. Also, in light of the fact that similar structure is not present in all the residual spectra, we are certain that the curvature evident in the residuals marked in Figs. 3.3*a* and *b* do not represent polarisation excess in the 6177 Å band.

To emphasise any enhancements in continuum polarisation curve, polynomial fits were used to normalise the residuals to zero slope. Care was exercised in carrying out the fits since it was conceivable that improper removal of the curve could introduce false structure or remove real effects. This is especially critical near the broad diffuse feature at 6177 Å. For this reason, only low order polynomial fits, usually third- or fifth-order, were used in the normalisation. Fig. 3.4 shows a typical fit to a residual spectrum. Clearly, no structure of the width of the DIBs is present in the fit. Therefore, we are confident that, in carrying out this step, we have removed only the smooth curve associated with the continuum and residual instrumental polarisation while retaining the small-scale (< 50 Å) structure expected if the diffuse bands are indeed polarised. The rectified residual spectra are shown in Figs. 3.5*a*, *b* and *c*.

The residuals show significant structure in the regions of the telluric lines. Because these lines are relatively narrow, even small displacements in the line positions between the spectra will produced S-shaped structure in the ratio. However, this effect is not expected to be quite as severe in the diffuse bands of interest since the widths of the bands ($\sim$5–40 Å) are larger than those of the telluric lines ($\sim$2–3 Å).

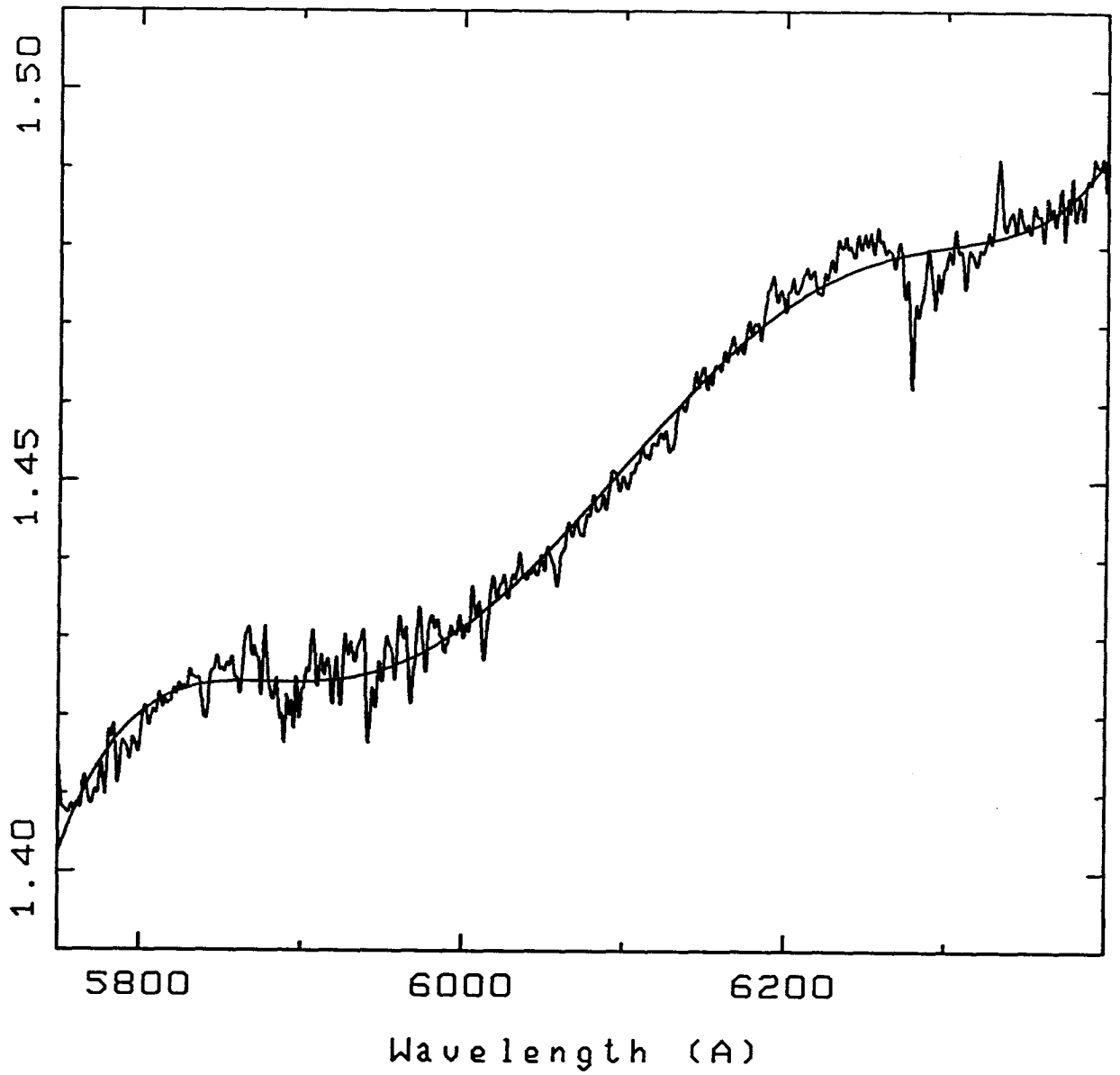

Figure 3.4: Typical rectification of the (7 Aug 1990 UT) residual spectrum of HD 183143. A fifth-order polynomial has been fitted to selected continuum points.

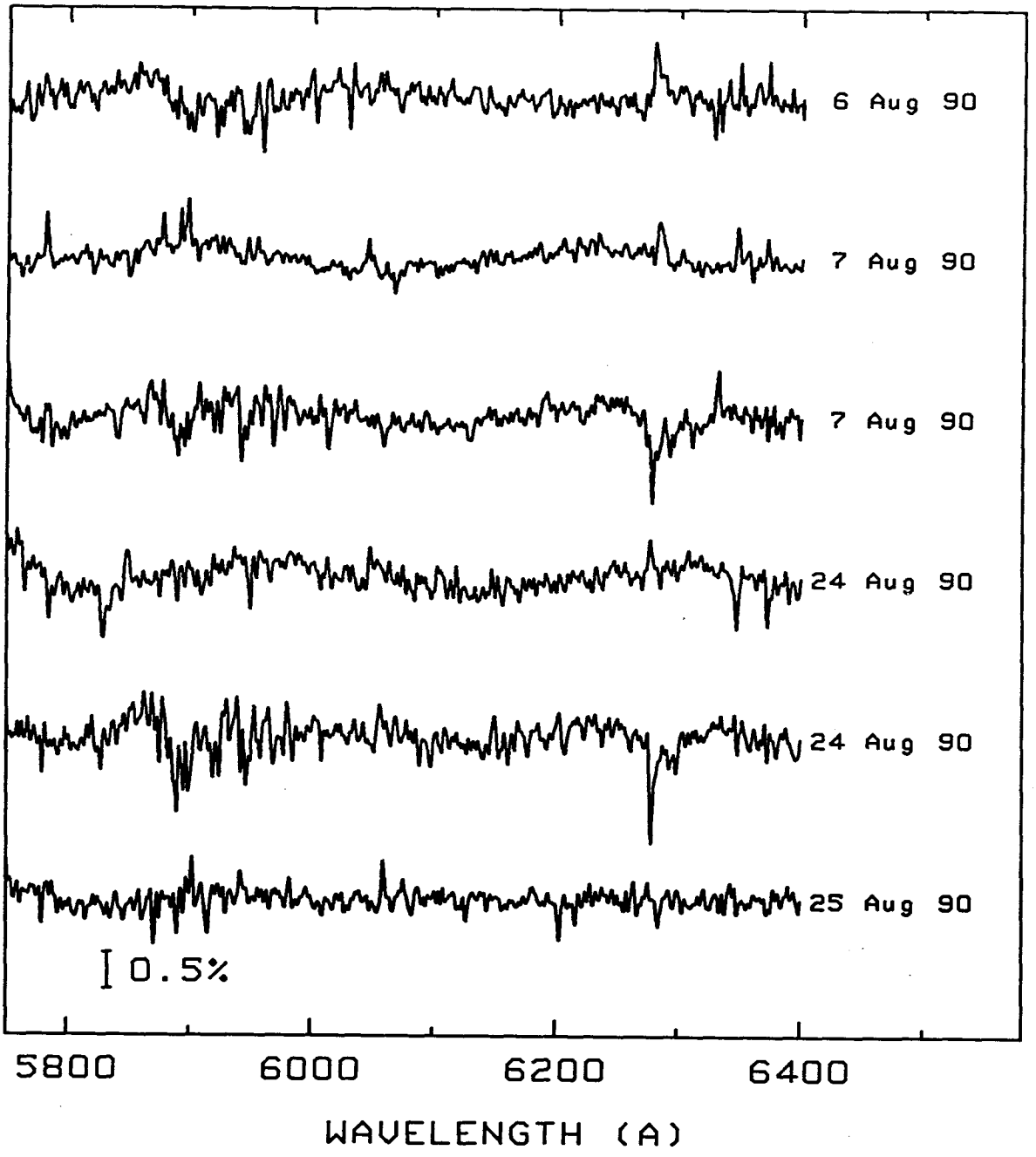

Figure 3.5: (*a*) Rectified residual spectra of HD 183143, formed by dividing polynomial fits into the residual spectra of Fig. 3.3*a*.

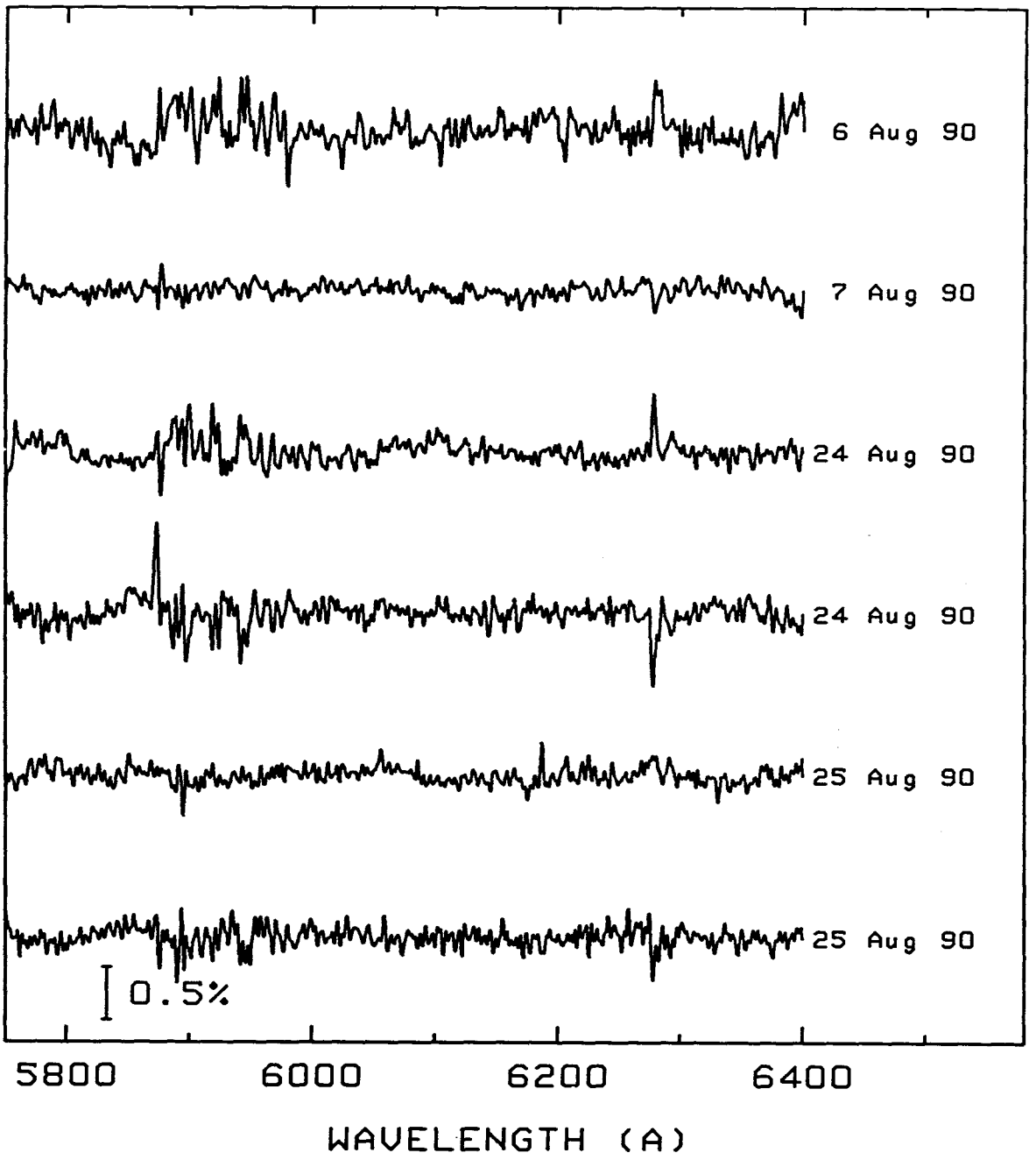

Figure 3.5: (*b*) Rectified residual spectra of 55 Cyg, formed by dividing polynomial fits into the residual spectra of Fig. 3.3*b*.

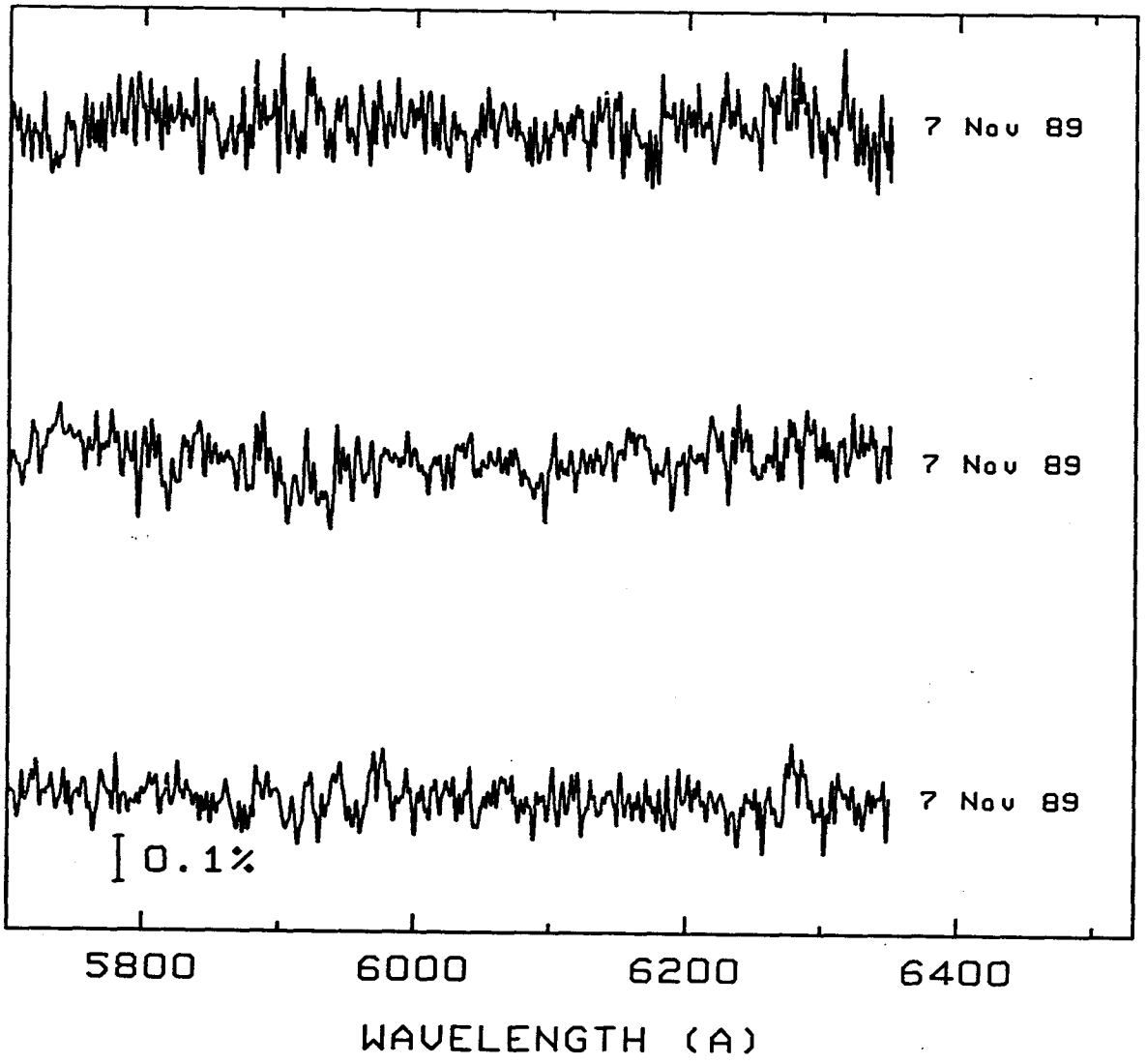

Figure 3.5: (*c*) Rectified residual spectra of ζ Per, formed by dividing polynomial fits into the residual spectra of Fig. 3.3*c*.

Figs. 3.5*a, b* and *c* also show residual effects resulting from the spectra being obtained through different air masses. Due to the combination of this effect and the sequence in which the measurements were taken (cf. Section 3.2), on nights when multiple pairs were obtained, the first pair shows residual absorption whereas the second shows residual emission. This effect should cancel by taking the mean of all the residuals.

(We used the spectra of α Cyg to check for polarisation structure within the water-vapour and oxygen bands themselves. Ratios were computed in the same way as for the program stars and the mean of those ratios is shown in Fig. 3.6. No polarisation structure within the telluric bands is evident.)

To improve the S/N of the spectral ratios and cancel the residual effects in the telluric bands caused by the variable air mass, the ratios of each star were averaged. The mean spectral ratios for HD 183143, 55 Cyg and ζ Per are shown together with representative spectra in Figs. 3.7*a, b* and *c*. The formal standard deviation of the ratios are 0.07, 0.03 and 0.03%, respectively.

The apparent S-shape profile appearing in the region of the narrow 5780 Å band in the mean ratio of HD 183143 (Fig. 3.7*a*) is not a polarisation effect; it is caused by small diplacements in the line positions despite the attempts to align the spectra before forming the individual spectral ratios. Similar effects occur in the sharper stellar and telluric lines of the spectrum. In fact, the nearby He I λ5875 line shows nearly identical S-shaped structure and we have used it to try to remove the effect in the 5780 Å band. The residual in the vicinity of the He I line was scaled according to the ratio of the band and the stellar line intensities and then subtracted from the residual effect at the DIB. Fig. 3.8 shows good cancellation of the effect from the 5780 Å DIB.

Note that the S-shaped structure in the region of the 6284 Å DIB in the mean residual spectrum of HD 183143 (Fig. 3.7*a*) is also caused by small misalignments between the spectra used to form the individual ratios. This structure is associated with the bandhead of telluric O_2 and not with the 6284 Å DIB.

No obvious polarisation structure associated with the DIBs is present in any of the mean residual spectra. Upper limits to the differential polarisation in the four strongest bands at 5780, 5797, 6177 and 6284 Å are given in Table 3.3 for each of the program stars. The upper limits represent the standard deviation across the entire band.

Our final result was obtained by combining the mean residual spectra of HD 183143

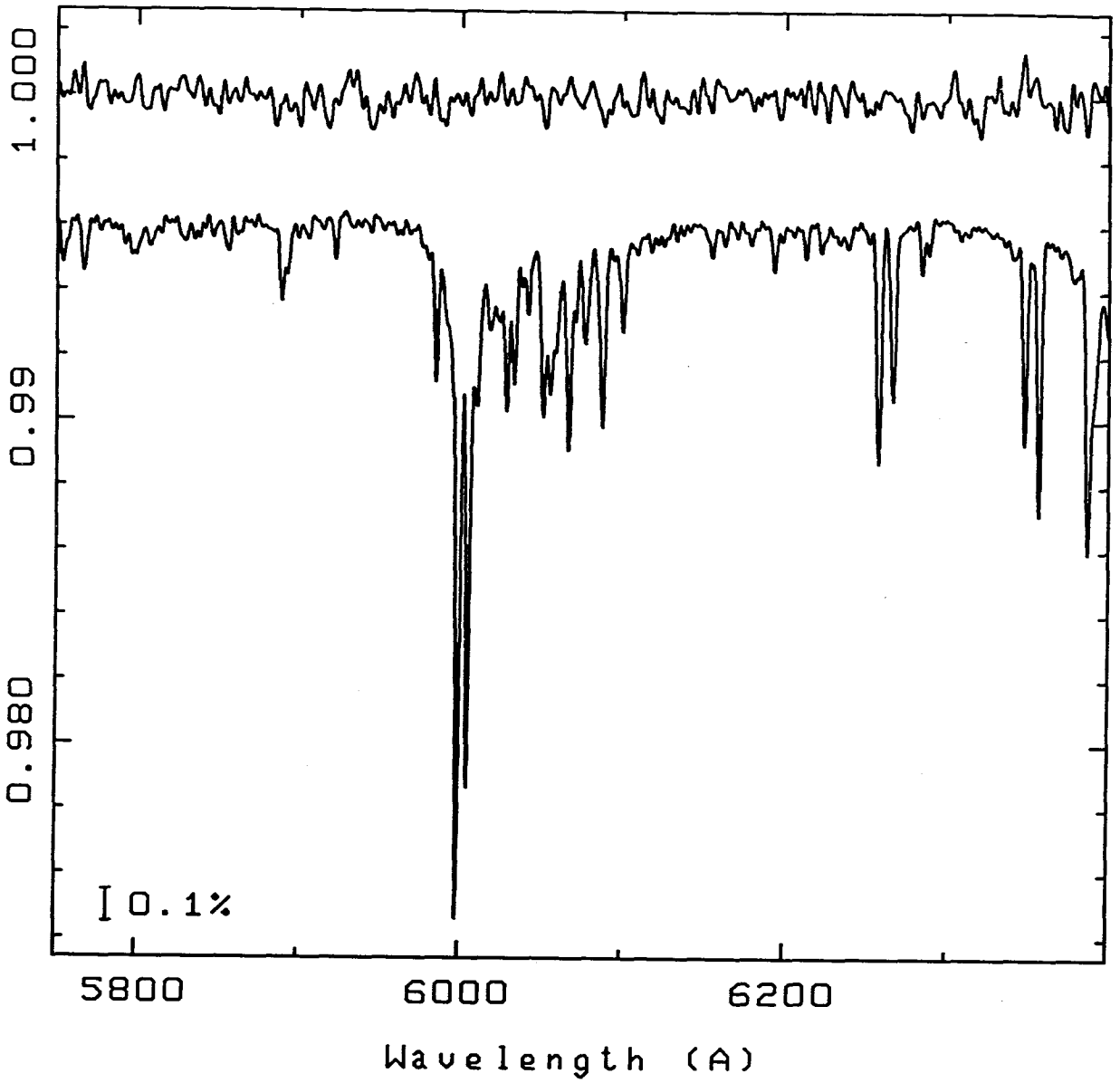

Figure 3.6: Mean residual spectrum of the standard unpolarised star α Cyg. A representative spectrum (not to scale) is shown below. The error bar indicates the intensity scale with respect to the continuum level.

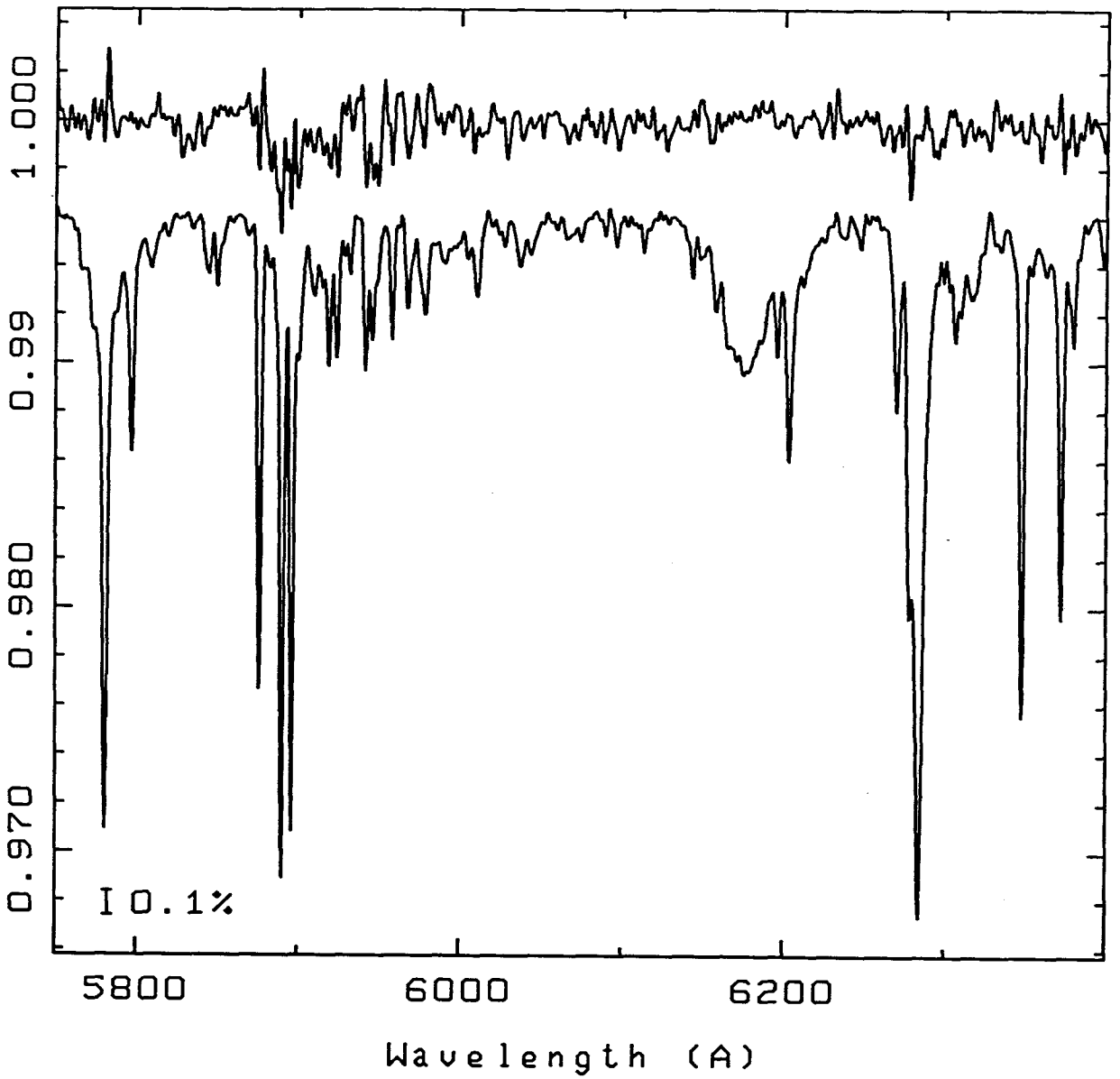

Figure 3.7: (*a*) Mean residual spectrum of HD 183143. A representative spectrum (not to scale) is shown below. The error bar indicates the intensity scale with respect to the continuum level.

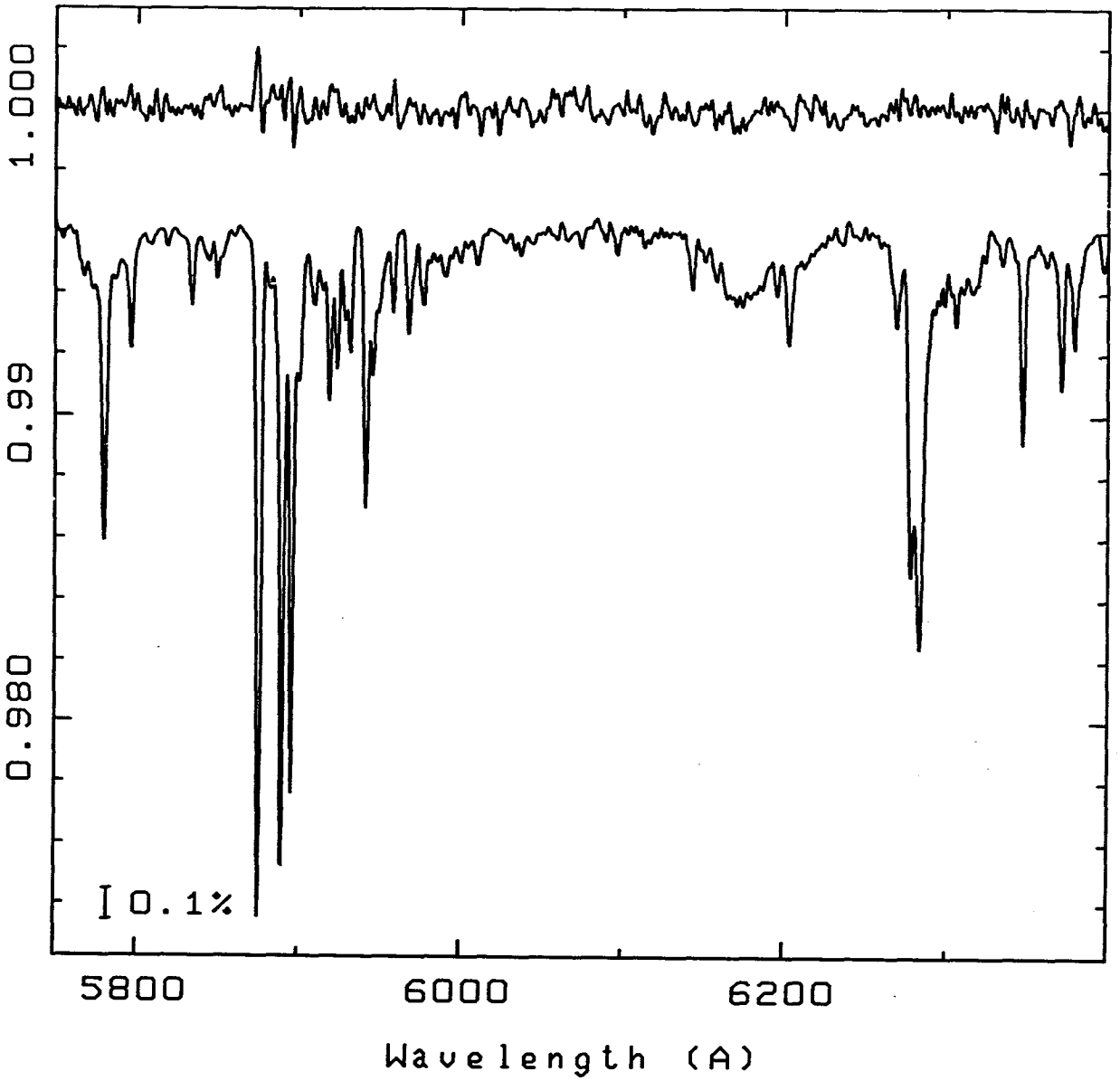

Figure 3.7: (*b*) Mean residual spectrum of 55 Cyg. A representative spectrum (not to scale) is shown below. The error bar indicates the intensity scale with respect to the continuum level.

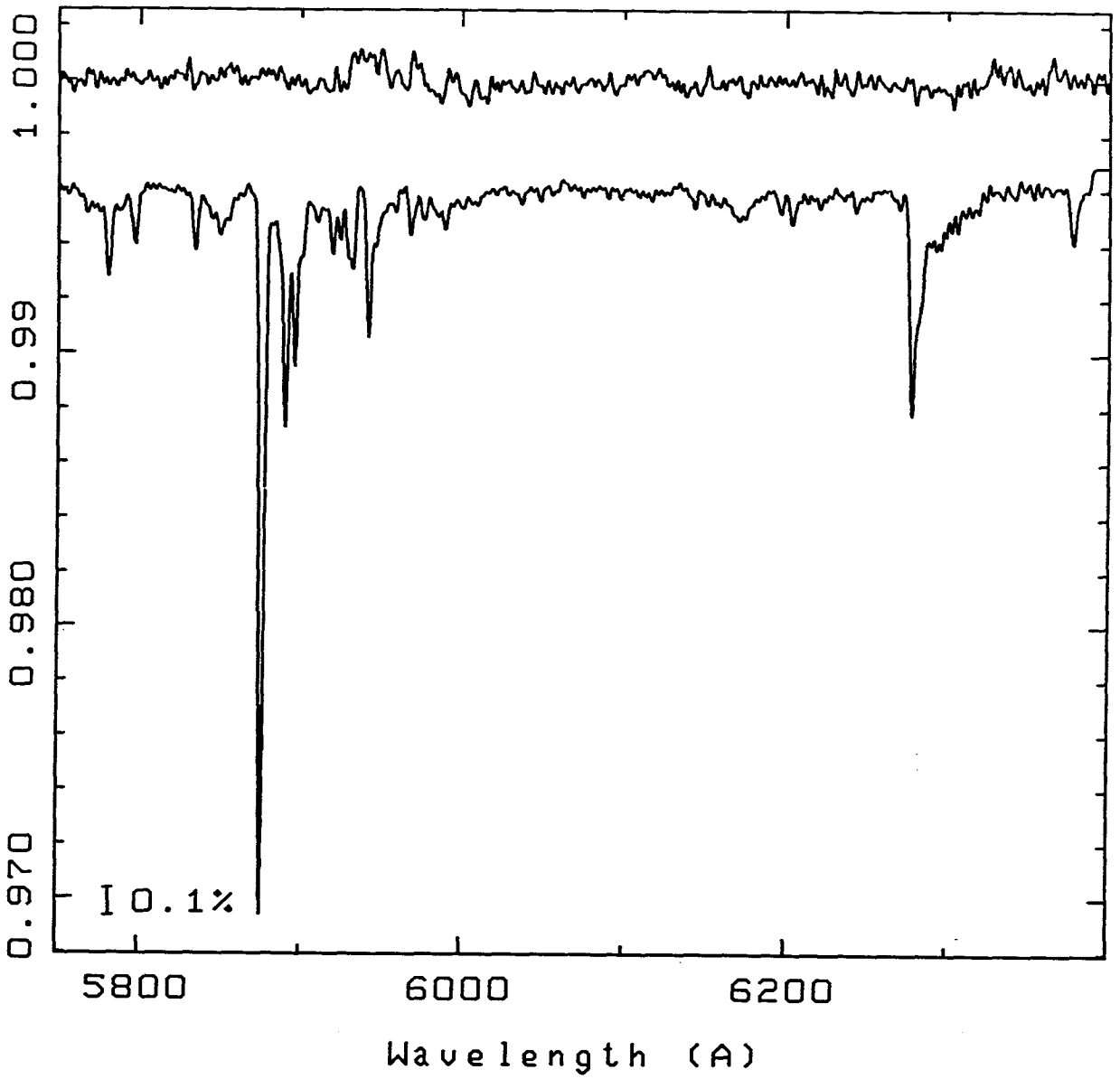

Figure 3.7: (c) Mean residual spectrum of ζ Per. A representative spectrum (not to scale) is shown below. The error bar indicates the intensity scale with respect to the continuum level.

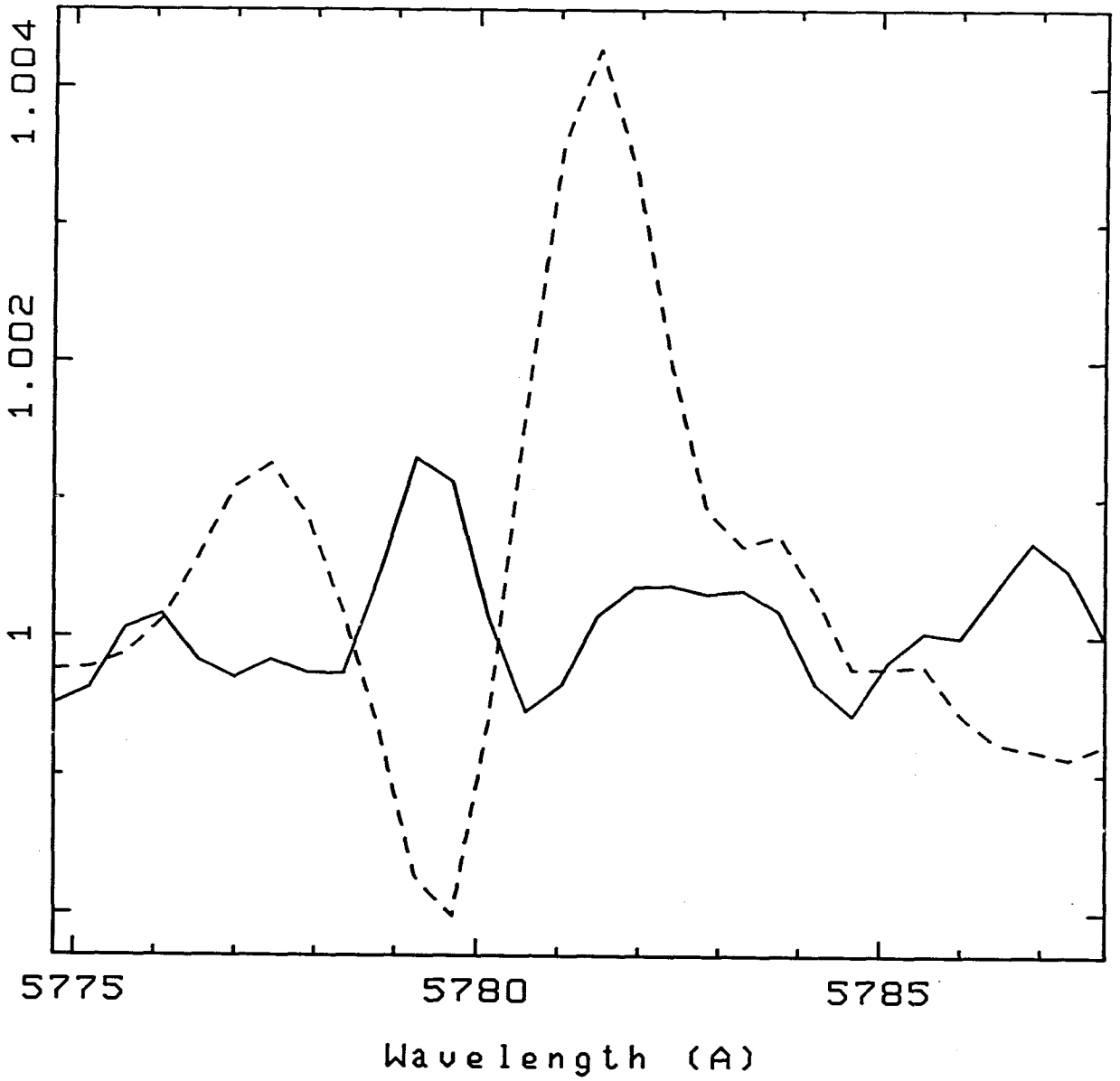

Figure 3.8: S-shaped structure (dashed line) is apparent in the mean residual spectrum of HD 183143 in the region of the 5780 Å band. The He I λ5875 line shows nearly identical structure (Fig. 3.7). The effects were caused by small displacements in the line positions. In order to remove the effect from the band, the residual in the vicinity of the stellar line was scaled according to the ratio of the band and He I line intensities and subtracted from the residual structure at the DIB. The result is shown by the solid line.

Table 3.3: Upper Limits ($\pm 1\sigma$) to the Polarisation in the Diffuse Interstellar Bands

	5780 Å	5797 Å	6177 Å	6284 Å
Star	(%)	(%)	(%)	(%)
HD 183143	0.01	0.01	0.04	0.07
55 Cyg	0.02	0.02	0.03	0.01
ζ Per	0.04	0.01	—	0.01
Mean[a]	0.01	0.01	0.02	0.03

a) Mean residual spectrum of HD183143 and 55 Cyg.

and 55 Cyg and is shown in Fig. 3.9. Upper limits to the change of polarisation through each band were then estimated by the standard deviation within each profile. (The mean residual spectrum of ζ Per was not used in the calculation because the strengths of the bands in its spectrum are much weaker than in the others.) As listed in Table 3.3, the upper limits are 0.02, 0.01, 0.01, 0.02 and 0.03% in the 5780, 5797, 6177 and 6284 Å bands, respectively.

3.5 Discussion

We may better understand our results by comparing them with model predictions, following the approaches of Martin and Angel (1974, 1975) and Fahlman and Walker (1974). If we make the assumption that the diffuse interstellar bands, extinction and continuum polarisation all arise from the same aligned grains, then we may make specific predictions as to the size of the polarisation effect within the features.

Martin and Angel (1974) have modelled the wavelength dependence of polarisation across the diffuse bands assuming the interstellar grains causing the continuum polarisation are infinitely long circular cylinders aligned by the "perfect" Davis-Greenstein mechanism.[3] The diffuse features were assumed to arise from impurities, i.e., atoms or molecules, dispersed through those same grains. The impurities produced specific wavelength dependent changes in the index of refraction related to the profile of the DIB. Without knowing the precise nature of the impurities, the index of refraction over an absorption feature were determined by the observed width, central wavelength and depth of the feature. It was also dependent on the index of refraction assumed outside the absorption features. Martin and Angel (1974) assumed the index of refraction of the interstellar grains producing the continuum polarisation to be purely or almost purely dielectric. They computed models for the range of continuum refractive indices from $m = 1.5 - 0i$ to $1.5 - 0.1i$.

Their primary result was that, in general, the polarisation profile of a diffuse band has the same shape as its extinction profile. Quantitatively, they expressed this in the

[3]In the theory of Davis and Greenstein, the interstellar grains are assumed to be aligned by the Galactic magnetic field and spin about their short axes. Details of the Davis-Greenstein mechanism may be found in Davis and Greenstein (1951), Davis (1958) and Jones and Spitzer (1967).

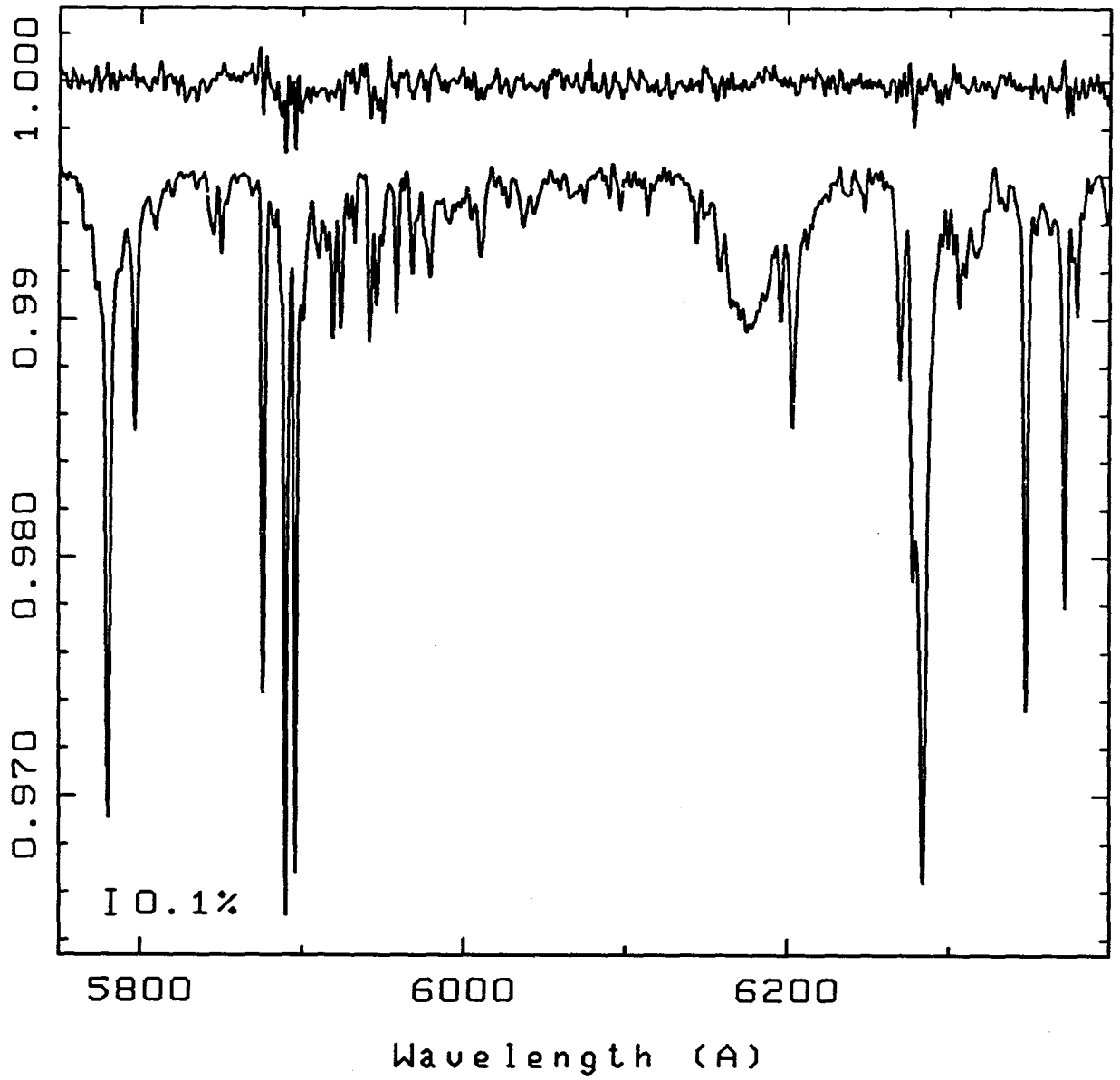

Figure 3.9: Mean residual spectrum formed from the average of all the residual spectra of HD 183143 (Fig. 3.7*a*) and 55 Cyg (Fig. 3.7*b*). A representative spectrum (not to scale) of HD 183143 is shown below. The error bar indicates the intensity scale with respect to the continuum level.

following way:

$$\frac{\Delta P(\lambda)}{P(\lambda)} = \frac{f\Delta\tau(\lambda)}{\tau(\lambda)} \tag{3.1}$$

(from Martin and Angel 1974) where ΔP is the change of polarisation from the adjacent continuum polarisation P, $\Delta\tau$ is the change in optical depth from the adjacent continuum optical depth τ and f is a model-dependent parameter.

We have used their result to predict the size of the polarisation effect in the diffuse bands of our data. For f, we adopted a value of 1.4, in agreement with Martin and Angel (1974, 1975) and Fahlman and Walker (1974). The continuum polarisation, $P(\lambda)$, was calculated using the empirical formula describing the wavelength dependence of optical polarisation from Serkowski, Matthewson and Ford (1975):

$$\frac{P(\lambda)}{P(\lambda_{max})} = \exp\left[-K\ln^2\left(\frac{\lambda}{\lambda_{max}}\right)\right] \tag{3.2}$$

where λ_{max} is the wavelength of maximum polarisation, $P(\lambda_{max})$, and $K = -0.10 + 1.86\lambda_{max}$ from the improved fit of Wilking, Lebofsky and Rieke (1982). We used the values of λ_{max} and $P(\lambda_{max})$ given by Serkowski *et al.* (1975) and listed in Table 3.1. The optical depth, $\tau(\lambda)$, over the wavelength range of our spectra was computed from the relation $A_V = 1.086\tau_V$ (Mihalas and Binney 1981) and the $1/\lambda$ extinction law. We assumed a ratio, R_V, of total to selective extinction of 3.2 which is suitable for all the program stars (Johnson 1968) and used the colour excesses listed in Table 3.1. The change in optical depth $\Delta\tau(\lambda)$ across a band from the continuum optical depth was calculated from the following equation:

$$\Delta\tau(\lambda) = \ln\left(\frac{I_\lambda}{I_c}\right) \tag{3.3}$$

where I_λ is simply the intensity at each point in the band profile and I_c is the continuum intensity. For I_λ, we used the mean of all our spectra rectified to a continuum value of unity, so that $I_c = 1$.

In calculating the predicted ΔP, we did not attempt to divide out the telluric α-band of oxygen from any of the spectra. Since the telluric band dominates the spectrum of ζ Per in the region of the 6284 Å, we have used the mean spectrum of HD 183143 to calculate ΔP and then scaled the computed value of ΔP to the level appropriate for ζ Per.

In Figs. 3.10*a, b* and *c*, we have plotted the differential polarisation (ΔP) profile predicted using Eqn. 3.1 in the region of the 5780 and 5797 Å bands, the 6177 Å band and

the 6284 Å band. The observed residual spectra of Figs. 3.7*a, b* and *c* are plotted on the same figures for the purpose of comparison. Those figures show no polarisation structure within the 5780, 5797 and 6284 Å DIBs at a level significantly smaller that the predicted effect. In the case of HD 183143, the observed ΔP in those bands is at least an order of magnitude less than that predicted.

Similarly, in the 6177 Å band of HD 183143, there is no statistically significant polarisation structure, the magnitude of the predicted ΔP being four times the standard deviation of the observed ΔP in the band. We cannot make the same claim in the 6177 Å band of 55 Cyg since there the noise level of our results is similar in magnitude to the predicted polarisation effect.

Have we overestimated the expected amount of polarisation in the DIBs due to grains? Since the degree of polarisation predicted by the model depends on the assumed composition of the grains and would be largest for dielectric grains (Greenberg 1978), it is important to establish whether the dielectric assumption is valid. According to Chlewicki and Greenberg (1990), the strong linear polarisation observed in the 3.08-μm ice band and the 9.7-μm silicate feature (Lonsdale *et al.* 1980) demonstrates convincingly that the polarising grains are most likely dielectric. In addition, Mie theory calculations show that conducting grains, with refractive indices that are strongly a function of wavelength, tend to produce more structure in the wavelength dependence of the polarisation than is observed (cf. Martin 1975; Greenberg 1978; Chlewicki and Greenberg 1990). Indeed according to Chlewicki and Greenberg (1990), the interstellar polarisation curve is well matched using a simple size distribution of dielectric grains.

The model of Martin and Angel (1974) produces results that are consistent with those of others. Greenberg and Stoeckly (1971), Kelly (1971), Bromage (1972), and Greenberg and Hong (1974, 1976) have computed the wavelength dependence of polarisation across the 4430 Å band. Their models were similarly computed by treating the DIBs as fine structure in the general extinction curve. Despite the different optical properties, alignment mechanisms and shapes of the grains assumed in the computations, the results are remarkably consistent. Of note is the general agreement that the polarisation profiles tend to mimic the extinction profiles of the bands. One exception is given by Greenberg and Hong (1974) who predicted anomalous dispersion[4] through the polarisation profile.

[4]Dispersion is defined by Greenberg and Hong (1974) as apparent "emission" at shorter wavelengths

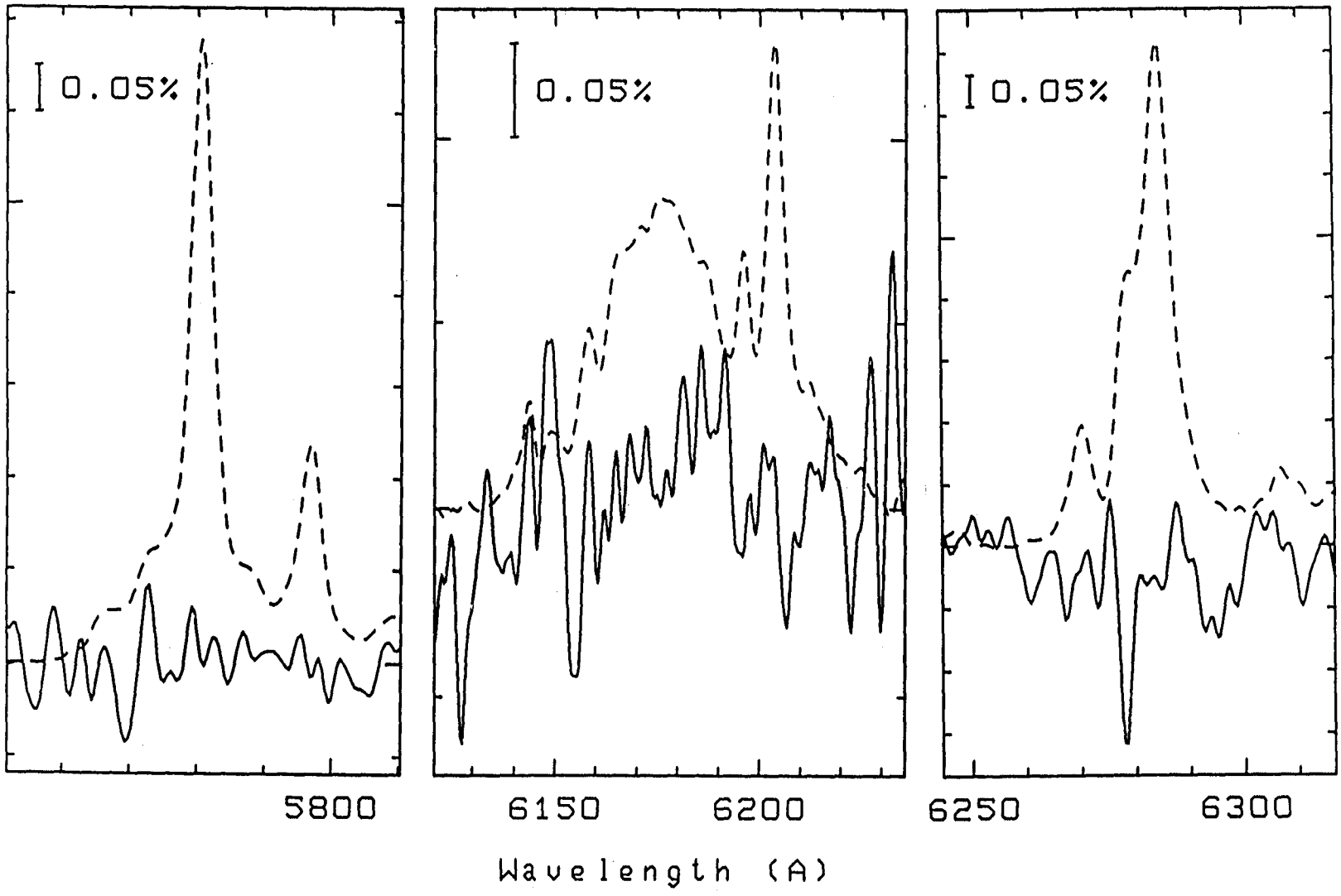

Figure 3.10: (*a*) Differential polarisation ΔP in the $\lambda\lambda$5780, 5797 (left panel), λ6177 (middle panel) and λ6284 (right panel) bands of HD 183143. The predicted ΔP was obtained by Eqn. 3.1 and is indicated by the dashed curve; the observed ΔP is given by the solid curve.

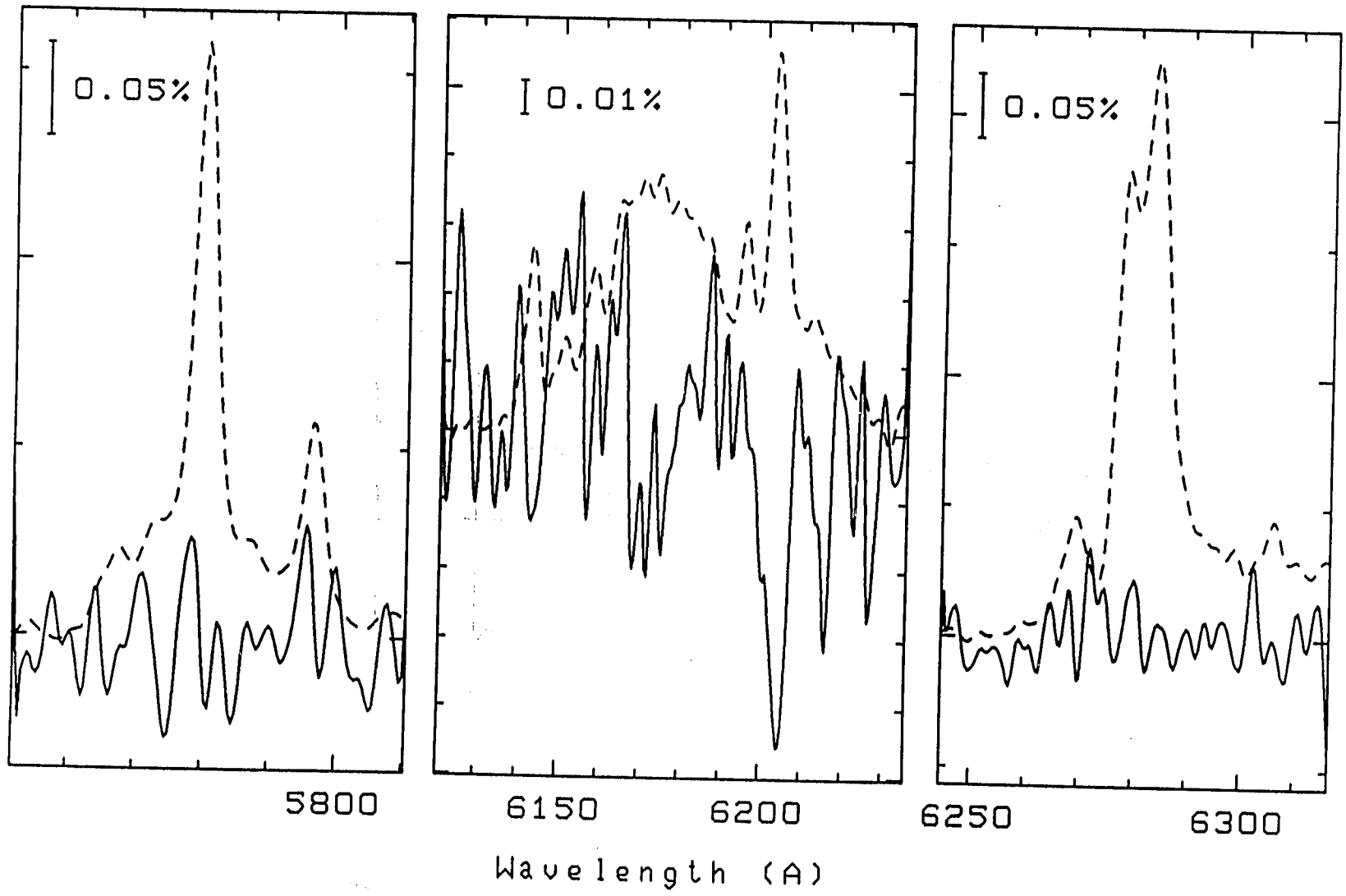

Figure 3.10: (*b*) As Fig. 3.10*a* for 55 Cyg.

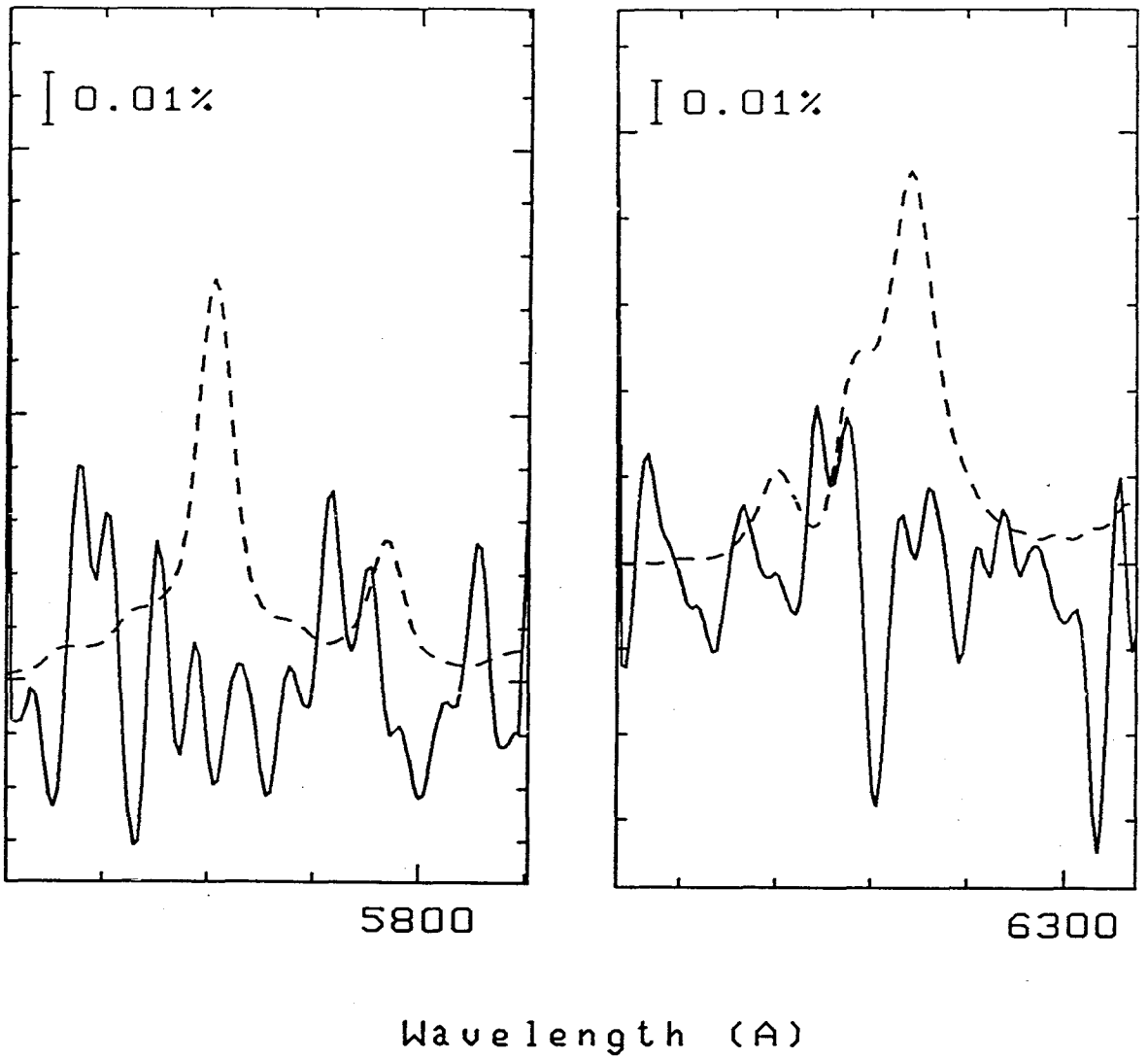

Figure 3.10: (*c*) As Fig. 3.10*a* for ζ Per. The predicted ΔP in the 6177 Å band is not shown because the band is very weak in this star.

However, as pointed out by Fahlman and Walker (1974), the magnitude of the polarisation predicted by the model of Greenberg and Hong (1974) is of the same order of magnitude as that computed by Eqn. 3.1. In any case, we feel that Eqn. 3.1 gives a reasonable estimate of the size of the polarisation effect if the diffuse bands are caused by the interstellar grains responsible for the visible continuum polarisation.

Our results support those of A'Hearn (1972), Martin and Angel (1974, 1975) and Fahlman and Walker (1975), and represent an order of magnitude improvement in the upper limit to the polarisation change set by those authors. We find no evidence for the differential polarisation effect reported by Gammelgaard and Rudkjobing (1973) in the 6177 Å band in any of the stars observed in this program. We would have observed this effect as a dimunition of the polarisation in the 6177 Å band.

3.6 Interpretation

A straightforward interpretation of the results of Sections 3.4 and 3.5 is that the DIBs do not originate in the solid grains which produce the visible continuum polarisation. That polarisation is produced by a population of partially-aligned elongated grains, which are also responsible for the visible extinction (cf. Smith *et al.* 1977).

There are two plausible explanations for the lack of polarisation structure in the DIBs. The first explanation is simply that the DIBs have a non-grain origin, presumably molecular. (This is because there is no known mechanism which could efficiently align the molecules (Chlewicki *et al.* 1986; van der Zwet 1986).) A further discussion of the molecular-hypothesis is beyond the scope of this thesis. Recent articles by Chlewicki *et al.* (1986) and van der Zwet (1986) outline the arguments in favour of a molecular origin for the bands.

The second explanation (for the lack of polarisation structure in DIBs) is that the bands arise from a population of grains distinct from those producing the visible continuum polarisation (Martin and Angel 1974; Chlewicki *et al.* 1986). Obviously, the grains responsible for the DIBs would have to be inefficient at polarising the stellar light. Two possibilities that would suit this requirement are spherical or unaligned grains.

Existing observational data place rather stringent constraints on the optical properties

and absorption at longer wavelengths about the center of the band.

and sizes of these grains. Although some show very slight asymmetry, the intrinsic profiles of many of the DIBs are highly symmetric (cf. Section 3.1.2). Therefore, large grains ($a \simeq 0.1\mu$m) can be excluded as the possible carriers of the bands since they would produce strong asymmetry in the band profiles. Since small particles are relatively inefficient scatterers in the visible, dispersion effects in the line profiles should be small (Chlewicki *et al.* 1986); hence the bands produced in such grains could have symmetric profiles.

However, Greenberg and Hong (1974) have computed the DIBs produced by model grains of various sizes whose shapes resemble spheres, spheroids and infinite cylinders.[5] Using the usual Clausius-Mosotti equation to introduce the impurities into the host material, they found that the only way to symmetrize the profiles was to put the the impurities into the very small particles (i.e., $a \ll \lambda$). Even under that condition, some asymmetry of the profiles persists so long as the impurity centers are located in non-spherical grains.

Chlewicki *et al.* (1986) computed similar models using the more accurate Purcell-Shapiro equation which better takes into account the interaction between the electric field produced in the impurity centre and the external field. They remark that in the small-grain limit, the lines tend to be asymmetric with a steeper *redward* edge.

Moreover, if the DIBs are formed in the very small grains then one would expect the strengths of the bands to correlate with the far-UV extinction, which appears to be produced by a population of $\sim 0.01\mu$m grain. However, as described in Section 3.1.2, several statistical studies show poor correlations of the 4430, 5780 and 6284 Å DIBs with far-UV extinction.

As Chlewicki *et al.* (1986) conclude,

> Insofar as particles are concerned, the only remaining sizes to be considered as potential diffuse line carriers are in the intermediate range ($0.02 < a < 0.1\mu$m). The typical size of "diffuse line" particles indicated by the observed profiles [see their Fig. 5] is $\sim 0.05\mu$m. However, using absorbers embedded in the intermediate-size particles, it is difficult to explain both the details of the individual profiles, such as the lack of broad wings in λ5780, and the large variety of observed line shapes.

The strength of the 4430 Å band does correlate with the 2175 Å extinction bump.

[5]They assumed the optical properties of "dirty ice" in their models. They also performed model calculations for core-mantle grains with the intention of determining whether the placement of the impurities, either in the cores or the mantles, have any affect on the symmetry of the resulting interstellar absorption bands (Greenberg and Hong 1976; Greenberg 1978).

(The positive correlation between these features does not contradict the lack of correlation between the 4430 Å band and far-UV extinction, since the 2175 Å feature also does not correlate with with far-UV extinction.) The 2175 Å extinction bump is often attributed to a population of small ($\sim 0.01\mu$m) graphite grains or "platelets" (Draine 1988). Recently, Clayton *et al.* (1991) have measured the polarisation across the 2175 Å bump of the supergiant α Cam. They found no statistically significant enhancement of polarisation in the bump. Therefore, the results of Clayton *et al.* and of this chapter do not contradict the possibility that the two features share a common origin.

In conclusion, it would seem that our results suggest that the bands are either molecular in origin, or are due to intermediate-sized ($0.02 < a < 0.1\mu$m) grains which are spherical or unaligned.

Chapter 4

Differential Polarisation Studies of Be Stars

4.1 Be Stars

4.1.1 Introduction

The most striking characteristic of Be stars, and that which distinguishes them from normal B stars, is the presence of emission in the Balmer series of hydrogen. For historical reasons, the term Be has been reserved only for the B stars of luminosity classes III, IV and V that have emisson lines, although emission in (predominantly) Hα is common in the supergiants. The underlying absorption spectra of Be stars are typical of normal B-type spectra in which the absorption lines have been broadened by rotation. The emission lines are usually superimposed on the broad absorption lines and most commonly occur at Hα and Hβ. If present at all, the emission decreases for the higher members of the Balmer series and disappears toward H20. Emission is also sometimes present in the singly ionized metallic lines such as Fe II. The presence of emission is not a rare anomaly in the spectra of B-type stars; in fact, the Be stars make up a significant ($\sim$ 20%) proportion of B stars. There are many excellent reviews of Be stars; some include the proceedings of IAU Symposium No. 70 (Slettebak 1976), Underhill and Doazan (1982), the proceedings of IAU Symposium No. 98 (Jaschek and Groth 1982) and the proceedings of IAU Colloquium No. 92 (Slettebak and Snow 1987).

The emission is thought to be produced in a flattened circumstellar envelope[1] of ionised gas extending to some 5–15 stellar radii. Much effort has gone into trying to understand how the extended circumstellar envelope is formed and how it is maintained (Plavec 1976). An important way of studying the envelopes around Be stars is by measuring the degree to which the light from these stars is polarised. Indeed, the presence of intrinsic polarisation in Be stars has provided compelling evidence for the disk-like nature of the circumstellar envelopes (Coyne 1976a). Furthermore, our understanding of the physical conditions inside the envelopes has been enhanced by studying the wavelength dependence of the continuum polarisation (Coyne 1976a; Coyne and McLean 1982). Since the mid-1970's, studies of the variations of polarisation across spectral features have proven particularly valuable in probing the dynamics, expecially the rotational and expansion velocities, of the gas in Be star envelopes (Coyne and McLean 1982).

4.1.2 The Be Phenomenon

The Be phenomenon represents one of a number of transient phases exhibited by stars of this type (Underhill and Doazan 1982; Dachs 1987). A Be star may undergo, in any order, transitions between the normal B, shell and Be phases. Each phase is distinguished by its own characteristic line spectrum. The Be phase is usually characterised by emission lines with (and sometimes without) shallow central depressions. The shell phase is identified by the presence of very deep, sharp absorption cores in the lines of hydrogen and ionised metals (e.g. Fe II, Ti II, Cr II) where usually the lowest Balmer and some metallic lines are also bordered by emission wings. (Such stars are normally referred to as shell stars in the literature.) It is also not uncommon for Be or shell stars to lose their emission or shell features completely and assume normal B phase characteristics. Transitions from one phase to another are gradual and can take anywhere from a few days to decades (Underhill and Doazan 1982). Following the example of Kitchin (1982), in this thesis, we do not distinguish between Be and shell phases but consider them to be different aspects of the same phenomenon.

The origin of the emission lines is attributed to recombination processes in a cool circumstellar envelope, the gas in which is ionised by the UV radiation of the star. Typical

[1]In this thesis, we use the term envelope to denote the outer regions of Be stars where the emission lines are produced.

electron densities of the envelopes are on the order of 10^{11}–10^{13} cm^{-3} (Underhill and Doazan 1982), and the masses of the envelopes range from 10^{-10}–10^{-8} $M_\odot$ (Baade 1987). The presence of Fe II implies electron temperatures of $\sim 10^4$ K. The intensities of the emission lines suggest that the envelopes in which they are formed must be extensive ($\sim$5–15 $R_\star$); the small displacements of the lines in the visible spectrum indicate low expansion velocities of the gas.

In contrast, far-UV observations indicate the presence of superionized regions with electron temperatures of $\sim 10^5$ K (Underhill and Doazan 1982). These superionized regions exhibit high expansion velocities which generally exceed the escape velocity at the star's photosphere and seem to imply the existence of a mass flux from the star (Doazan 1987; Dachs 1987). The mass flux in Be stars is highly variable; the strong variability might be a condition for the formation of the circumstellar envelopes (Underhill and Doazan 1982).

Besides B–Be phase transitions, Be stars frequently exhibit irregular or quasi-periodic variations in their emission-line profiles. Variations of V/R, the ratio of the strengths of the violet and red emission peaks, are common in Be stars with double-peaked emission lines. The timescales for V/R variations are of the order of years to decades (Dachs 1987).

Be stars may also display rapid periodic variations in the profiles of some of their underlying absorption lines. There is growing evidence that these variations are very common, and perhaps universal, among the early to mid B-type stars (Penrod 1986, 1987; Baade 1987). The variations can take either one or both of the following forms: (1) changes in the width and asymmetry of the absorption line; (2) several quasi-emission or absorption bumps travelling from blue to red across the line profile. Several models have been suggested to explain the line-profile variations such as nonradial pulsation (NRP), "spots" or "spokes" carried across the stellar disk by rotation, and binarity. The favoured explanation is NRP. Conceptually, NRP can be thought of as waves travelling around the equator of a star; the form of these waves is described by spherical harmonics. The mode of oscillation is specified by the quantum numbers, ℓ and m. In practice, sectorial modes ($\ell = |m|$), which divide the star into longitudinal strips each strip moving out of phase with its neighbours, have been found to best reproduce the line-profile variations (Walker 1991). A review of the theoretical aspects of NRP can be found in the book by Unno *et al.* (1989; and references therein).

In addition to line variability, many Be stars exhibit rapid photometric variations with periods of the order of fractions of a day or days; the amplitudes of the variations are small, typically 0^m01 to 0^m1 (Percy 1987). These rapid photometric variations have also been attributed to NRP (Percy 1987). Longer-term variations are also observed in Be stars and usually accompany high-amplitude changes in the line spectrum as well as phase transitions (Underhill and Doazan 1982).

Struve (1931) was the first to suggest a model for the Be phenomenon. In this model, the emission lines arise in a gaseous equatorial ring formed by the ejection of matter from a rapidly rotating star. It was implicitly assumed that all Be stars are rotating at their critical velocity. Although in general Be stars rotate faster than normal B stars, the rotational velocities of most Be stars do not approach the critical velocities required for mass ejection. In fact the largest observed $v \sin i$ is 400 km s^{-1}. Moreover, rotation alone is incapable of ejecting matter to large enough distances for the formation of the envelope (Underhill and Doazan 1982). Thus, later models have usually incorporated a mechanism for producing a mass flux from the star in addition to stellar rotation.

Recently, it has been suggested that NRP could provide the additional energy required to power a Be outburst (Penrod 1986, 1987). In this interpretation, low-ℓ pulsation modes produce shock waves which dramatically increase the scale height of the atmosphere such that, combined with the forces due to radiation pressure and rotation, material is thrown off the outer photosphere into a circumstellar disk. Wilson (1986) and Osaki (1986) have also discussed possible mechanisms for a generating a Be outburst from NRP.

Other models of note are the stellar wind model (Marlborough 1987; and references therein) in which the circumstellar envelope is formed by a radiation-driven rotationally distorted wind; the binary model (Kriz and Harmanec 1975; Harmanec 1982, 1987) in which the envelope is the result of mass accretion from a close companion filling its inner Lagrangian surface; and the magnetic-loop model (Underhill and Fahey 1984; Underhill 1987) in which the disk arises from "plumes" of plasma supported by closed magnetic structures located around the equatorial regions of the star, while plasma streams, along open magnetic field lines, form an expanding spiral as a result of rotation of the star.

4.1.3 Past Polarisation Studies of Be Stars

Polarisation studies of Be stars have contributed significantly to our understanding of the extended envelopes about these stars. The intrinsic polarisation of Be stars was first discovered by Behr (1959) because of temporal polarisation variations in the star γ Cas. This was followed by similar detections in χ Oph (Shakhovskoj 1962) and other Be stars (Shakhovskoj 1964; Coyne and Gehrels 1967). Subsequent polarimetric surveys have shown that about 50% of Be stars are intrinsically polarised (Serkowski 1970; Poeckert, Bastien and Landstreet 1979). The degree of continuum polarisation in the visible region of the spectrum of most Be stars is about 1% and never exceeds 2% (Underhill and Doazan 1982).

The intrinsic polarisation of the light from Be stars has a characteristic wavelength dependence which is distinct from that observed for interstellar polarisation. Serkowski (1968) first noticed that the polarisation in the emission-line stars decreases much more strongly (in the UV spectrum) across the Balmer limit than is the case with the interstellar polarisation. Coyne and Kruczewski (1969) later showed that the polarisation rises longward of the Paschen limit in a manner that is also unlike interstellar polarisation.[2] The wavelength dependence of the polarisation has provided valuable insight into the processes occuring in the Be star envelopes.

It is generally accepted that the intrinsic polarisation in Be stars is caused by the scattering of stellar radiation from free electrons in an extended envelope which is not spherically symmetric with respect to the observer.[3] This interpretation was first put forward by Shakhovskoj (1964) and Ruciński (1966, 1967) to explain the intrinsic polarisation of the eclipsing binary β Lyrae and later independently proposed by Coyne and Kruszewski (1969) to explain the polarisation of Be stars. In order to account for the wavelength dependence of the polarisation, Coyne and Kruszewski (1969) also proposed that the otherwise wavelength-independent polarisation produced by electron scattering could be modified by continuous absorption (before and after scattering) by partly ionised hydrogen in the envelope. In their model, hydrogen absorption and electron scattering are

[2]Examples of polarisation curves for Be stars may be found in Coyne and Kruczewski (1968) and Poeckert *et al.* (1979).

[3]The photosphere of a rotationally distorted star does not produce polarisation greater than 0.1% and therefore cannot be entirely responsible for the polarisation observed in Be stars (Nagirner 1962; Collins 1970; Ruciński 1970).

important sources of opacity, but at some wavelengths absorption is the dominant opacity while at other wavelengths electron scattering opacity dominates. Shortward of the Balmer limit, absorption dominates the electron scattering opacity such that the decrease in polarisation across the Balmer limit to shorter wavelengths is an inverse function of the bound-free hydrogen opacity at those wavelengths (Underhill and Doazan 1982).

More complex models of the intrinsic polarisation of Be stars have since been developed (Haisch and Cassinelli 1976; Capps, Coyne and Dyck 1973; Coyne and McLean 1975; Coyne and Vrba 1976; Poeckert and Marlborough 1977, 1978a, 1978b; Jones 1979). Such models usually assume a disk-shaped geometry[4] and include both bound-free and free-free processes.[5] In these models, the direction of the net polarisation is parallel to the polar axis of the star. Reviews of the various models may be found in Coyne (1976a) and Underhill and Doazan (1982).

Emission and absorption processes in the Balmer lines of Be stars modify the wavelength dependence of polarisation inside the lines; thus the polarisation profiles of the emission lines serve as further (independent) constraints on the models of Be stars (Coyne and McLean 1982). A decrease in polarisation across the Hβ emission feature in ζ Tau was first discovered by Serkowski as reported in Zellner and Serkowski (1972). Similar detections were announced by Clarke and McLean (1974a) at the IAU colloquium on photopolarimetry in 1972. Numerous studies have since verified those preliminary results. They are reviewed in Coyne (1976a), Coyne and McLean (1982) and only cited here: Clarke and McLean (1974b, 1975, 1976); Hayes and Illing (1974); Hayes (1975); Coyne (1974, 1976b); Coyne and McLean (1975); Poeckert (1975); Poeckert and Marlborough (1976, 1977, 1978a); McLean *et al.* (1979); McLean and Clarke (1976, 1979); and Clarke and Brooks (1984). With the exception of McLean *et al.* (1979), all of the measurements have been made using narrow-band (typically, 2–26 Å) photopolarimetric techniques.

From the early observations, the decrease in polarisation observed in the lower Balmer emission lines was found, to a first approximation, to vary inversely with the total intensity I of the emission line [i.e., $P_L = P_C/I$, where P_L and P_C are, respectively, the line

[4]Haisch and Cassinelli (1976) found that very flattened, disk-shaped envelopes are required to produce the observed levels of continuum polarisation when absorption is taken into account.

[5]Capps *et al.* (1973) showed that unpolarised free-free emission from the disk is required to account for the rapid decrease in polarisation between 0.9 and 2.2 μm.

polarisation and adjacent continuum polarisation] (cf. Coyne 1976a; McLean and Clarke 1976). This decrease was attributed to dilution of the continuum polarisation by the addition of unpolarised emission in the line[6] (Clarke and McLean 1974; Poeckert 1975).

This interpretation however appears to be too simplistic for some stars. For example, polarimetric measurements across the Hα line of γ Cas have shown that the polarisation in the blue wing of the line was smaller (Poeckert 1975; Mclean and Clarke 1976) than expected if the reduced polarisation was caused solely by the addition of unpolarised emission flux. Anomalous polarisation changes have also been reported for ϕ Per where the emission flux in Hα has been estimated to be about 0.5% polarised (Coyne and McLean 1975), and for ζ Tau where an *increase* in polarisation from the continuum value has been detected (McLean and Clarke 1976).

The highest resolution (0.45 Å) polarimetric observations (prior to this thesis) have been made by McLean *et al.* (1979) with a Digicon echelle spectropolarimeter. They measured the polarisation across the Hβ line of Be stars γ Cas and ϕ Per. Their data revealed variations in the line polarisation which had previously gone undetected due to the poor resolution of the earlier studies. The line polarisation was generally characterised by a systematic decrease in the polarisation (from the continuum value) toward the center of the line accompanied by an increase at the line center. There was also slight evidence in their data for changes in the position angle of the polarisation. McLean *et al.* (1979) pointed out that their results could not be explained solely in terms of dilution by unpolarised line emission, and suggested that absorption also plays an important role in determining the polarisation in the line profiles of Be stars.

Polarisation studies also offer an independent way of investigating the possible sources of the line profile variations observed in many Be stars (cf. Section 4.1.2). If NRPs are the source of these variations, then it should be possible to observe changes in the intrinsic polarisation of the star and these changes should correlate with the periods of the line profile variations[7] (Odell 1979; Stamford and Watson 1980). Short-term polarimetric variations, of the order of days or fractions of a day, have been reported by a number of authors (e.g.

[6]The continuum polarisation is produced in the denser regions closer to the star ($\lesssim 3$ R_*; Poeckert and Marlborough 1978a); the emission flux is produced in the outer regions where it is less scattered and therefore less polarised.

[7]NRPs distort the star from its spherical shape. Therefore, in the integrated light of the star, there should be a net polarisation.

Poeckert 1975; Clarke and McLean 1976; Poeckert and Marlborough 1978a; Poeckert *et al.* 1979). However, most attempts to find a correlation between the polarisation variations of Be stars (and other stars suspected of being nonradial pulsators) and their line-profile variations have thus far either failed or been inconclusive (e.g. Clarke 1986; Gies and McDavid 1987). Polarimetric variations consistent with a nonradial ($\ell = 2$) mode have been reported by Odell and Tapia (1981) and Odell (1981). All of these studies relied on wide-band (UBV) polarimetry.

In fact, with the exception of McLean *et al.* (1979), none of the studies of Be stars mentioned above has employed *spectropolarimetry*. Therefore, using our polarisation analyser and a CCD detector, we obtained moderate resolution (0.15 Å), high S/N (500–1000) spectra to investigate polarisation effects associated with two phenomena observed in Be stars:

1. We present a first attempt using spectroscopic techniques to measure excess polarisation associated with the line profile variations of OB stars. The prime candidates for this program were ζ Oph and ϵ Per, which display the largest amplitude variations ($\sim 1\%$) known among the OB stars.

2. We also observed three intrinsically polarised stars γ Cas, ϕ Per and 28 Cyg to investigate the polarisation effects across their Hβ emission lines in order to studying the nature of the extended circumstellar envelopes about these stars.

4.2 Observations

Table 4.1 lists the line profile variables and emission-line stars observed, their spectral types, visual magnitudes, $v \sin i$, NRP mode, the time separation between individual subfeatures (Δt),[8] intrinsic polarisation in the B band and the angle of polarisation. For the line profile variables, information regarding the mode and Δt were obtained from the given reference. We have also provided the reference from which the polarisation parameters were obtained.

All of the polarised spectra presented in this chapter were obtained with the UBC/DAO polarisation analyser described in Chapter 2 and the 488 nm beamsplitter cube. The ob-

[8] Δt has alternatively been refered to as the "period" of the variations by Gies and Kullavanijaya (1988). In this thesis, we use the notation of Walker *et al.* (1987).

Table 4.1: Program Stars for Be Star Polarisation Study

HD	Star	Spectral Type	V	$v \sin i$ (km s^{-1})	ℓ	δt (hrs)	P_B[c] (%)	ϕ_p	Reference
Line-profile Variables									
149757.....	ζ Oph	O9.5Ve[a]	2.56[a]	390[b]	8	2–3	...	...	Vogt and Penrod
24760.....	ϵ Per	B0.5V	2.89	153	3,4,5,6	4.5,3.8,3.0,2.3	...	...	Gies and Kullavanijaya (1988)
Emission-line Stars									
10516.....	ϕ Per	B2Vep	4.07	450	...	...	2.0	26°	Poeckert *et al.* (1979)
5394.....	γ Cas	B0IVe	2.47	300	...	...	0.8	105°	McLean *et al.* (1979)
191610.....	28 Cyg	B2.5Ve	4.93	310	...	...	0.5	180°	Coyne (1975)

a Hoffleit and Jaschek 1982

b Hutching and Stoeckley 1977

c Continuum polarisation measured with Johnson B filter

servations were made using the DAO 1.83-m telescope and Cassegrain spectrograph in six observing runs between June 1990 and July 1991. The 1800 lines mm^{-1} grating, blazed at 5000 Å, was used in the first order and gave a reciprocal dispersion of 10 Å mm^{-1}. The spectra were centred at Hβ λ4861 and some included He II λ4921.

Each star was monitored in a continuous series of integrations with the analyser rotated in position angle between each integration. Spectra of ζ Oph obtained in the June 1990 observing run were recorded with the Reticon detector. The integration time for each spectrum was 20 min; the mean S/N per diode was 600. The resolution of the data was 0.15 Å $diode^{-1}$. An RCA CCD (620×1024) detector was employed during the subsequent observing runs in September 1990 and January 1991. It gave a resolution of 0.15 Å $diode^{-1}$. Because of the low noise penalty per read out of the CCD, the integration times of the spectra were reduced, ranging from 20s–40s. We took advantage of on-chip binning to improve the signal in each spectral element without increasing the read out noise. The spectra were aligned along the columns of the CCD and were binned only in the direction cross-wise to the dispersion into one (September data) or three or more (subsequent data) columns.

A complete journal of the observations is presented in Table 4.2, listing typical integration times, mean S/N per diode, the number of spectra and the length (in hours) of each time series.

Spectra obtained in 1990 were taken with the temporary analyser mount mentioned in Section 2.4.1. Position angles were selected manually using five detents located every 40° at 180°, 140°, 100°, 60°, 20°. Rotation of the analyser was alternated between clockwise and counter-clockwise directions (as seen projected onto the sky), with exception of the September 1990 run. This was done in order to minimise spurious polarisation detections caused by systematic zero-point drifts in wavelength due to spectrograph flexure and the redward movement of the travelling subfeatures across the line profiles of the program stars (see Section 4.5.1). In September 1990, the analyser was always rotated in the clockwise direction. Also, three spectra at each rotation of the analyser were obtained in order to limit the amount of time spent in overhead [i.e. in reading out the CCD (20 s per read out) and rotating the analyser]. The median was taken of each set of three spectra to improve the S/N and reduce the effects of cosmic-ray spikes. The observing sequence finally adopted for the observing run in January 1991 was as follows: (1) one polarised

Table 4.2: Summary of Be Star Observations

Star	Date (UT)	t^a (hr)	Detector	N^b	Exposure Time (s)	S/N	Spectral Region	θ
ζ Oph.....	15 Jun 1990	3	DAO Reticon	9	1200	600	Hβ λ4861	20°, 60°, 100°, 140°, 180°
	15 Jun 1990[c]	3	UBC Reticon	14	900	600	Hβ, He I λ6678	—
ϵ Per.....	05 Jan 1991	7	RCA CCD	336	30	300	Hβ, He I λ4921	0°, 45°, 90°, 135°
ϕ Per.....	25 Sep 1990	$2\frac{1}{2}$	RCA CCD	105	40	280	Hβ λ4861	20°, 60°, 100°, 140°, 180°
γ Cas.....	23 Sep 1990	$4\frac{1}{2}$	RCA CCD	225	20	500	Hβ λ4861	20°, 60°, 100°, 140°, 180°
	24 Sep 1990	5	RCA CCD	255	20	500	Hβ λ4861	20°, 60°, 100°, 140°, 180°
28 Cyg.....	24 Sep 1990	4	RCA CCD	165	40	200	Hβ λ4861	20°, 60°, 100°, 140°, 180°

a) Total time coverage of time series.

b) Number of spectra in time series.

c) Unpolarised data set taken with DAO 1.22-m telescope.

spectrum at each of 0°, 45°, 90°, 135°, was obtained, and (2) the process was repeated in the reverse order, i.e., 135°, 90°, 45°, 0°. The polarisation analyser was operated remotely for these runs.

On one night (15 June 1990 UT), a times series of Reticon spectra was obtained of ζ Oph in natural light using the coudé spectrograph of the DAO 1.22-m telescope with the 1200 lines mm^{-1} grating, blazed at 6000 Å. These observations were timed to coincide with the polarimetric observations at the 1.83-m telescope. The reciprocal dispersion was the same as that used at the 1.83-m telescope, namely, 10 Å mm^{-1}. The spectra were centred at about 6650 Å and included both Hα λ6563 and He I λ6678.

In addition to the program stars, standard stars known to be unpolarised were observed in an identical manner on each night of the observations. These stars are listed in Table 4.3 along with their visual magnitudes, spectral type and the source from which they were taken.

Iron-Argon comparison spectra were recorded approximately every 1/2 hour to 45 min in order to monitor possible wavelength shifts due to spectrograph flexure.

4.3 Data Reduction

The Reticon data were processed following the procedures described in Section 3.3. Reductions of the CCD data were carried out using routines in the software package IRAF (Image Reduction and Analysis Facility). The first task in the reductions was to subtract a bias frame from each data frame. The bias frame was formed from the median of all (usually 9-10) zero-second exposures taken throughout the night. Because the bias level or offset in each frame tends to fluctuate from one exposure to another, individual bias levels, calculated from the overclock pixels and recorded in the image header, were first subtracted from all the frames including the bias frames using the DAO-written task `subocpm`.

No flat-fielding of the data was done, avoiding the unnecessary addition of noise which could undermine the precision of our results. Instead we followed a procedure of forming residual spectra similar to the one carried out in Chapter 3. In this case, however, residual spectra were computed by dividing each spectrum by a mean spectrum (cf. Section 4.5). Besides cancelling the variations in sensitivity between the individual diodes, this method

Table 4.3: Standard Unpolarised Stars for Be Star Polarisation Study

HD	Star	Spectral Type	V	References
127762.....	γ Boo	A7 III	3.03	Appenzeller (1966)
172167.....	α Lyr	A0 Va	0.03	Appenzeller (1966)
432.....	β Cas	F2 III	2.27	Serkowski (1974)
197345.....	α Cyg	A2 Iae	1.25	Clarke and Brooks (1984)

reveals the presence of wavelength-dependent polarisaton in the line profiles.

The spectra were extracted from the two-dimensional CCD spectrum images in one of two ways. Where the spectra had been binned (on-chip) into a single column, only that column was extracted from each spectrum using the IRAF task `toonedspec` in `noao.proto`. The data in three or more column bins were extracted individually using the task `apsum` in `noao.twodspec.apextract`. This task displays the cross-sectional profile of the 2D spectrum and allows the user to define the width of the aperture used in the extraction. The aperture widths, taken to be the width of the profile at half-maximum, were typically 3-4 pixels. The spectra were traced along the center of the profile at various positions on the dispersion axis in order to account for any distortions in the spectra or misalignments of their dispersion axes. The spectra were then extracted by summing (unit weights) the pixels within the apertures at each point along the dispersion axis. The extraction parameters, such as the aperture width and the tracing information, were stored in a database directory. No sky-background subtraction was performed on the data since the spectra were obtained with an image slicer and therefore contain negligible contributions from the sky.

In the case where the data were binned in three or more columns, the residual spectra were formed from the 2D spectrum images *before* being extracted. Because the task `apsum` had difficulty tracing the poorly defined profiles of the residual spectra, the same parameter values defined in the extraction of the spectra corresponding to those residuals were used as defaults in the residual extraction.

The residual spectra formed from the CCD were then rectified using a second-order Legendre polynomial so that their mean intensity levels were equal to one. Second-order cubic splines were used to rectify the Reticon residual spectra.

4.4 Polarisation Analysis

The polarisation data for this analysis consisted of a set (or sets) of residual spectra for each star (each spectrum having been divided by an average spectrum and rectified) obtained at (4–5) different rotations of the analyser (cf. Section 4.2). The analysis of the observations involved computing the differential polarisation ΔP and the position angle ϕ_p at wavelengths λ_i, where $i = 1, 2, \ldots, N$ across a given spectral feature. We have

defined ΔP and ϕ_p by Eqn. 1.5 of Section 1.2 to be

$$I^i_{res}(\theta) = 1 + \Delta P^i \cos[2(\theta^i - {\phi_p}^i)] \tag{4.1}$$

where we have written $I(\theta)/I_{avg}$ (in Eqn. 1.5) as $I_{res}(\theta)$ to denote the rectified residual spectra and P (in Eqn. 1.5) as ΔP to denote the differential measurements (cf. Section 2.3). Here θ takes the values of the position angles of the analyser for which each series of I^i_{res} was obtained.

From Eqn. 4.1, we were able to determine the wavelength dependence of polarisation across a spectral feature and investigate possible changes in the position angle through the line profile. We introduce the terms "differential polarisation (ΔP) spectrum" and "position angle (ϕ_p) spectrum" to describe the wavelength dependence of ΔP and ϕ_p.

Since the number of wavelength points N was in general large (ranging from 500 to 2000), a FORTRAN program was written by the author to calculate ΔP and ϕ_p by least-squares fits to $I^i_{res}(\theta)$ at each point in the given wavelength region. Because the function I^i_{res} depends nonlinearly on θ, the Levenberg-Marquardt least-squares fitting routine `MRQMIN` from Numerical Recipes (Press, Flannery, Teukolsky and Vettering 1986) was used. The intensities $I^i_{res}(\theta)$ were weighted according to σ_i^{-2} in the fit where σ_i is the standard deviation of the i^{th} data point. In our analysis, we assumed that all data points had the same standard deviation, $\sigma_i = \sigma$, and set σ to be the standard deviation measured in the continuum regions of the residual spectra. The uncertainties associated with the fitted parameters were also provided by the least-squares fitting routine (cf. Numerical Recipes).

Like most nonlinear least-squares fitting algorithms, the Levenberg-Marquardt method requires a good intial guess. We calculated the initial parameters using a Fourier series truncated to the first harmonic. Thus,

$$\Delta P = [a_1^2 + b_1^2]^{\frac{1}{2}} \tag{4.2}$$

$$\phi = \frac{1}{2} \arctan(\frac{b_1}{a_1}) \tag{4.3}$$

where

$$a_1 = \frac{2}{\pi} \int_0^\pi I_{res}(\theta) \cos 2\theta \, d\theta \tag{4.4}$$

$$b_1 = \frac{2}{\pi} \int_0^\pi I_{res}(\theta) \sin 2\theta \, d\theta \tag{4.5}$$

and we used the trapezoidal rule to do the numerical integrations.[9] Using these initial parameters, the Levenberg-Marquardt algorithm typically converged in 3–4 iterations.

4.5 Results and Discussion

4.5.1 Differential Linear Polarisation Associated with Line-Profile Variations

4.5.1.1 ζ Oph

The bright O9.5 Ve star, ζ Oph, was the first object investigated for excess polarisation associated with the line-profile variations of the star. It is the prototype of a class of nonradially pulsating stars with rapid rotation ($v \sin i \geq 170$ km s^{-1}; Unno *et al.* 1989). It was the first star in which travelling subfeatures within the absorption lines were detected (Walker, Yang and Fahlman 1979) and displays some of the largest variations known ($\sim$1%) among the OB stars. Since one might expect the size of any polarisation excess to be correlated with the strength of the variations, ζ Oph is probably one of the best candidates for this program.

The time series of polarised spectra of ζ Oph at Hβ is shown in Fig. 4.1. The corresponding analyser position angle is given above and to the left of each spectrum. The spectra have been smoothed by a Gaussian transfer function with a σ value of 0.23 Å. Small variations are just noticeable in the line profiles. These variations are best seen in the residual spectra shown in Fig. 4.2, formed by dividing the individual spectra by the mean of all the spectra in the series. The "bumps" moving across the line profiles are much like those observed by Walker, Yang and Fahlman (1979) and Vogt and Penrod (1983)

[9]The reader may wonder why we did not use a more sophisticated numerical integration algorithm. Initially our choice was for the sake of convenience. Since then, we have become aware that the trapeziodal rule is extremely accurate for periodic data at equally spaced points (modulo the periodicity). This is discussed in more detail by Kahaner, Moler and Nash (1989; p. 162). Because of this requirement for equally spaced points modulo the periodicity, this exceptionally high accuracy is obtained only for the case of ϵ Per and not for any of our other observations.

and are most consistent with the $\ell = |m| = 8$ mode of pulsation.[10]

As a check that any apparent polarisation effect seen in the polarised spectra did not arise from another (time-dependent) variation, we carried out an identical analysis on the unpolarised spectra. The corresponding times series at He I 6678 is shown in Fig. 4.3. Only those spectra whose mid-exposure times coincided with those of the polarised spectra are presented. In some cases, adjacent spectra were averaged in order that their mid-exposure times match more closely the times of the polarised spectra. The residual spectra formed in the same way described above are shown in Fig. 4.4. Despite the striking differences between the two line profiles in Figs. 4.1 and 4.3, their residuals (Figs. 4.2 and 4.4) are remarkably similar.

To compare directly the variations in both lines, the residual spectra were interpolated with a *sinc* function onto the same velocity scale. Rest wavelengths were taken from (Moore 1959). The result of the transformation is shown in Fig. 4.5 where the residuals within a pair of polarised and unpolarised residuals (with corresponding mid-exposure times) are shown superimposed. Some show slight velocity shifts with respect to each other which is due to the fact that the mid-exposure times of the spectra within a pair were not always the same. (The time difference never exceeded five minutes.) Also because the He I line is weaker than Hβ, it is not unexpected that the amplitudes of the subfeatures in the He I line should be correspondingly smaller. Despite the smaller amplitudes, the visibility of the subfeatures is better in the He I line, most probably because of the inverse correlation between the resolution of the bumps and the intrinsic widths of the lines (Kennelly, Walker and Hubeny 1990). Nevertheless, in general, the match between the bump patterns within each pair is very good.

In order to analyse the subfeatures for polarisation using the method of Section 4.4, it was necessary to shift the residual spectra so that the subfeatures were aligned. We used the unpolarised residual spectra for this purpose. To calulate the shifts, the displacements

[10] An approximate value of $|m|$ was calculated from the formula

$$|m| = \frac{2\pi(v \sin i)}{a_0} \Delta t \tag{4.6}$$

(Walker *et al.* 1987) where a_0 is the acceleration of the subfeature at line center and Δt is the average time separation between successive subfeatures. The values of a_0 and Δt were measured from the unpolarised residual spectra in Fig. 4.2 to be 3197 km s^{-1} d^{-1} and 0.1309 d, respectively, and $v \sin i = 379$ km s^{-1} from Unno *et al.* (1989). We obtained $|m| \simeq 6$.

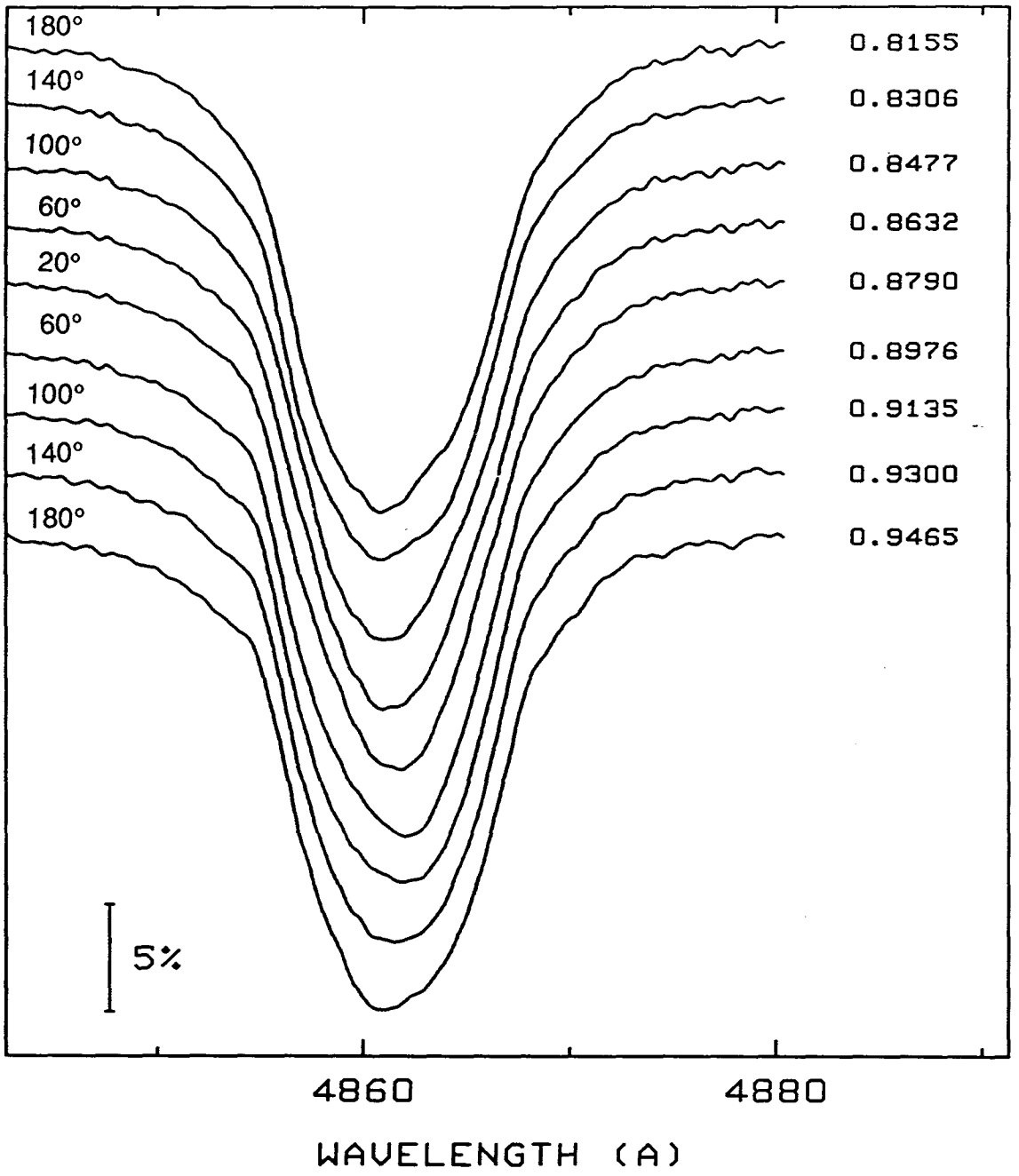

Figure 4.1: Polarised spectral time series of ζ Oph at the Hβ λ4861 line. The analyser position angle is shown above and to the left of each spectrum. The corresponding mid-exposure time in fractions of a day from the barycentric JD 2,448,057 is given to the right of each spectrum. The intensity scale with respect to the continuum is indicated by the error bar.

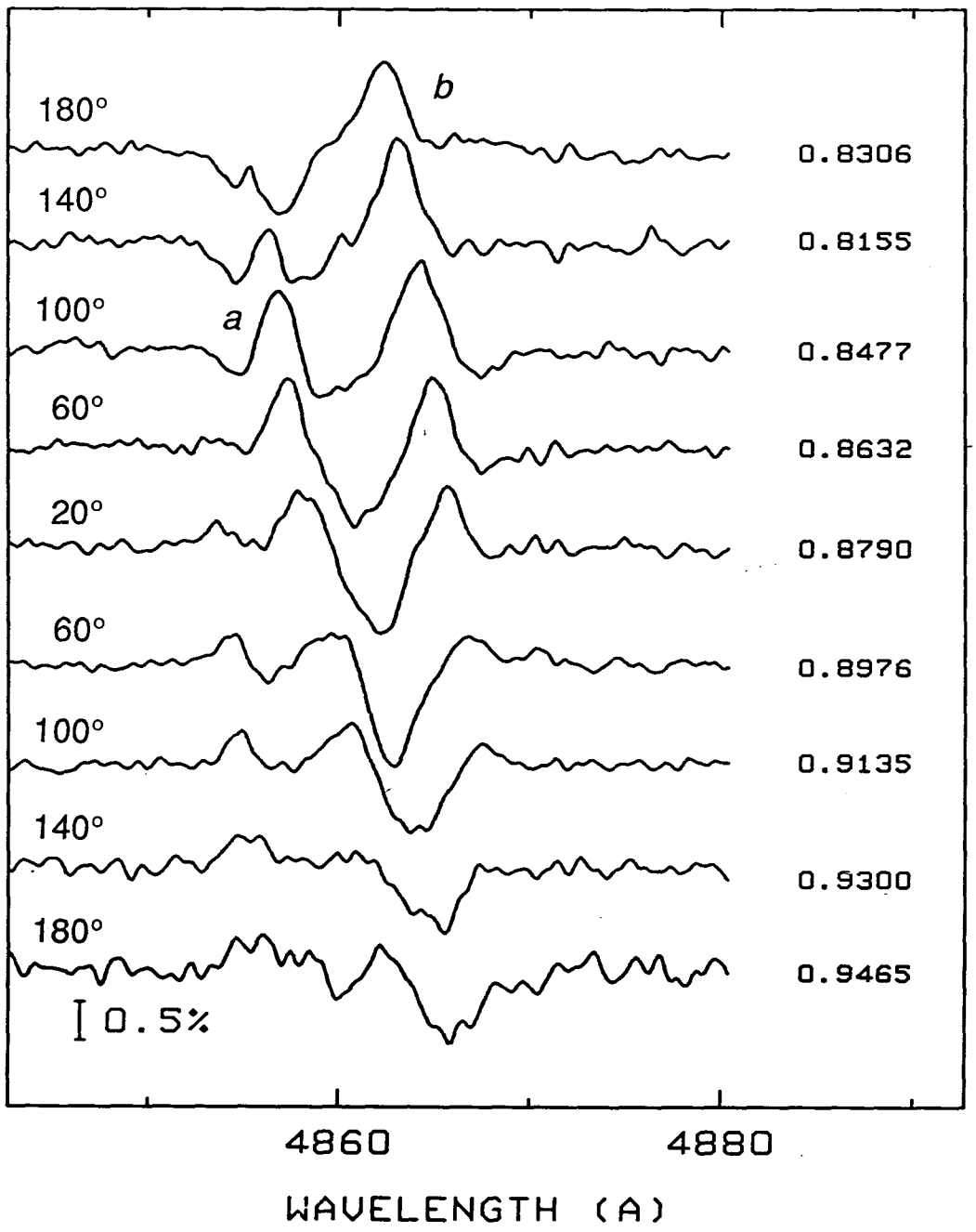

Figure 4.2: Polarised residual time series of ζ Oph at the Hβ λ4861 line formed by dividing the individual spectra in Fig. 4.1 by their mean spectrum.

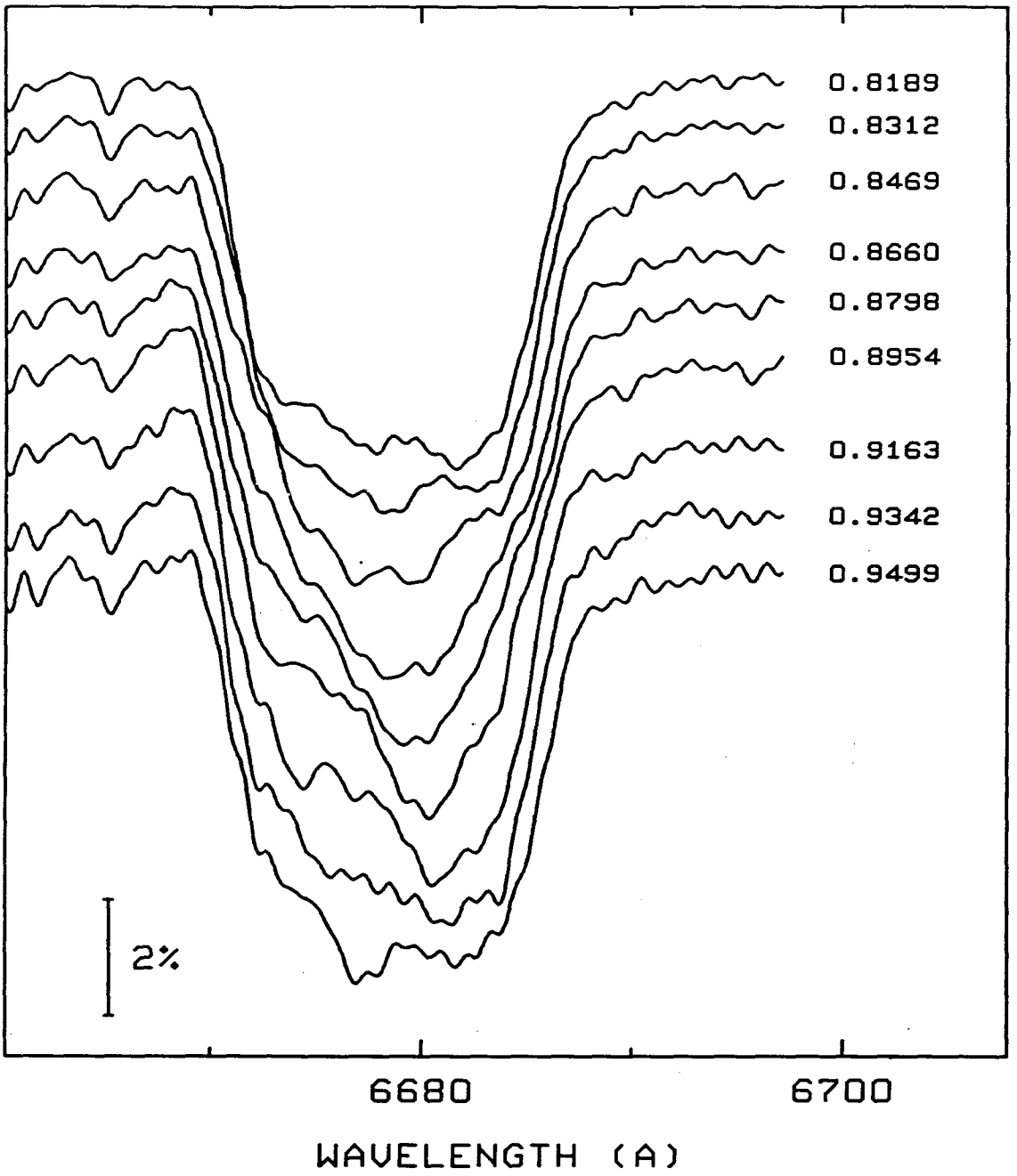

Figure 4.3: Unpolarised spectral time series of ζ Oph at the He I λ6678 line. The corresponding midexposure time in fractions of a day from the barycentric JD 2,448,057 is given to the right of each spectrum. The intensity scale with respect to the continuum is indicated by the error bar.

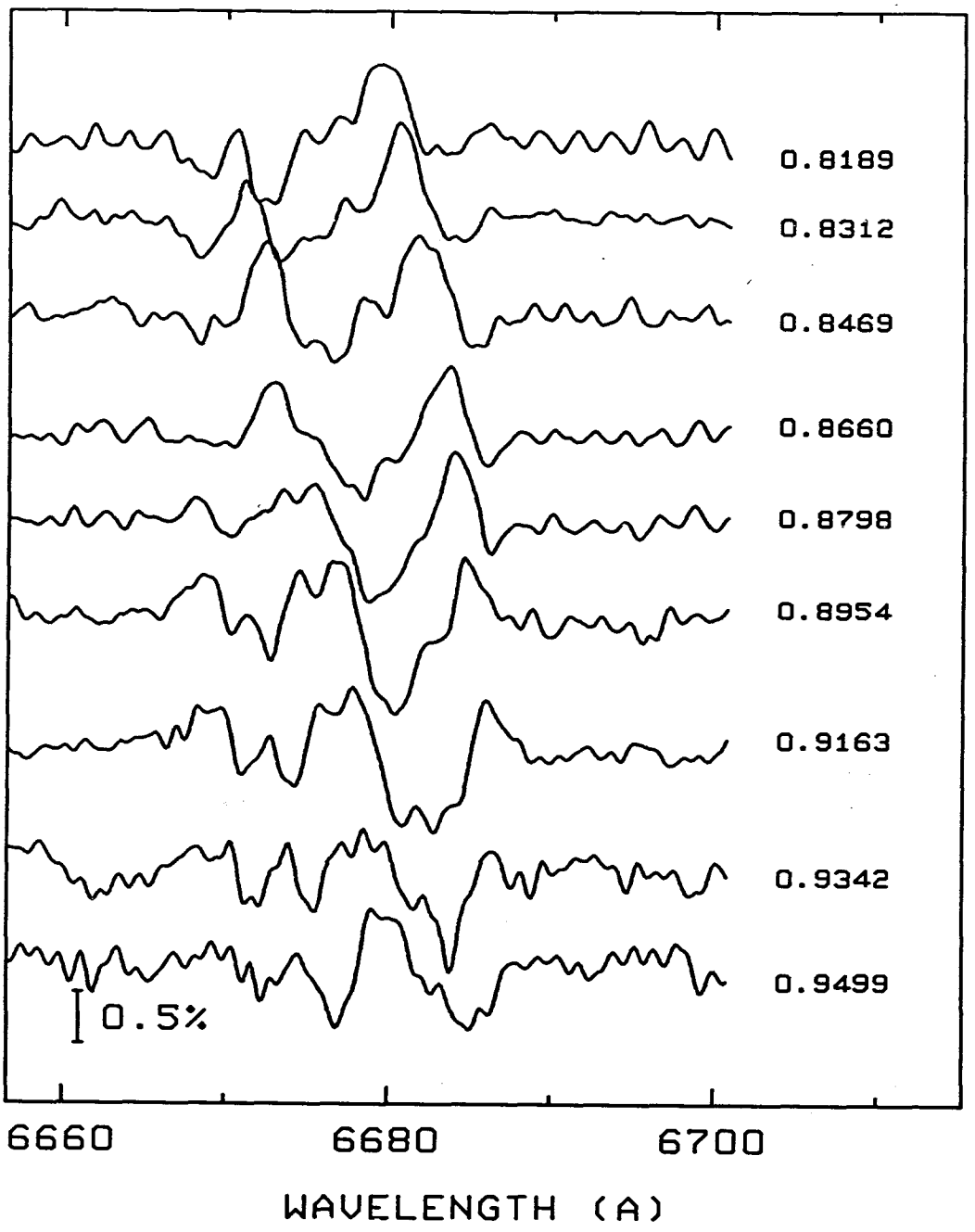

Figure 4.4: Unpolarised residual time series of ζ Oph at the He I λ6678 line formed by dividing the individual spectra in Fig. 4.3 by the their mean spectrum.

(in velocity) of the bumps from the line center were measured as a function of time and a line fitted to the points corresponding to each bump. Taking the average shift derived from the two fits, the residuals were then shifted according to their respective mid-exposure times. As shown in Fig. 4.6, besides aligning the bumps within each series of polarised and unpolarised residuals, this step also improved the alignment within the residual pairs whose mid-exposure times did not exactly coincide.

We applied the polarisation analysis outlined in Section 4.4 to the both polarised and unpolarised datasets. In both cases, the data were divided into two subsets, one containing the first five residual spectra and the other containing the last five, so that the middle spectrum was included in both sets. In this way the subset containing the polarised data comprised one complete sequence of residuals taken at the five position angles of the analyser.

The results for the polarised and unpolarised datasets are compiled in Figs. 4.7 and 4.8, respectively. The results of the first subsets are plotted in Figs. 4.7*a* and 4.8*a* and those of the second subsets are shown in Figs. 4.7*b* and 4.8*b*. In the middle and upper panels of each of those figures are plotted the differential polarisation (ΔP) spectrum and the position angle (ϕ_p) spectrum in the region of the line profile. Typical 2σ errors in ΔP and ϕ_p from the least-squares fit, at each wavelength point are given by the error bars in the respective panels. The middle residual spectrum from each subset (corresponding to 100°) is also plotted in the lower panel of each figure for comparison.

There is evidence for pronounced structure in the ΔP spectra of Figs. 4.7*a* and *b* that appears to be strongly correlated with the bump pattern in the Hβ profile. However, we feel, in view of the significant scatter in both ΔP and ϕ_p in the region of the line profile, that it is unlikely that this structure represents an actual polarisation effect. In fact, the structure in ΔP is almost certainly caused by systematic (time-dependent) variations in the subfeatures of the line profile.

Besides their systematic movement across the line profiles, the subfeatures also display other variations which could complicate the polarisation analysis. As a bump emerges from, or disappears into, a line wing, there is a systematic increase, or decrease, in its amplitude (cf. Unno *et al.* 1989). An example of type of behaviour is shown by subfeature *b* in Fig. 4.2. Furthermore, it is not unusual for individual subfeatures to decay in amplitude or suddenly disappear as they traverse the line profile (Yang, Ninkov and

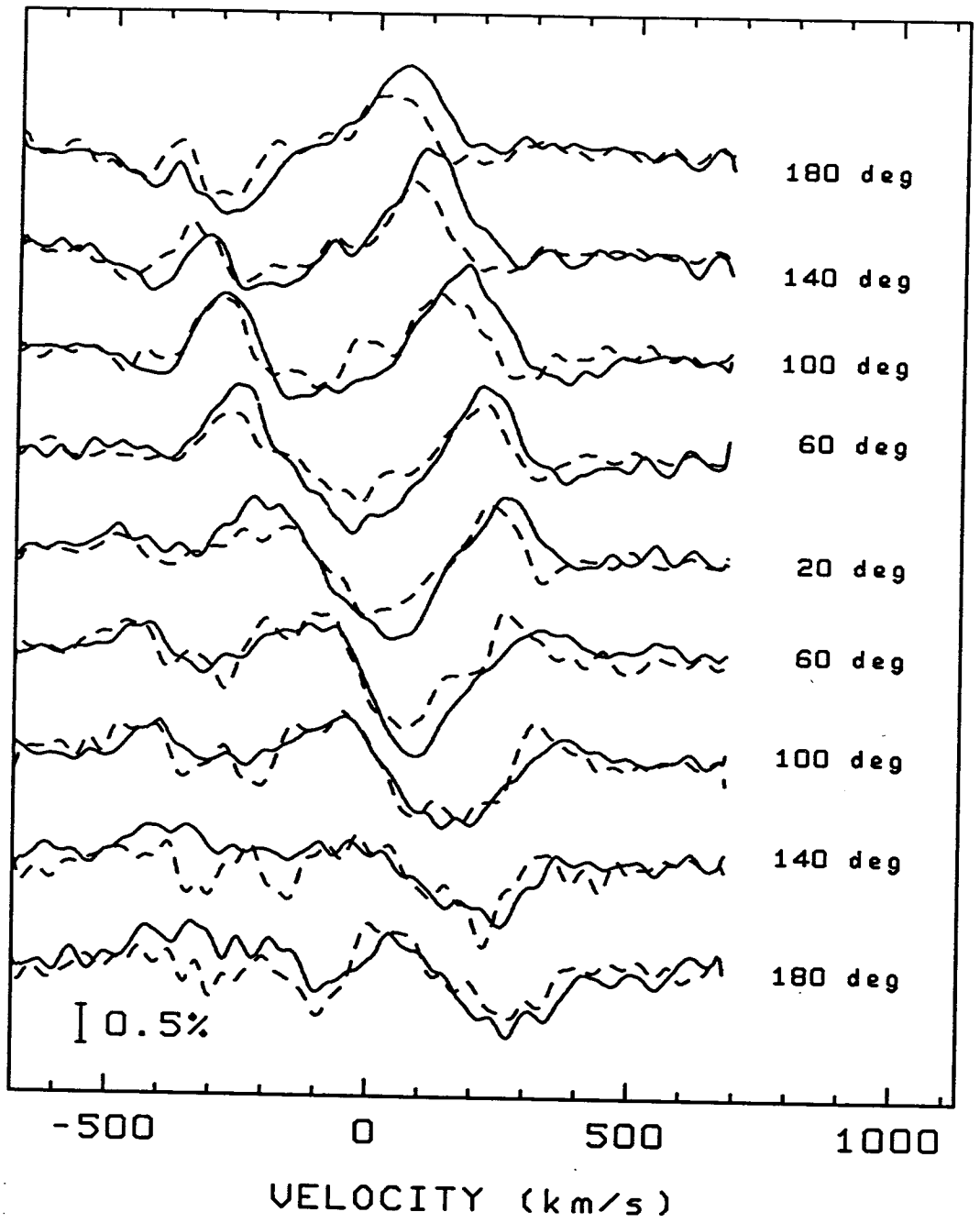

Figure 4.5: Superposition of polarised and unpolarised residual time series of ζ Oph at Hβ (Fig. 4.2) and He I λ6678 (Fig. 4.4). The residual spectra have been interpolated onto the same velocity scale. The analyser position angle corresponding to the polarised residuals is given to the right of each pair of residual spectra.

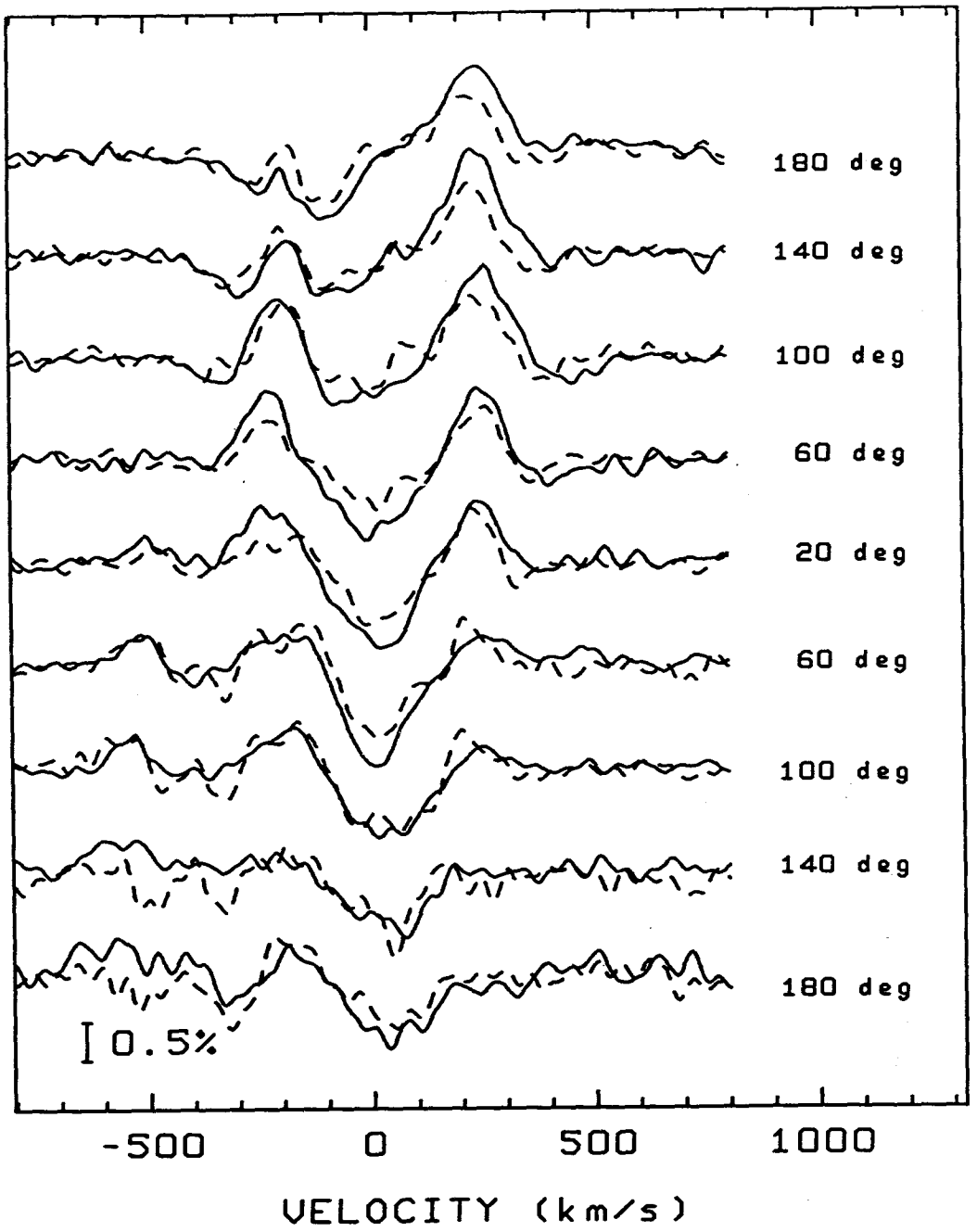

Figure 4.6: As Fig. 4.5, but with the subfeatures aligned.

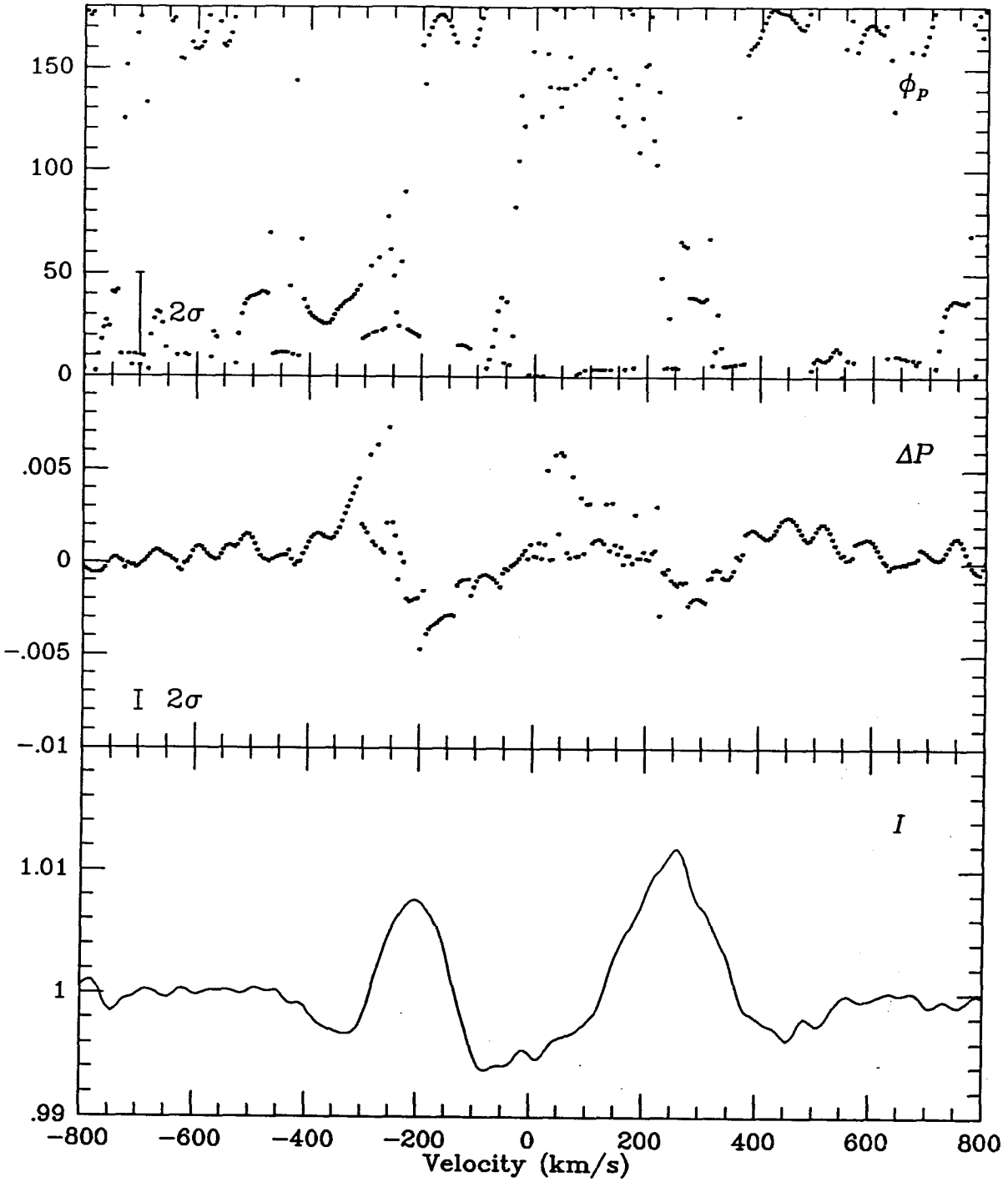

Figure 4.7: (*a*) Results of the polarisation analysis of the first five (first subset) polarised residual spectra of Fig. 4.6 for ζ Oph. The differential polarisation (ΔP) spectrum and position angle (ϕ_p) spectrum are plotted in the middle and upper panels respectively. The middle residual spectrum from the first subset (corresponding to 100°) is shown in the lower panel for comparison.

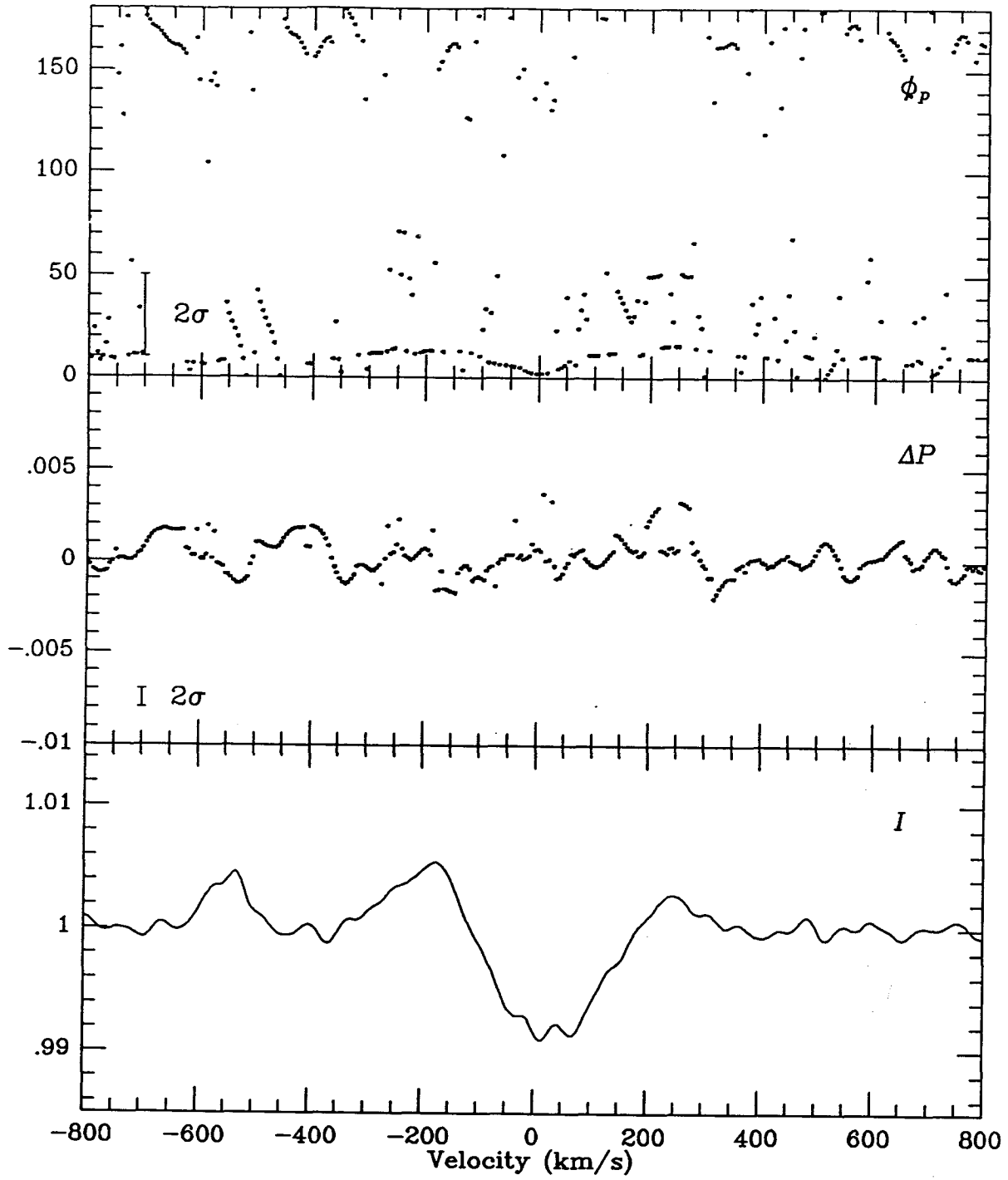

Figure 4.7: (b) Results of the polarisation analysis of the last five (second subset) polarised residual spectra of Fig. 4.6 for ζ Oph. The differential polarisation (ΔP) spectrum and position angle (ϕ_p) spectrum are plotted in the middle and upper panels respectively. The middle residual spectrum from the second subset (corresponding to 100°) is shown in the lower panel for comparison.

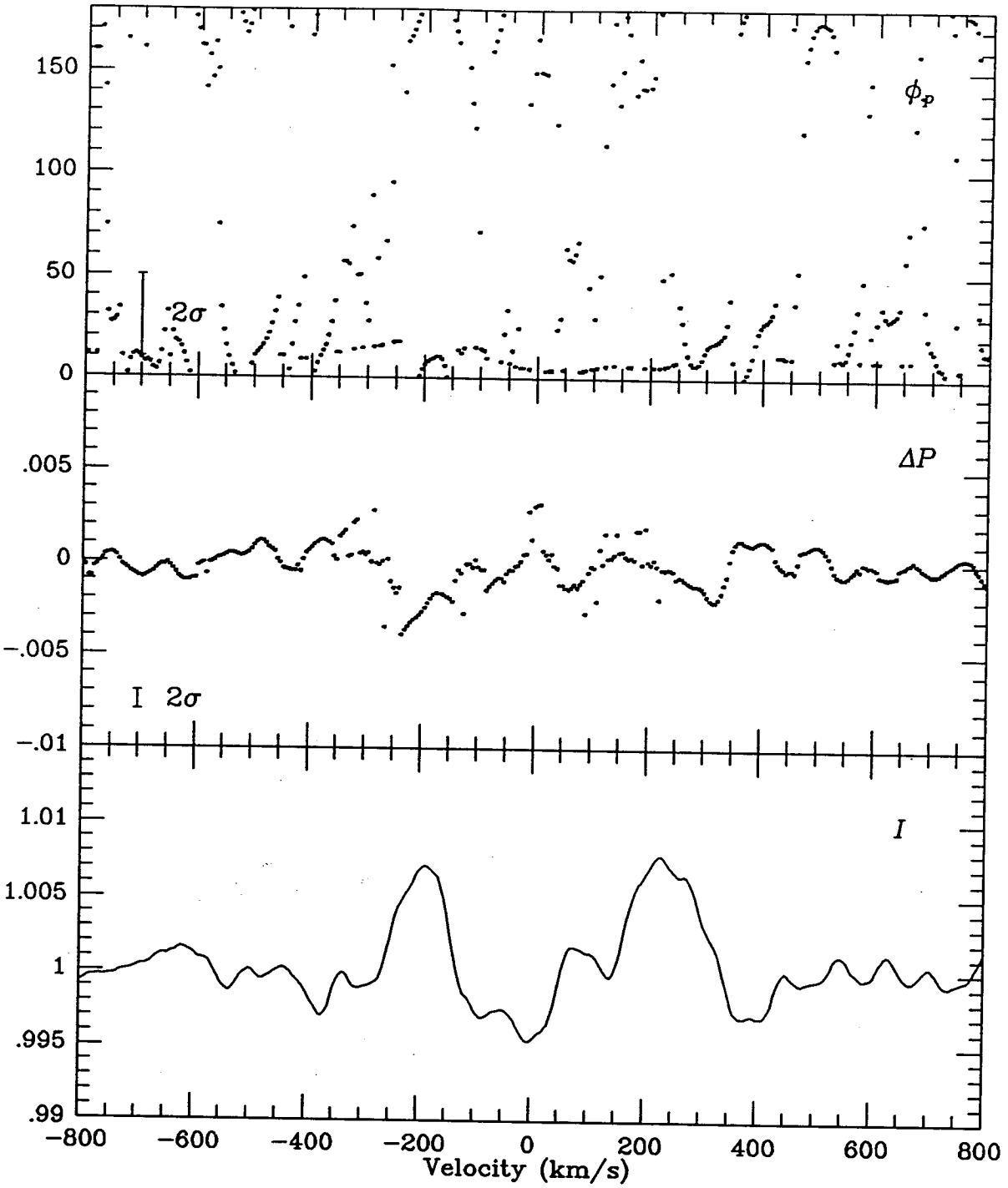

Figure 4.8: (a) Results of the polarisation analysis of the first five (first subset) unpolarised residual spectra of Fig. 4.6 for ζ Oph. The differential polarisation (ΔP) spectrum and position angle (ϕ_p) spectrum are plotted in the middle and upper panels respectively. The middle residual spectrum from the first subset (corresponding to 100°) is shown in the lower panel for comparison.

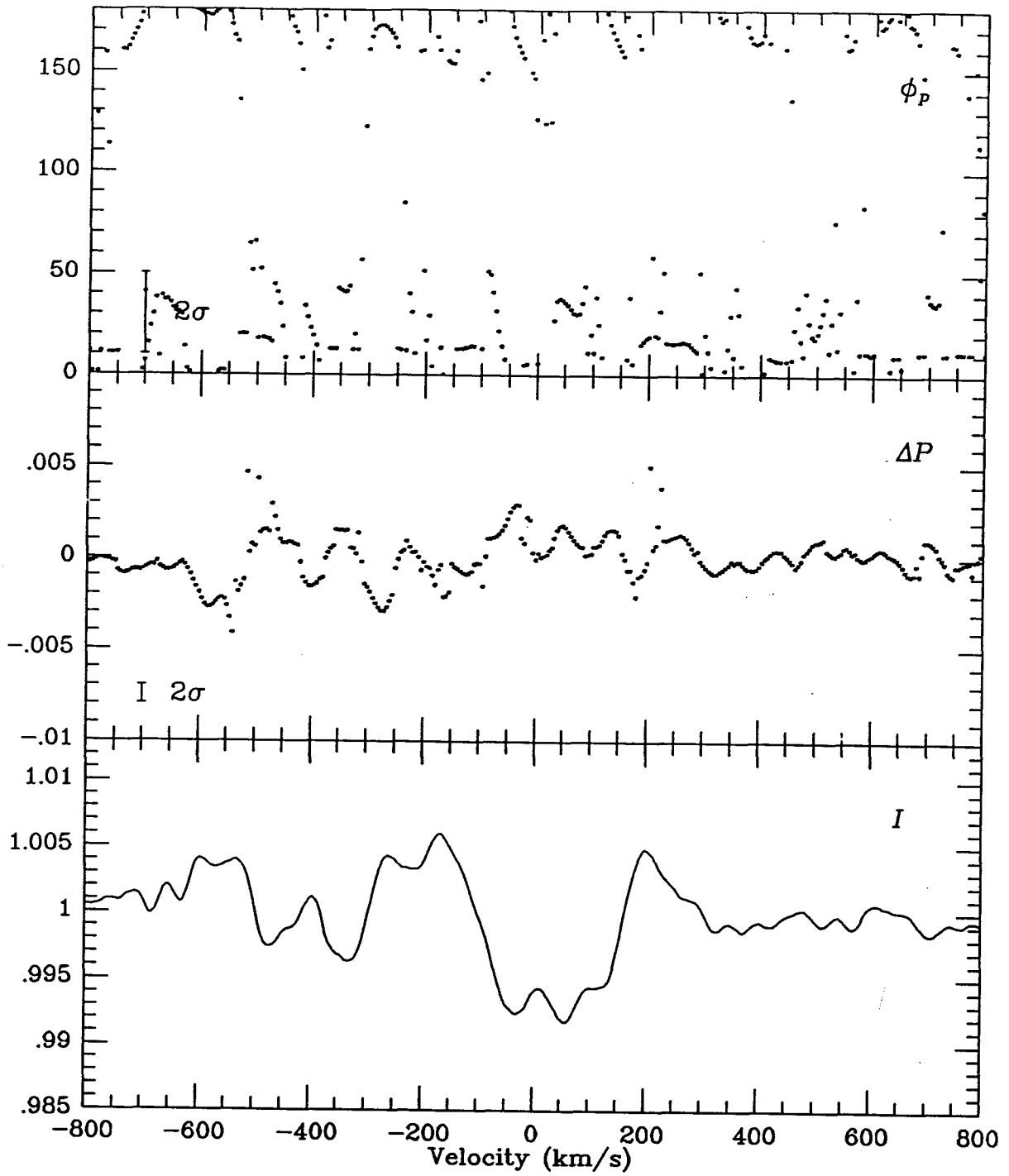

Figure 4.8: (*b*) Results of the polarisation analysis of the last five (second subset) unpolarised residual spectra of Fig. 4.6 for ζ Oph. The differential polarisation (ΔP) spectrum and position angle (ϕ_p) spectrum are plotted in the middle and upper panels respectively. The middle residual spectrum from the second subset (corresponding to 100°) is shown in the lower panel for comparison.

Walker 1988). In fact, the amplitude of subfeature a appears to diminish as it approaches the line center. It is clear from Eqn. 4.1 that the magnitude of these variations will be reflected in ΔP and ϕ_p, producing spurious structure in the both spectra.

Figs. 4.8a and b were generated using the unpolarised dataset and are therefore measures of the systematic variations in the line profile. The same general structure in the ΔP spectrum of Figs 4.7a, b (polarised dataset) was found in Figs. 4.8a, b (unpolarised dataset). The similarity between both figures strongly indicates that the structure observed in Figs 4.7a, b is spurious and arose from systematic changes in the line profile of ζ Oph. This would also explain the significant scatter in both ΔP and ϕ_p.

In an effort to minimise the sytematic effects in the polarised residuals, we subtracted the unpolarised residual spectra from their corresponding polarised residual spectra and repeated the analysis of Section 4.4 on the *differenced* spectra. As shown in Fig. 4.9, some bump pattern remained in those spectra because (as mentioned above) the amplitudes of the bumps were not the same in both line profiles. Analysis of the first and last five differenced spectra revealed no significant structure in the ΔP spectrum of either subset. The results of the analysis are shown in Figs 4.10a and b. The standard deviation from the mean of all the points in ΔP for the first subset is 0.07% and for the second subset is 0.08%. As our final result we combined the ΔP spectra for both subsets. The mean spectrum shows no evidence for polarisation structure associated with the line profile variations of ζ Oph, exceeding the standard deviation of 0.05%.

Notes: A curious feature of the ΔP spectra of Figs. 4.7, 4.8 and 4.10 is the ripple-like structure present (particularly) in the regions outside the line profile. If the analysis of Section. 4.4 is of random noise, then one might expect this scatter to be reflected in ΔP spectrum at the same level. The "ripple" pattern hints at the presence of periodic variations in the residual spectra which is reproduced in ΔP. These variations are most probably artifacts of the geometrical arrangement of the diodes in the Reticon array.

Each diode in the array is read out by one of four video lines; every fourth diode in the array is read out by the same video line. Differences between the gains and zero-points of the video-line amplifiers combine to produce a variety of patterns which repeat every n^{th} diode in the array where n is an integral multiple of four (Walker *et al.* 1985). Although the processing procedures outlined in Section 3.3 were designed to remove such patterns, some low-level pattern usually persists especially if the diode-to-diode variations are not

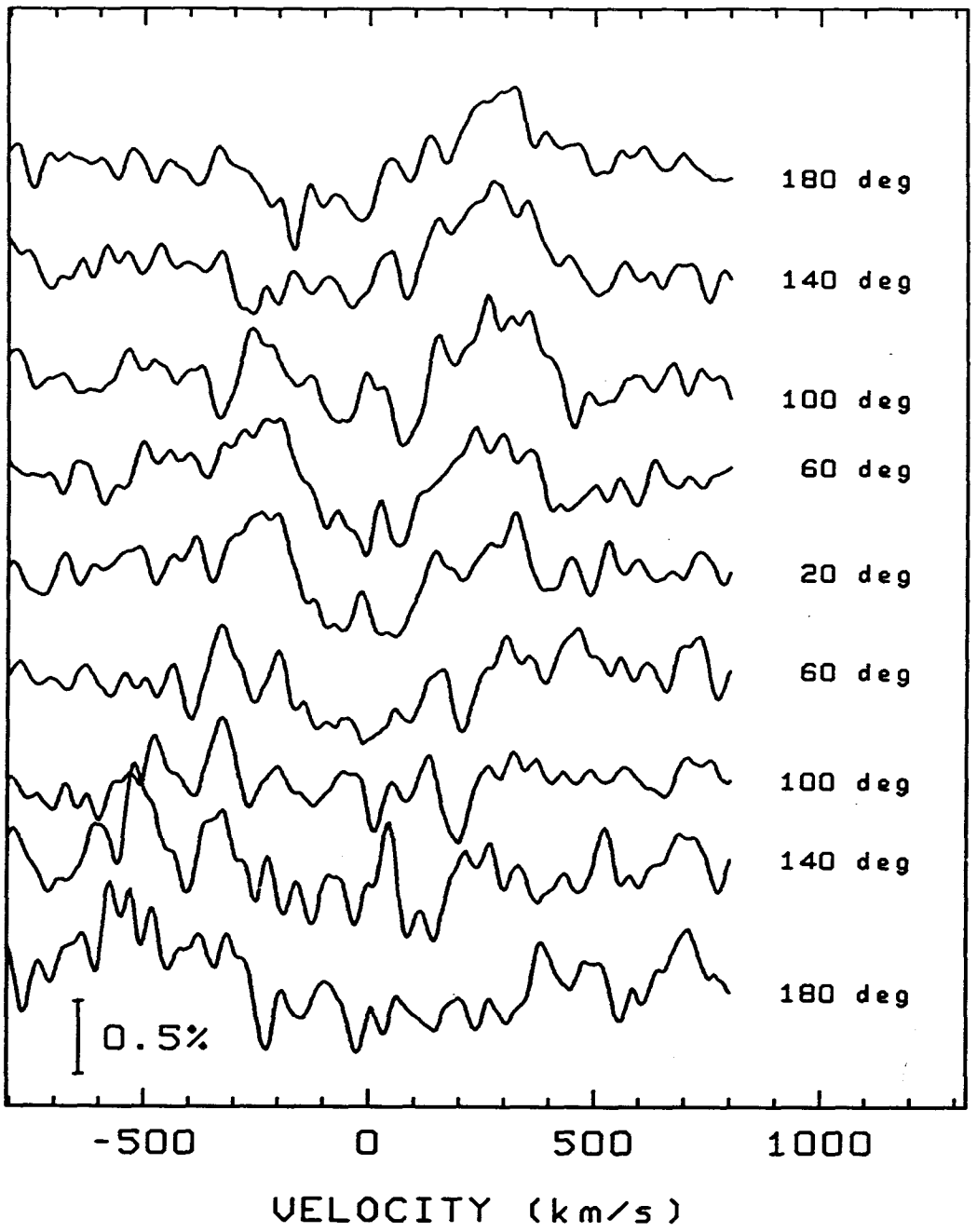

Figure 4.9: Differenced time series formed by subtracting the unpolarised residual spectra from the corresponding polarised residual spectra in Fig. 4.6.

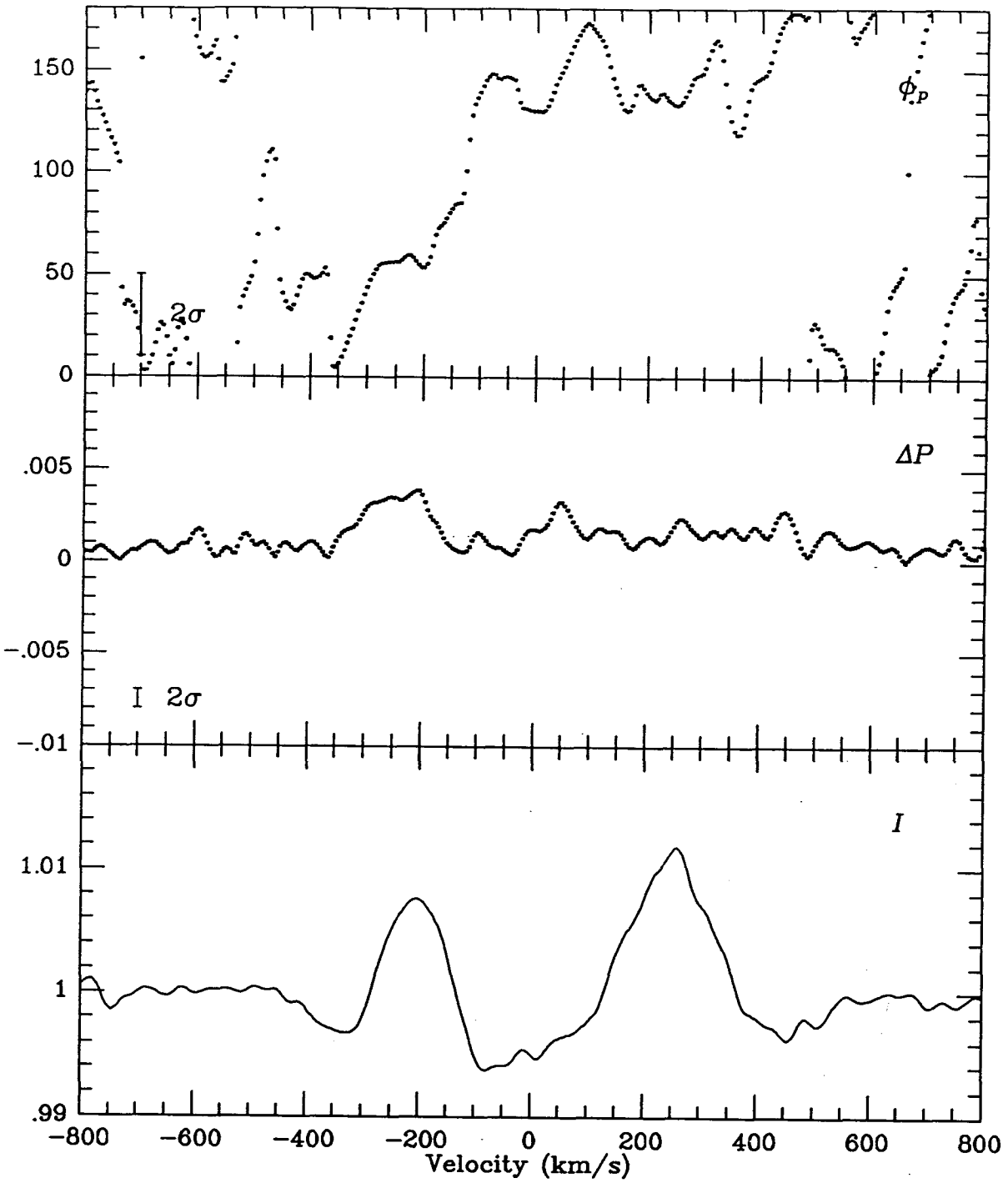

Figure 4.10: (*a*) Results of the polarisation analysis of the first five (first subset) differenced spectra of Fig. 4.9 for ζ Oph. The differential polarisation (ΔP) spectrum and position angle (ϕ_p) spectrum are plotted in the middle and upper panels respectively. The middle residual spectrum from the first subset (corresponding to 100°) is shown in the lower panel for comparison.

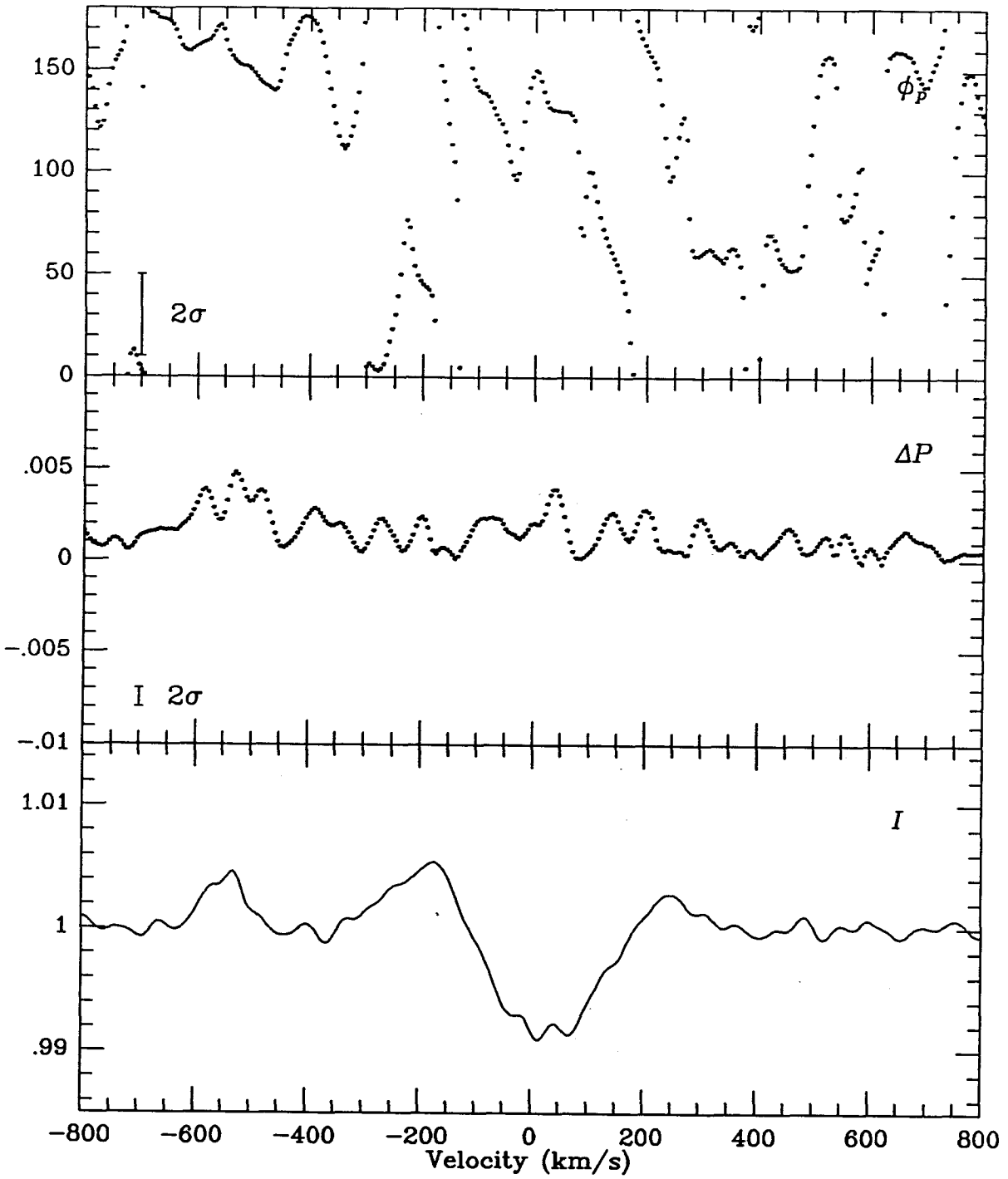

Figure 4.10: (*b*) Results of the polarisation analysis of the last five (second subset) differenced spectra of Fig. 4.9 for ζ Oph. The differential polarisation (ΔP) spectrum and position angle (ϕ_p) spectrum are plotted in the middle and upper panels respectively. The middle residual spectrum from the second subset (corresponding to 100°) is shown in the lower panel for comparison.

perfectly removed. Thus the intensity is a periodic function of diode number and this periodicity is reproduced in the polarisation measurements. Even though the residuals have been shifted with respect to each other, a *periodic* effect remains and would still be reflected in the polarisation. In contrast, CCDs generally do not suffer from this "ripple" effect (see for example Figs. 4.20*a, b*).

The ϕ_p spectra of Figs. 4.7, 4.8 and, in particular, 4.10 also show evidence for systematic effects. In the absence of polarisation, we would expect ϕ_p to exhibit random scatter (with amplitude $\sim 1/|\Delta P|$; as is evident in Fig. 4.19) as a function of wavelength. We suspect that the sytematic changes in ϕ_p are caused by time-dependent variations in the line profile. At a particular wavelength λ_1, the least-squares fit of Eqn. 4.1 to $I_{res}(\theta)$ will yield a certain value of ϕ_p. At the next wavelength point λ_2, ϕ_p will take a different value. Since the amplitude of the bumps varies continuously with wavelength (i.e., λ_1 and λ_2 are correlated), ϕ_p will also vary in a continuous manner. Further study of this effect would be of interest.

4.5.1.2 ϵ Per

We also looked for polarisation associated with the line profile variations of the bright B star ϵ Per. Like ζ Oph, ϵ Per also exhibits exceptionally large line profile variations, with the amplitudes of the travelling subfeatures approaching 1% in this star.

In an effort to reduce the systematic errors encountered in the analysis of the ζ Oph data (see Section 4.5.1.1), we decided to take a different approach for our polarimetric observations of ϵ Per. Recall from the last section that a major problem with the previous observations was the fact that the positions and shapes of the subfeatures in the line profile had changed significantly between spectra at the different position angles of the analyser. The systematic differences in the spectra produced spurious structure in the polarisation spectrum which could have been mistakenly interpreted as a real effect. The most practical solution to the problem was to use a CCD detector which, because of its low read out noise ($\sim 50e^-$ for the RCA CCD compared with $\sim 500e^-$ for the Reticon), permitted rapid switching between position angles of the analyser. An integration time of as little as 30 s was used for the ϵ Per observations; thus, one sequence of position angles (corresponding to 0°, 45°, 90° and 135°) took approximately 3 min, and very little shift of the subfeatures occurred over the sequence.

Drifts in the zero-point of the detector array from spectrograph flexure were estimated from the line positions in the Fe-Ar arc spectra obtained every half hour during the night. The zero-point shifts amounted to no more than one pixel for the entire night and were therefore negligible between spectra of any given set. Displacements of the moving bumps in the lines between those spectra were also small. Gies and Kullavanijaya (1988) calculated the time for a single bump of the most dominant mode ($\ell = 4$) to traverse the entire line profile to be $\simeq$7 hrs. If Hβ is roughly 15 Å wide (measured at the continuum) then the rate at which the subfeature crosses the line profile is approximately 0.04 Å min^{-1}. At that rate, the subfeature has travelled 0.1 Å in the time it takes to complete one sequence of position angles. This shift is small compared to the width ($\simeq$4 Å) of the subfeature.

Spectral time series of ϵ Per at Hβ and He I 4921 are shown in Figs. 4.11*a* and *b*, respectively. The corresponding residual time series at Hβ and He I 4921 are presented in Figs. 4.12*a* and *b*. The spectra have been averaged in 1/2-hour bins in order to clearly display the line profile variations of this star. Each binned spectrum is the composite of 24 spectra obtained at all the different position angles of the analyser and therefore contains no polarisation information. The residual spectra were computed by dividing the spectra in Figs. 4.11*a* and *b* by the mean of all the spectra in the time series. Gies and Kullavanijaya (1988) attributed the line profile variations of ϵ Per to sectorial NRP modes with $\ell = |m| = 3$, 4, 5 and 6.

In order to carry out the analysis of Section 4.4, residual spectra were again computed but in a slightly different way from those in Fig 4.12*a, b*: Each spectrum within a set (considered to be one complete sequence of position angles) was divided by the mean of the spectra in that set. This would reveal any polarisation effects in the line profile by removing the component of the profile that is independent of position angle. In order to improve the S/N ratio, the residuals at each position angle were then combined in 1/2-hour bins, resulting in 14 binned residuals at each position angle. Since each binned residual was the average of six residual spectra, each spectrum having been taken with the analyser alternated between clockwise and counterclockwise rotations, the effects of wavelength shifts due to spectrograph flexure and the movement of the subfeatures across the line profile were expected to average out.

No obvious polarisation structure above the level of the noise was apparent in any of

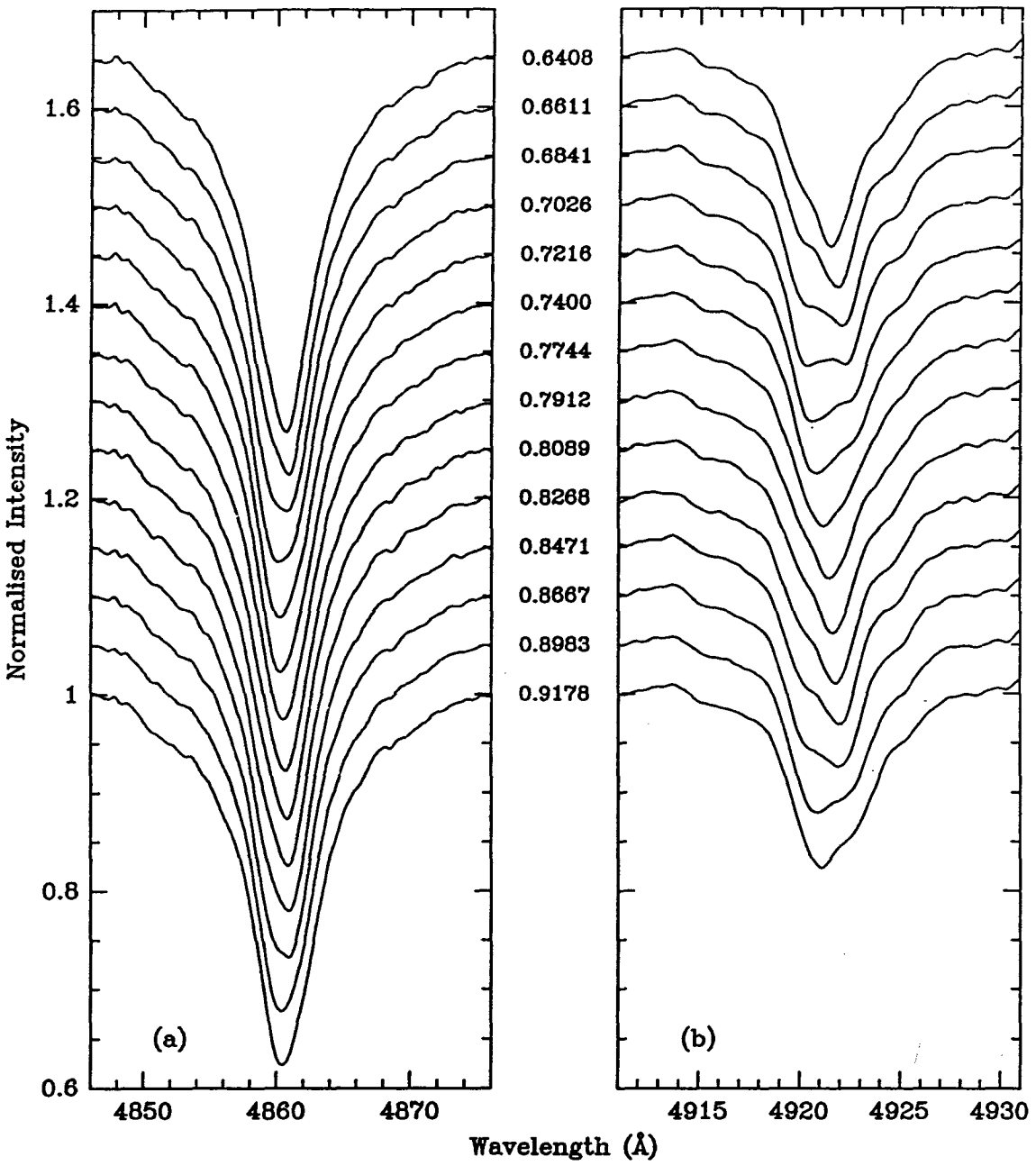

Figure 4.11: (*a*) Spectral time series of ϵ Per at Hβ. Each spectrum is the average of 24 spectra. The corresponding midexposure time in fractions of a day from the barycentric JD 2,448,261 is given to the right of each spectrum.
(*b*) Spectral time series at He I λ4921. The corresponding midexposure time in fractions of a day from the barycentric JD 2,448,261 is given to the left of each spectrum.

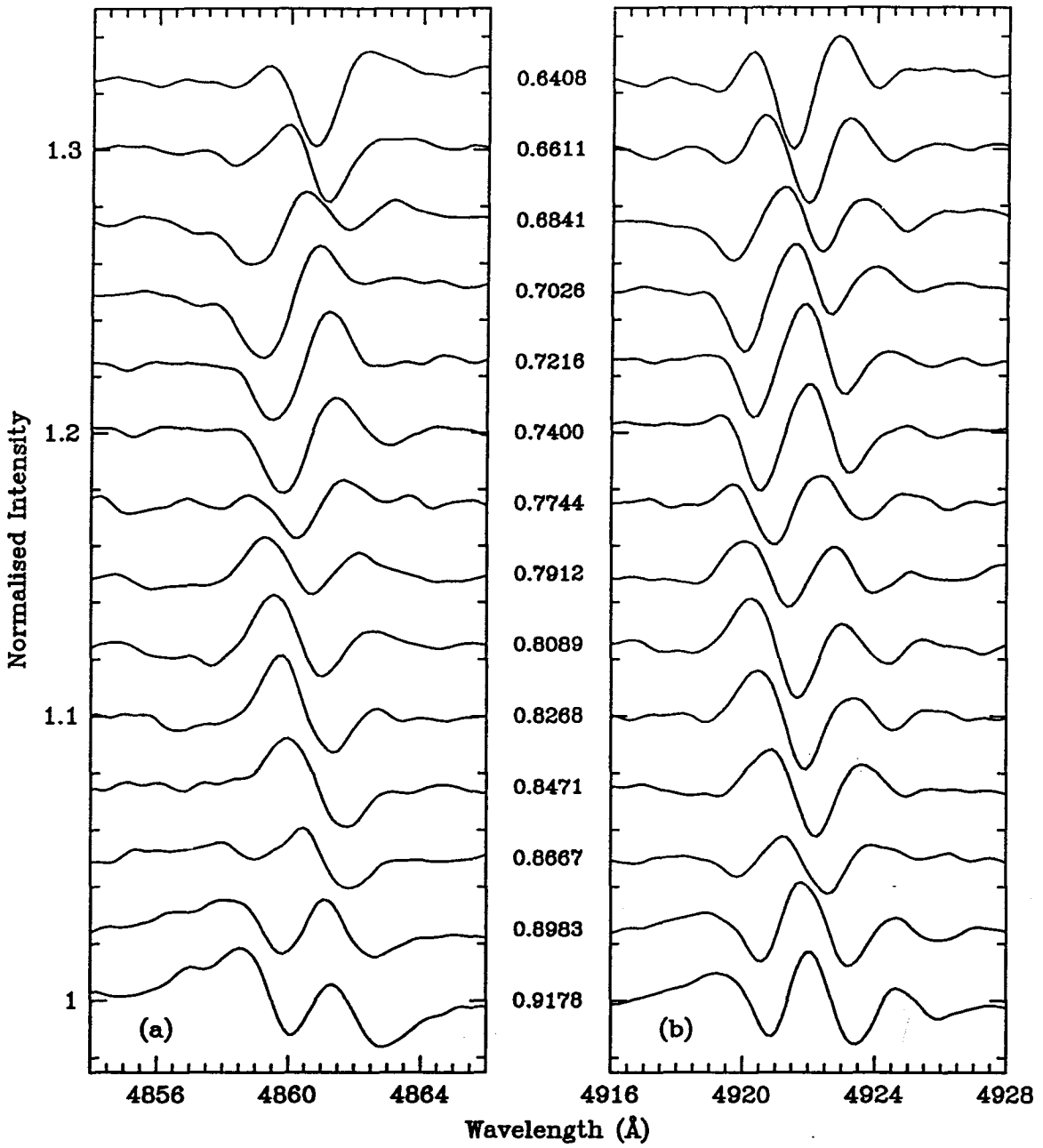

Figure 4.12: (*a*) Residual time series of ϵ Per at Hβ formed by dividing the mean spectrum into the individual spectra in Fig. 4.11*a*.
(*b*) Residual time series at He I λ4921 formed by dividing the mean spectrum into the individual spectra in Fig. 4.11*b*.

the sets of residual spectra. As an example, we present only one of these sets in Fig. 4.13. The residuals have been smoothed by a Gaussian function with a σ of 0.27 Å and the S/N ratio of each of the residuals is ~ 150. Analysis of all the sets of residual spectra by the method outlined in Section 4.4 revealed no polarisation structure across either the Hβ or He I 4921 profile, and an upper limit (1σ) of 0.15% was established by the results. We present in Fig. 4.14 only the result of the polarisation analysis on the residual spectra of Fig. 4.13.

4.5.1.3 Interpretation

Our observations of ζ Oph and ϵ Per represent the first spectroscopic polarisation measurements of the line profile variations of OB stars. We are not aware of any theoretical predictions of polarisation in the travelling subfeatures for any of the three models invoked to explain these variations. However, the upper limits obtained in this study should provide additional constraints on the possible sources of the line profile variations.

4.5.2 Differential Polarisation Measurements Across the Hβ Line of Be Stars

We investigated the wavelength dependence of polarisation across the Hβ emission line of the Be stars γ Cas, ϕ Per and 28 Cyg. Polarimetric observations of γ Cas were made on two consecutive nights to investigate reports in the literature of variable polarisation.

Residual spectra were formed in the manner outlined above for ϵ Per. Since we were only interested in the polarisation variation across the entire line profile rather than in discrete moving subfeatures within the profile (as in Section 4.5.1.2), nightly averages of all the residuals at each position angle were formed for all the stars. Thus the data were reduced to a single set of residual spectra per night of observations for each star. The residual spectra of ϕ Per, γ Cas and 28 Cyg are shown, respectively, in Figs. 4.15, 4.16*a, b*, 4.17. The residuals have been smoothed by a Gaussian function with a σ value of 0.27Å. The S/N of each of these spectra is typically between 1000 (for ϕ Per) and 4000 (for γ Cas). With the exception of 28 Cyg, all the residual plots show well-defined structure at Hβ. Moreover, the degree of structure clearly varies as a function of the analyser position angle.

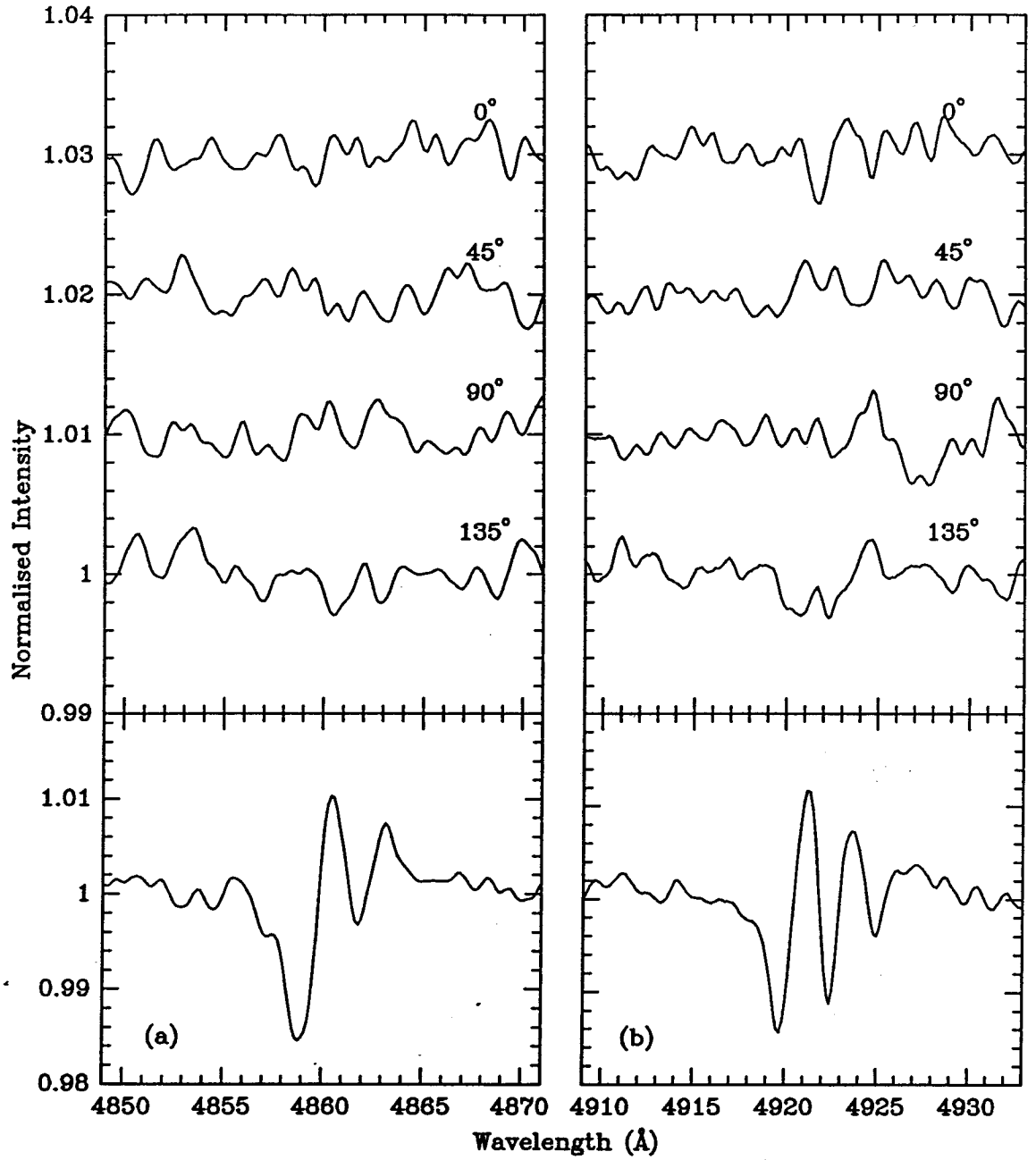

Figure 4.13: (*a*) Mean residual spectra of ϵ Per corresponding to barycentric JD 2,448,261.6841 at Hβ. Residual spectra were calculated by dividing the individual spectra within a set (considered to be one complete sequence of position angles) by the mean of the spectra in that set. Six of these residual spectra at each position angle were averaged to form the mean residual spectra shown in the upper panel. The corresponding analyser position angle is shown to the right of each mean residual spectra. The residual spectrum of Fig. 4.12 corresponding to the above BJD is shown for comparison in the lower panel. (*b*) Mean residual spectra corresponding to barycentric JD 2,448,261.6841 at He I λ4921.

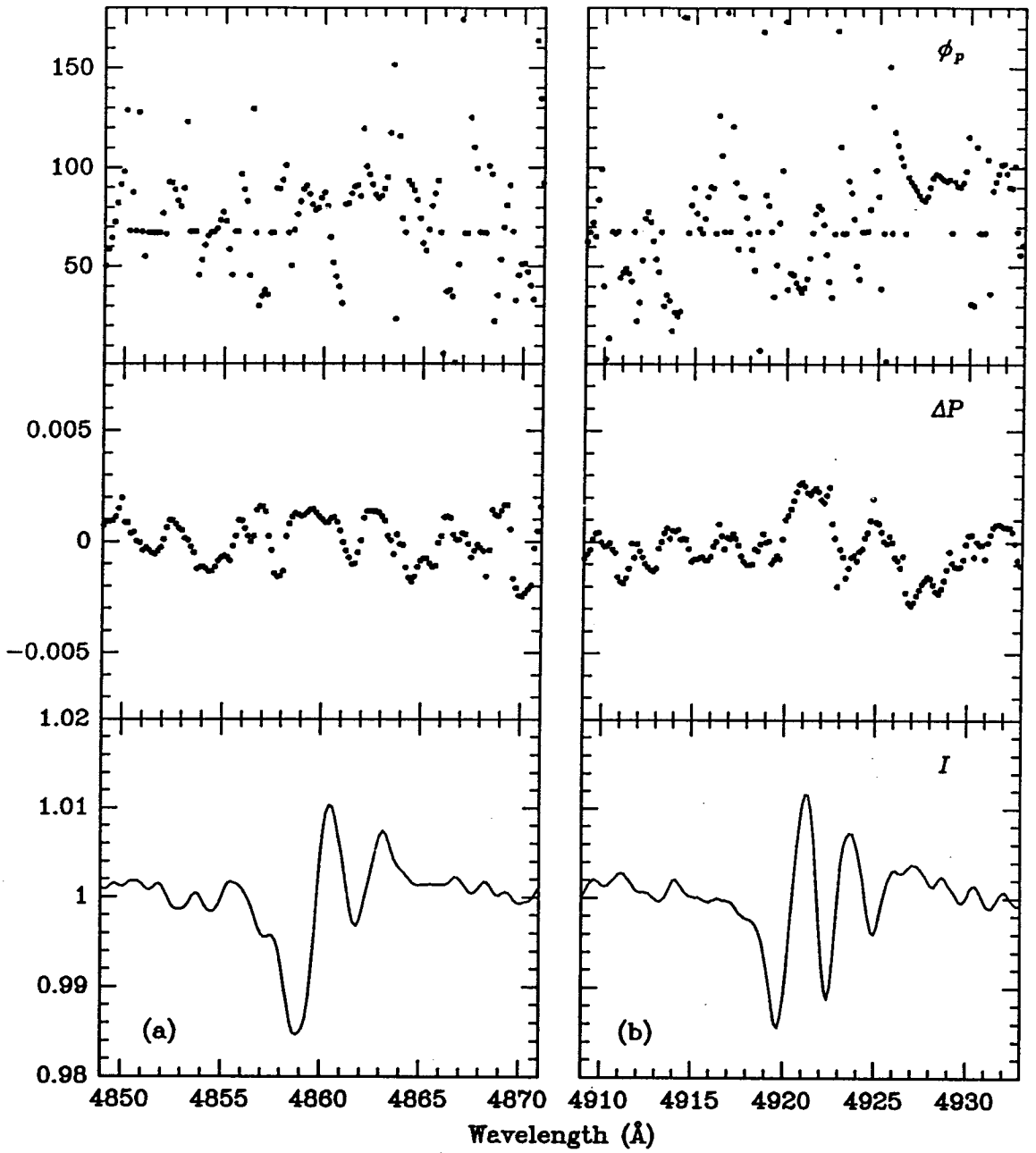

Figure 4.14: (*a*) Results of the polarisation analysis of the mean residual spectra of Fig. 4.13 at Hβ for ϵ Per. The differential polarisation (ΔP) spectrum and position angle (ϕ_p) spectrum are plotted in the middle and upper panels respectively. The residual spectrum of Fig. 4.12 corresponding to barycentric JD 2,448,261.6841 is shown for comparison in the lower panel.
(*b*) Results of the polarisation analysis of the mean residual spectra of Fig. 4.13 at He I λ4921 for ϵ Per.

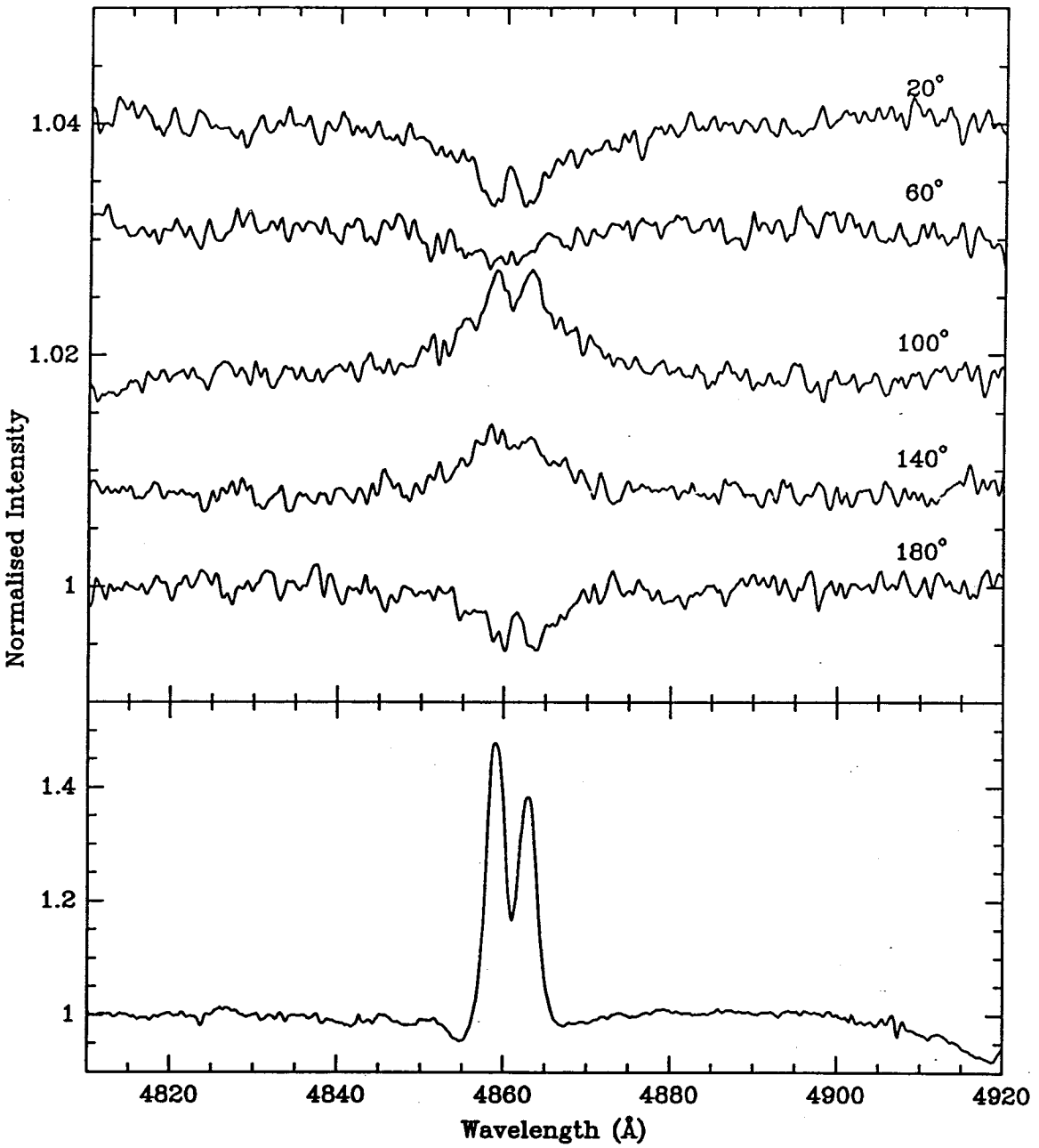

Figure 4.15: Mean residual spectra of ϕ Per at Hβ. Residual spectra were calculated by dividing the individual spectra within a set (considered to be one complete sequence of position angles) by the mean of the spectra in that set. All of the night's residual spectra at each position angle were averaged to form the mean residual spectra shown in the upper panel. The corresponding analyser position angle is shown to the right of each mean residual spectrum. The average spectrum of all the night's observations normalised to the continuum is shown for comparison in the lower panel.

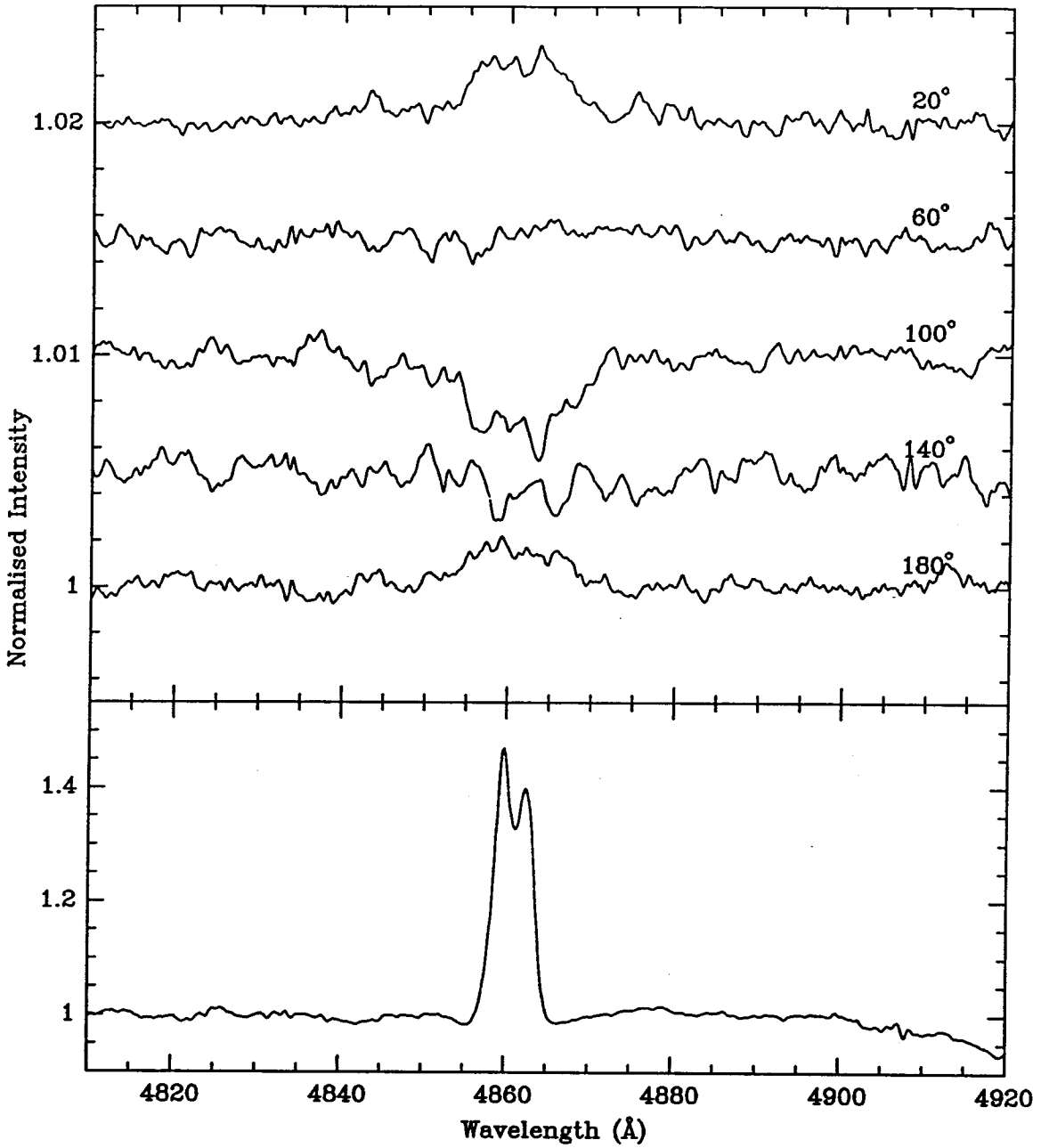

Figure 4.16: (*a*) As Fig. 4.15 for γ Cas. The observations were taken on 23 Sep 1990 UT.

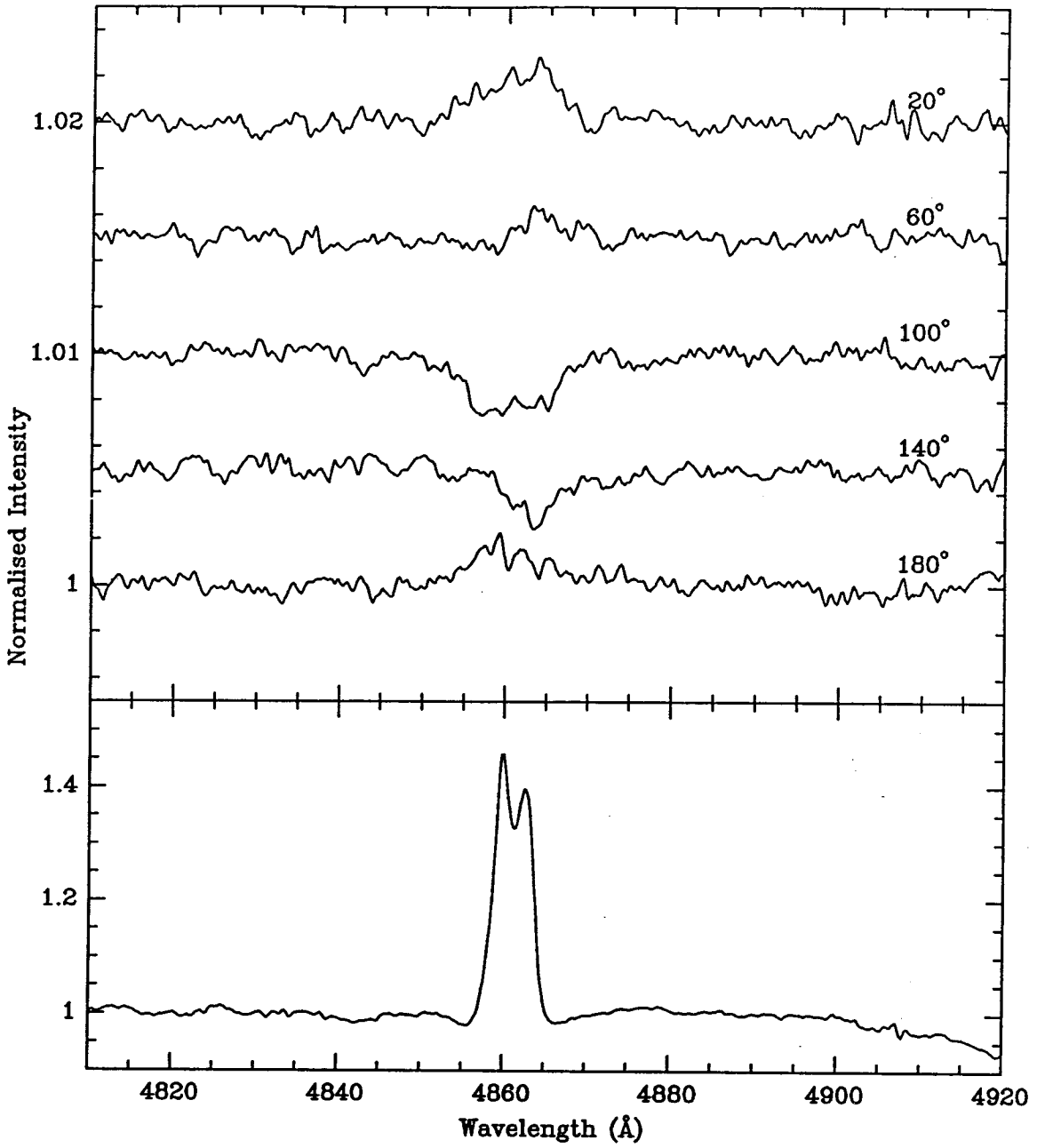

Figure 4.16: (*b*) As Fig. 4.15 for γ Cas. The observations were taken on 24 Sep 1990 UT.

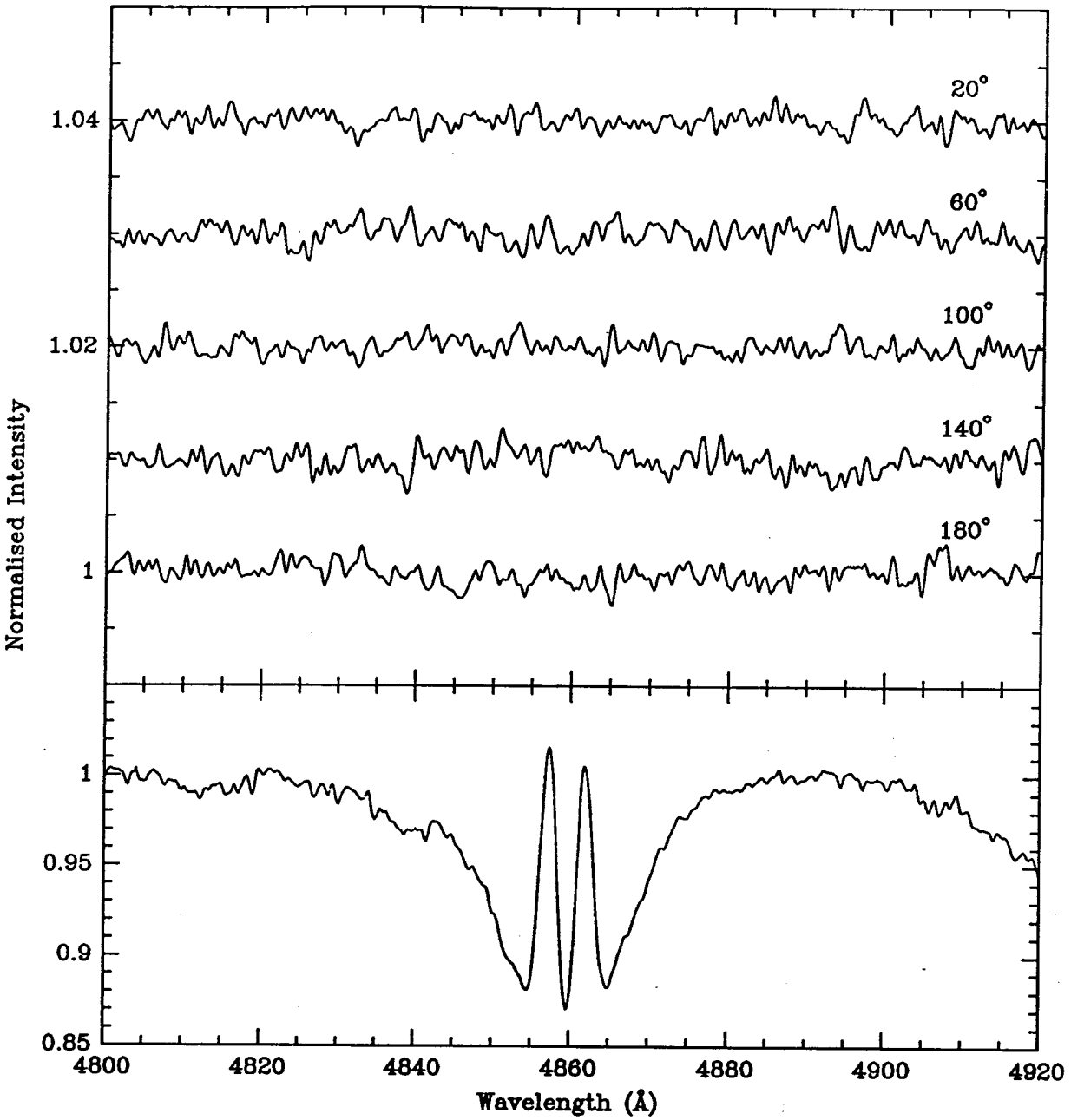

Figure 4.17: As Fig. 4.15 for 28 Cyg.

To ensure that the structure seen in the residual spectra did not originate in the instrument, we computed (in the same manner as for the program stars) residual spectra of unpolarised standard stars obtained on each night of the observations. They were generally very similar; as a sample we present only Fig. 4.18. No structure across Hβ is evident in the residual plots.

The residual spectra for all the program stars were analysed using the method described in Section 4.4. The normalised intensity profile I (lower panel), differential polarisation (ΔP) spectrum (middle panel) and the position angle (ϕ_p) spectrum (upper panel) in the region of Hβ are plotted in Figs. 4.19, 4.20*a, b* and 4.21 for ϕ Per, γ Cas, and 28 Cyg, respectively. The normalised intensity I in each figure represents the nightly mean of all the spectra for each star. The dashed line in the figures denotes the "predicted" change in polarisation if the effect is caused only by the addition of unpolarised flux to the line (see discussion below). The error bars in the respective panels represent the formal 2σ errors in ΔP and ϕ_p from the least-squares fit, at each wavelength point inside the Hβ profile. Outside Hβ, the error in ϕ_p tended to be larger ($\pm 20°$). This simply reflects the fact that outside the line profile the least-squares fits of Eqn. 4.1 are largely to noise.

Before discussing the results presented in Figs. 4.19 and 4.20*a, b*, it is important to realise that, as a consequence of measuring ΔP (instead of absolute P), the measured position angles ϕ_p are offset by $\pm 90°$ from the true or absolute values. The reason for this is as follows: Suppose (as shown in part (a) of Fig. 4.22) we have measurements of the continuum polarisation at the two orthogonal position angles ϕ_p and $\phi_p \pm 90°$, where the intensities are I_{max} and I_{min} respectively. The emission lines of Be stars are represented, in part (b) of Fig. 4.22, by an additional component of unpolarised radiation which is added to I_{max} and I_{min} in the same absolute amount. Our data reduction procedure is equivalent to normalising the intensities, I_{max} and I_{min}, to the same continuum value, which amplifies the I_{min} emission component. This is illustrated in part (c) of Fig. 4.22. Our analysis procedure is sensitive only to the *difference* between the two intensities. But, as shown in part (d) of Fig. 4.22, the measured intensity is a *maximum* at an angle of $\phi_p \pm 90°$, which contradicts the definition of I_{max} set out in Section 1.2.

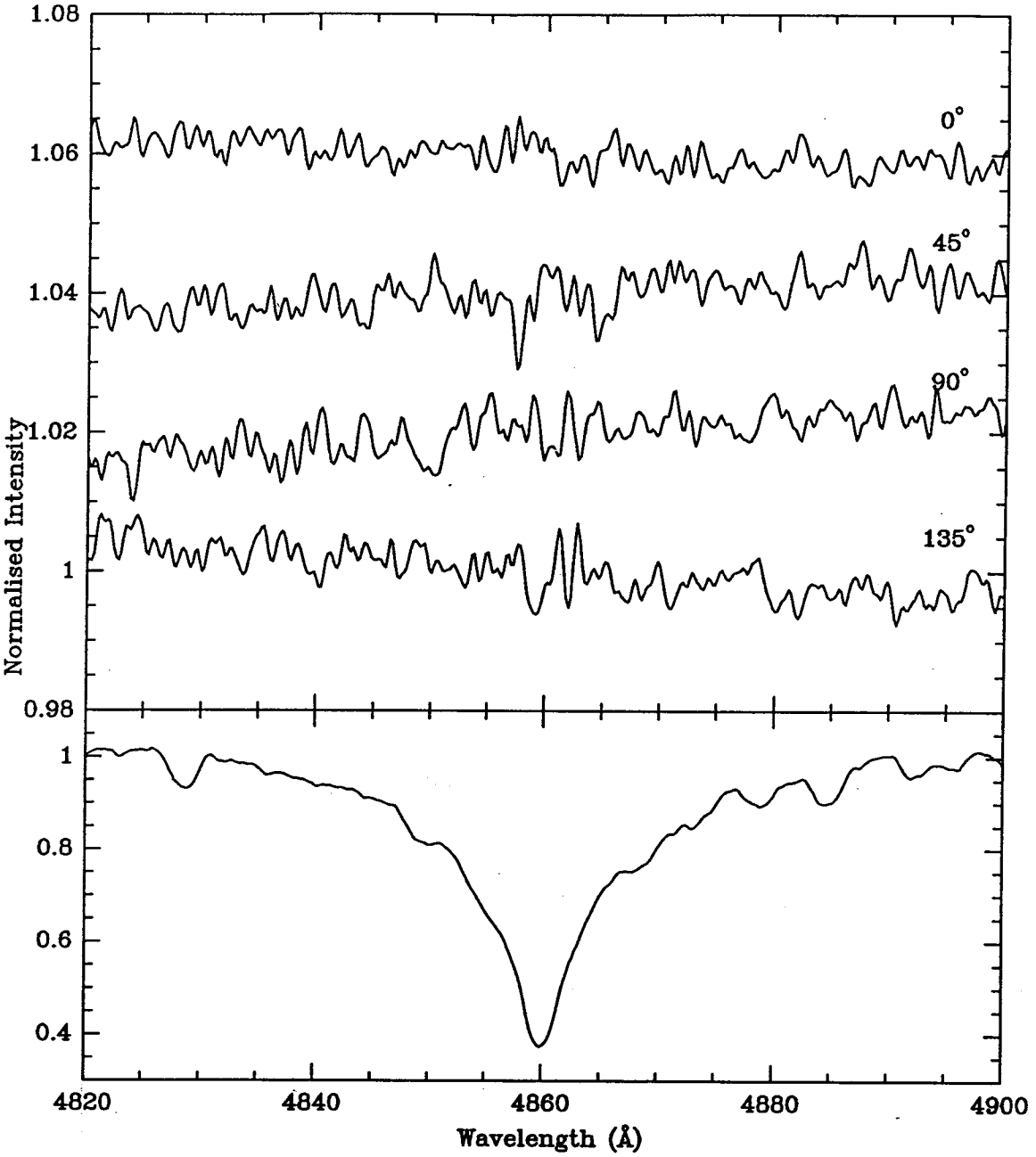

Figure 4.18: As Fig. 4.15 for γ Boo.

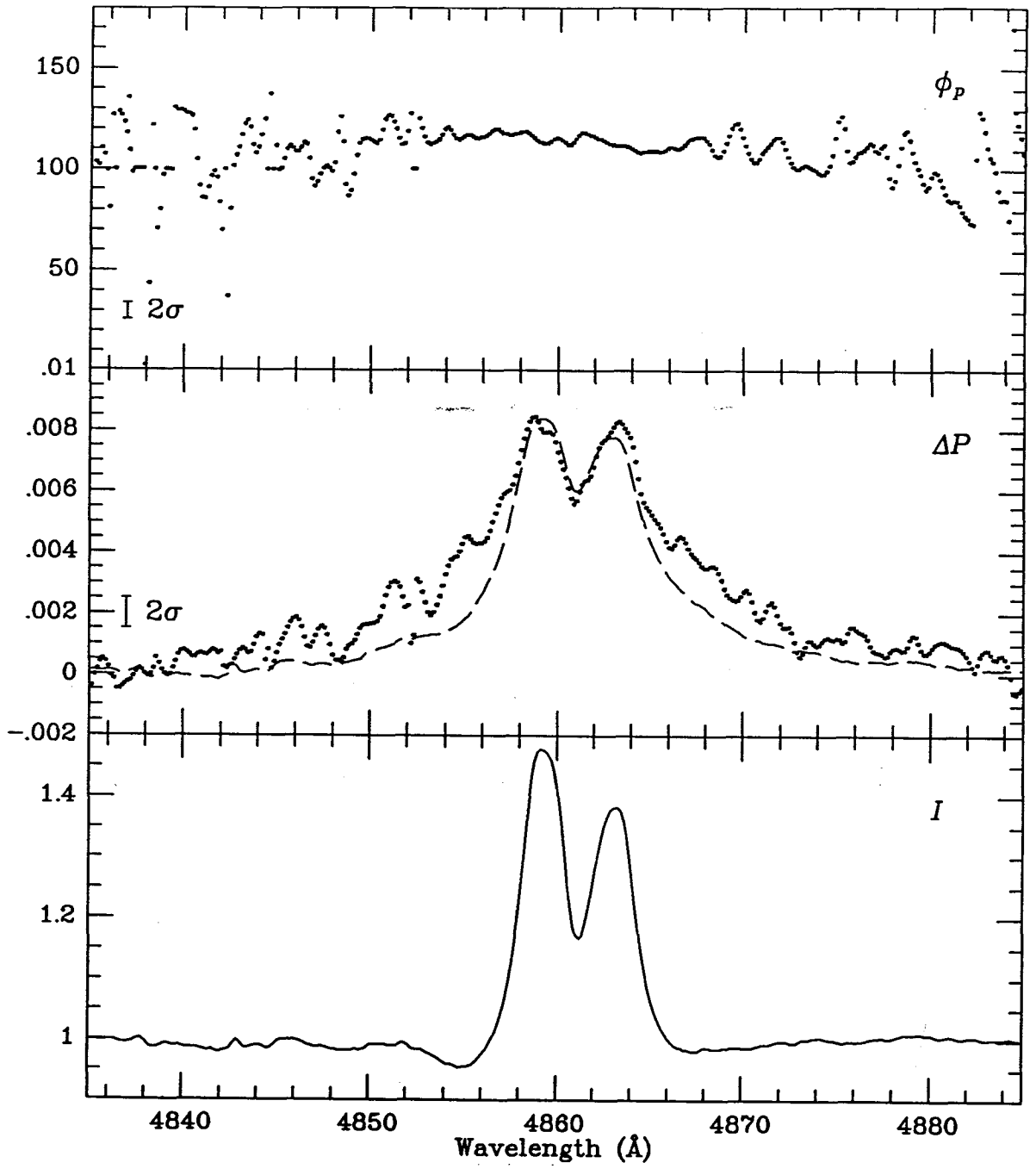

Figure 4.19: Results of the polarisation analysis of the mean residual spectra of Fig. 4.15 at Hβ for ϕ Per. The differential polarisation (ΔP) spectrum and position angle (ϕ_p) spectrum are plotted in the middle and upper panels respectively. The average spectrum of all the night's observations normalised to the continuum is shown for comparison in the lower panel. Note that the measured position angles ϕ_p are offset by ± 90 from the true values. To obtain the true ΔP and ϕ_p, the following transformation must be made:

$$\Delta P \rightarrow -\Delta P$$

$$\phi_p \rightarrow \phi_p \pm 90^\circ$$

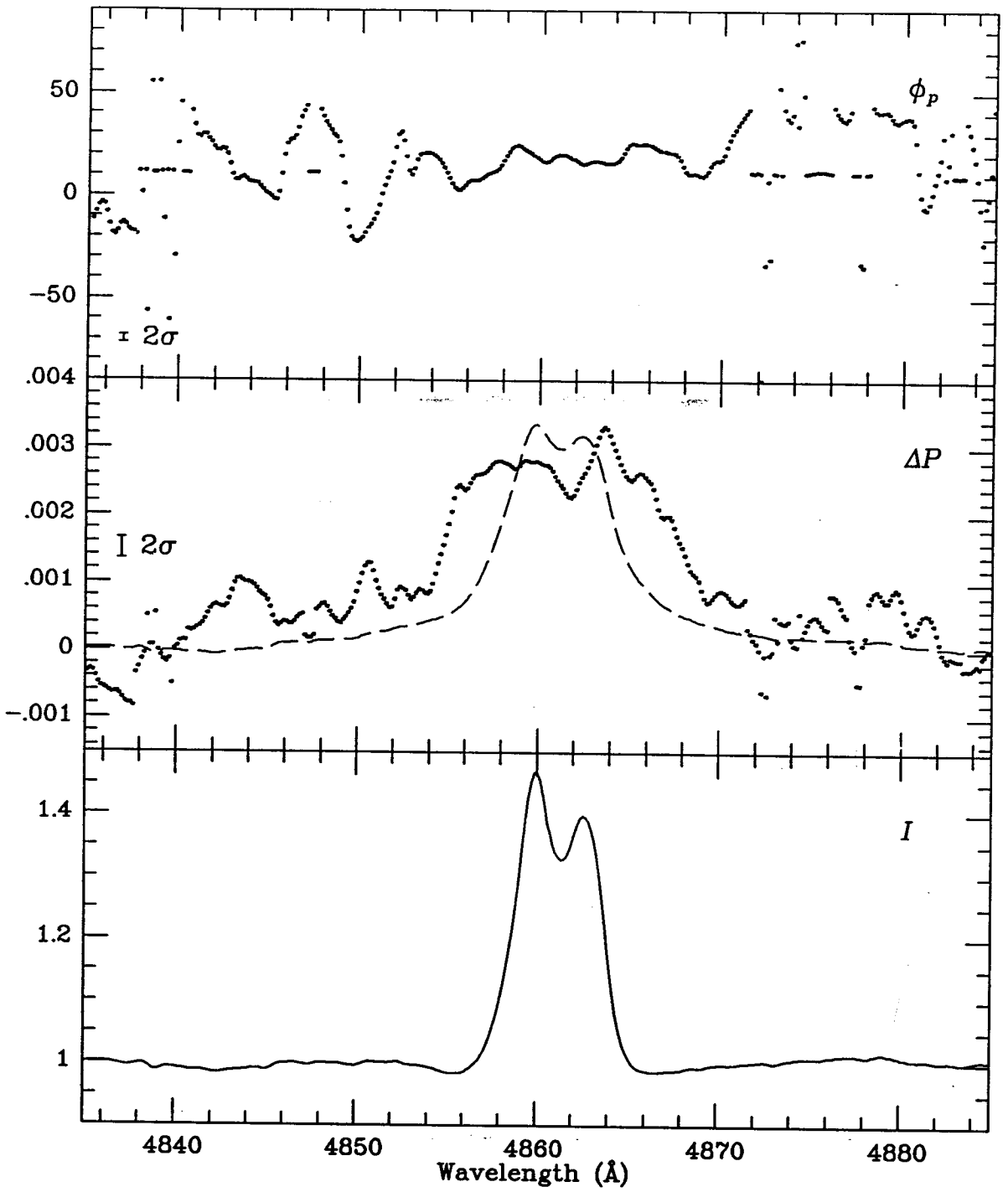

Figure 4.20: (*a*) As Fig. 4.19 for γ Cas. The observations were taken on 23 Sep 1990 UT.

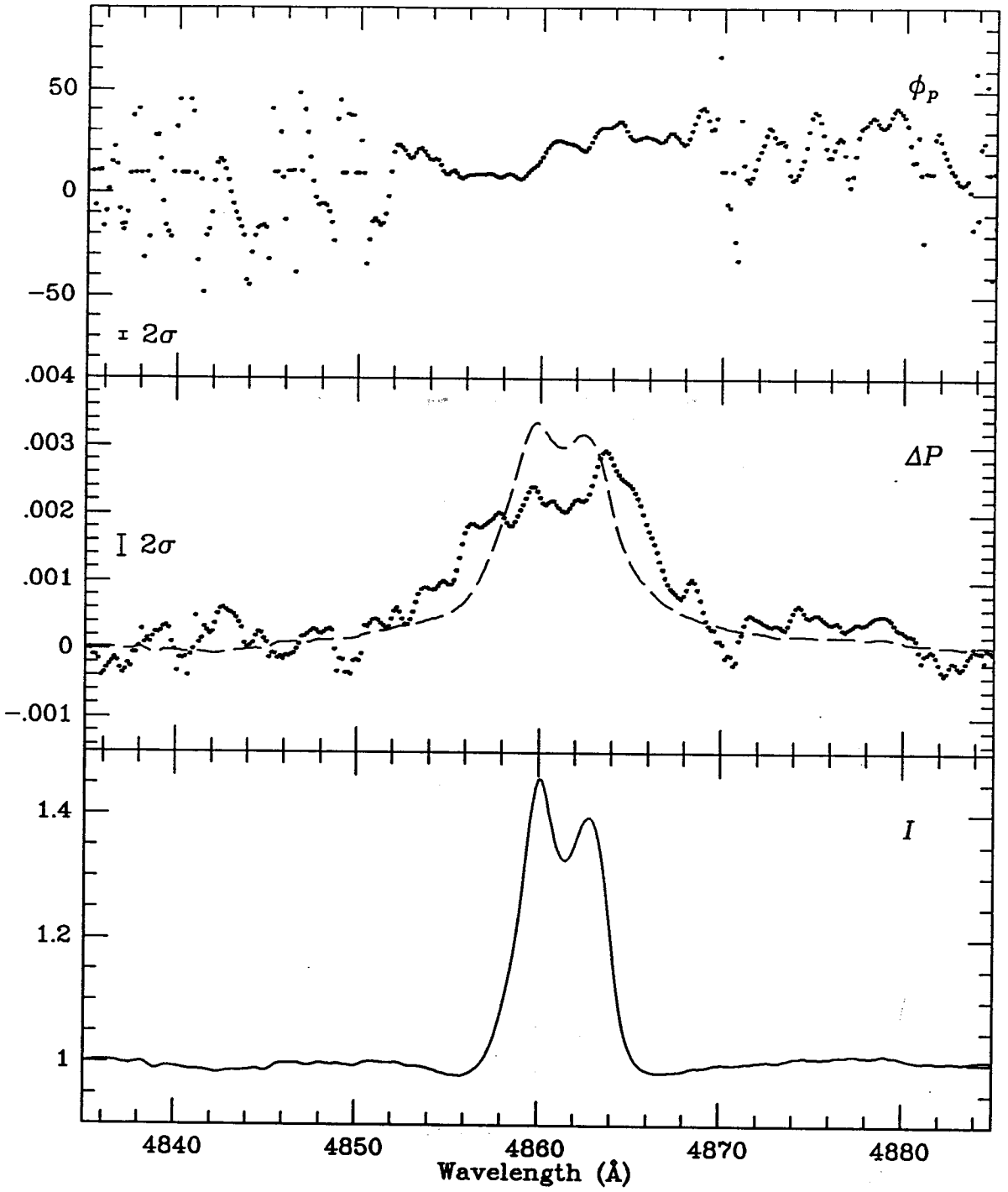

Figure 4.20: (*b*) As Fig. 4.19 for γ Cas. The observations were taken on 24 Sep 1990 UT.

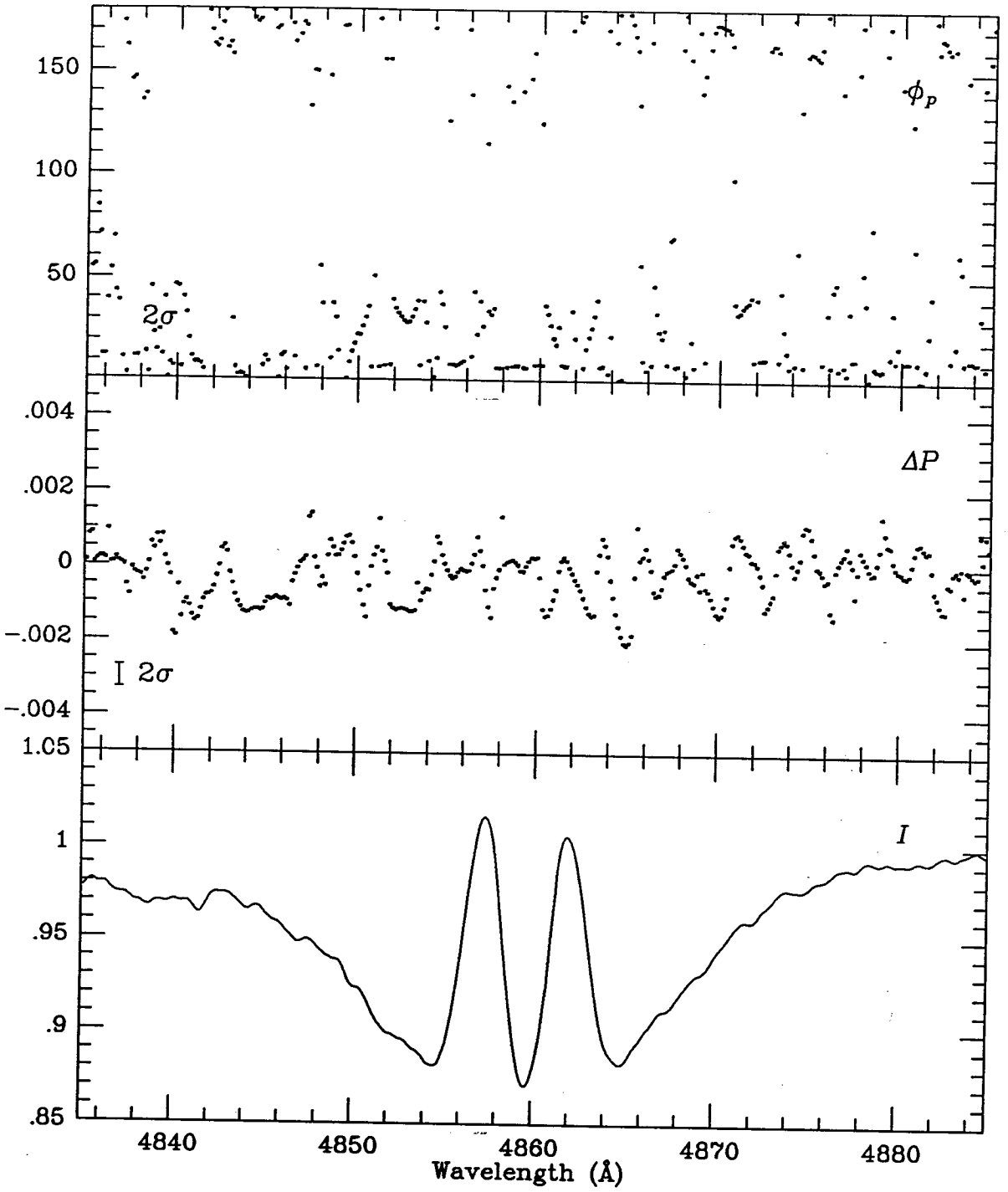

Figure 4.21: As Fig. 4.19 for 28 Cyg.

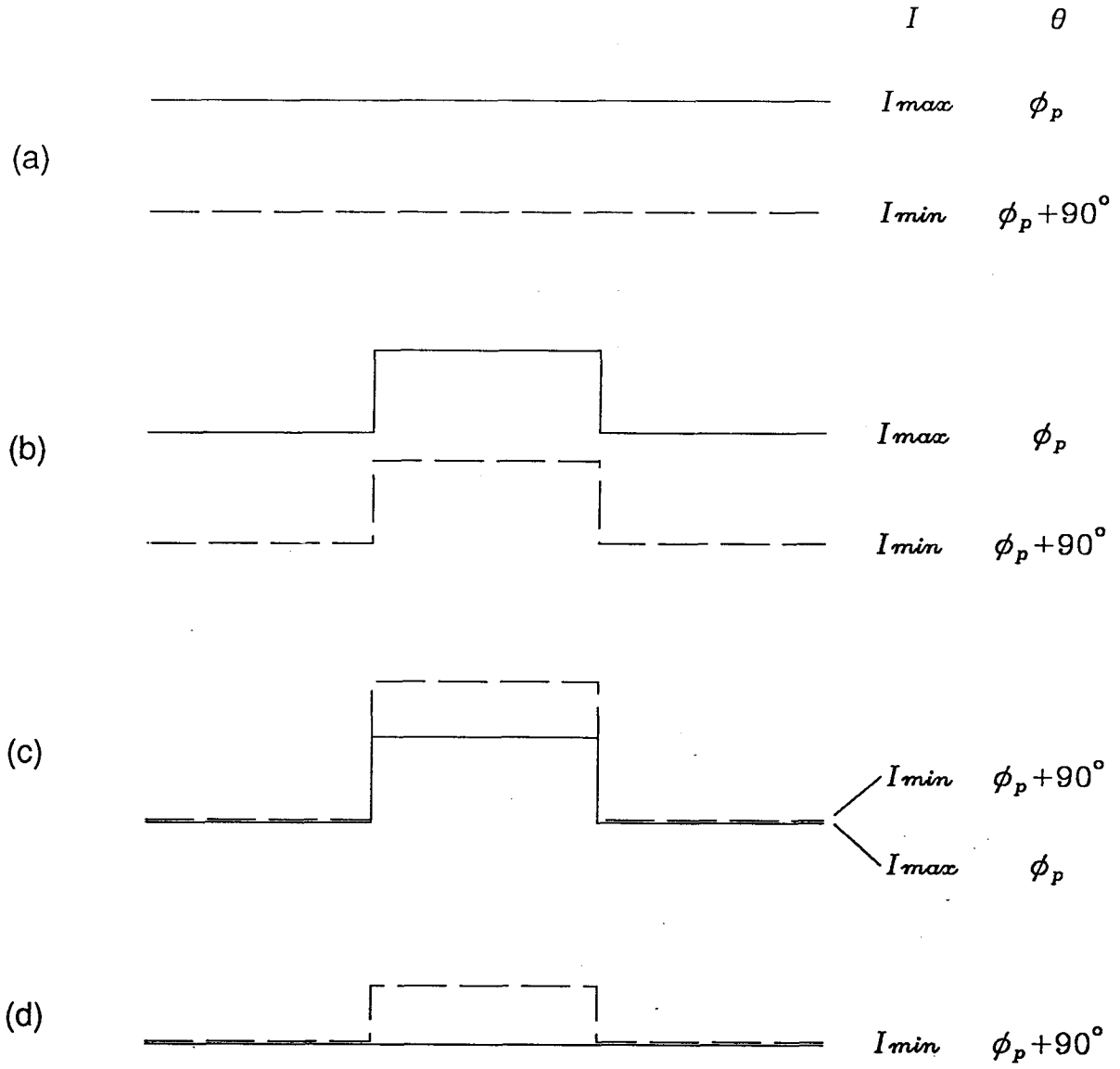

Figure 4.22: Explanation of why the measured position angles ϕ_p are offset by $\pm 90°$ from the true values.
(*a*) Continuum polarisation measurements at the two orthogonal position angles ϕ_p and $\phi_p + 90°$ corresponding to intensities I_{max} and I_{min}.
(*b*) Addition of unpolarised (emission) component in the same absolute amount.
(*c*) Our reduction procedure normalises I_{max} and I_{min} to the same continuum value, which amplifies the I_{min} emission component.
(*d*) Our analysis procedure is sensitive only to the difference between the two intensities. The measured intensity is a *maximum* at an angle of $\phi_p \pm 90°$, contradicting the definition of I_{max} in Section 1.2.

Therefore, to obtain the true ΔP and ϕ_p, we must make the transformation[11]

$$\Delta P \rightarrow -\Delta P \tag{4.7}$$

$$\phi_p \rightarrow \phi_p \pm 90^\circ \tag{4.8}$$

In this thesis, however, we have elected to present our data in terms of the measured ΔP and ϕ_p in order to allow straightforward comparison between the ΔP and emission profiles of Figs. 4.19 and 4.20*a, b*.

4.5.2.1 Physical Interpretation

We interpret our results in terms of the stellar wind model of Poeckert and Marlborough (1978a).[12] Although their model is – by their own admission – ad hoc (as are all Be star models), it nevertheless provides a conceptual framework for understanding the complex wavelength dependence of the polarisation and position angle across the Hβ profile in Figs. 4.19, 4.20*a, b*. It is also the only detailed radiative transfer model which attempts to account for the polarisation changes observed in the emission lines of Be stars. An equally valuable analytical discussion is given by McLean (1979).

Both absorption and emission processes in the envelopes of Be stars influence the wavelength dependence of the degree and position angle of the polarisation across the line profile. A significant result of the computations of Poeckert and Marlborough (1978a) is that line absorption plays an important and perhaps a dominant role in determining the detailed polarisation structure of Be-star line profiles. However, the general characteristics of this structure may be interpreted in terms of simpler qualitative arguments. In the following, we first examine the effects of line absorption on the degree and position angle of polarisation across a (rotationally-broadened) profile before looking at the effects of line emission.

Consider the simple case of a differentially rotating axisymmetric disk-like envelope inclined at some arbitrary angle to the observer, shown in Fig. 4.23. The stellar flux is polarised by scattering in the envelope. The degree and direction of polarisation *projected onto the sky* are indicated by the bold vectors in Fig. 4.23. The net polarisation is

[11] We point out that if the polarisation *increases* through the line then the transformation is unnecessary by the same arguments given in the text.

[12] The details of Poeckert and Marlborough's model are described in Marlborough (1969) and Poeckert and Marlborough (1977, 1978a, 1978b).

simply the vector integral of the individual polarisations over the disk. Because the degree of polarisation is larger (smaller) for scattering matter in the 3 and 7 (1 and 5) orientations,[13] the net plane of polarisation lies along the projected rotation axis (the 3 and 7 orientations).

Absorbing matter within the disk along the line of sight to positions 1 and 5 in Fig. 4.23 *increases* the net polarisation by preferentially absorbing direct (unpolarised) light and scattered light which is polarised in the direction perpendicular to the net polarisation. Because this matter has a relatively small Doppler shift, it has the largest effect at the center of the line profile (as shown in part (a) of Fig. 4.23).

On the other hand, absorbing matter within the disk along the line of sight to positions 3 and 7 in Fig. 4.23 preferentially absorbs light which is strongly polarised in the same direction as the net polarisation. In a rotating disk, this matter has the most effect in the line wings and produces polarisation minima in the blue and red wings of the line profile. If the rotational velocity of the envelope decreases with radius (as in a Keplerian disk), absorption at larger radii occurs at smaller Doppler shifts, so the resulting polarisation minima move towards the line center (as shown in part (a) of Fig. 4.23). If the envelope is rotating only (i.e., there is no expansion or contraction), these minima should similarly be symmetric with respect to the line center.

The explanation for the position-angle changes across the line profiles is slightly more complicated. Consider a rotationally broadened spectral line produced by the disk shown schematically in Fig. 4.23. In (say) the blue wing, the scattered flux in the approaching half of the disk (positions 2, 3 and 4) is affected by line absorption whereas the flux in the receding half of the disk (positions 6, 7 and 8) is affected only by continuum absorption. Therefore, the scattered flux at wavelengths in the blue wing of the line is more attentuated for the approaching half of the envelope and less attenuated for the receding half. Of course, the opposite is true for wavelengths in the red wing. Because for each wing the integration of the scattered light is not symmetrical with respect to the rotation axis, the net plane of polarisation varies systematically across the line profile (as

[13]Radiation scattered through a large angle with respect to the direction of the incident radiation will be strongly polarised. If the unpolarised incident wave is represented by the superposition of two orthogonal linearly polarised waves with equal electric field strengths $E^i_{\parallel} = E^i_{\perp}$, then the scattered components (E^s) are related to the incident components (E^i) by $E^s_{\perp} \propto E^i_{\perp}$ and $E^s_{\parallel} \propto E^i_{\parallel} \cos\theta$ where the symbols $\parallel$ and $\perp$ denote the parallel and perpendicular planes of polarisation with respect to the plane of scattering.

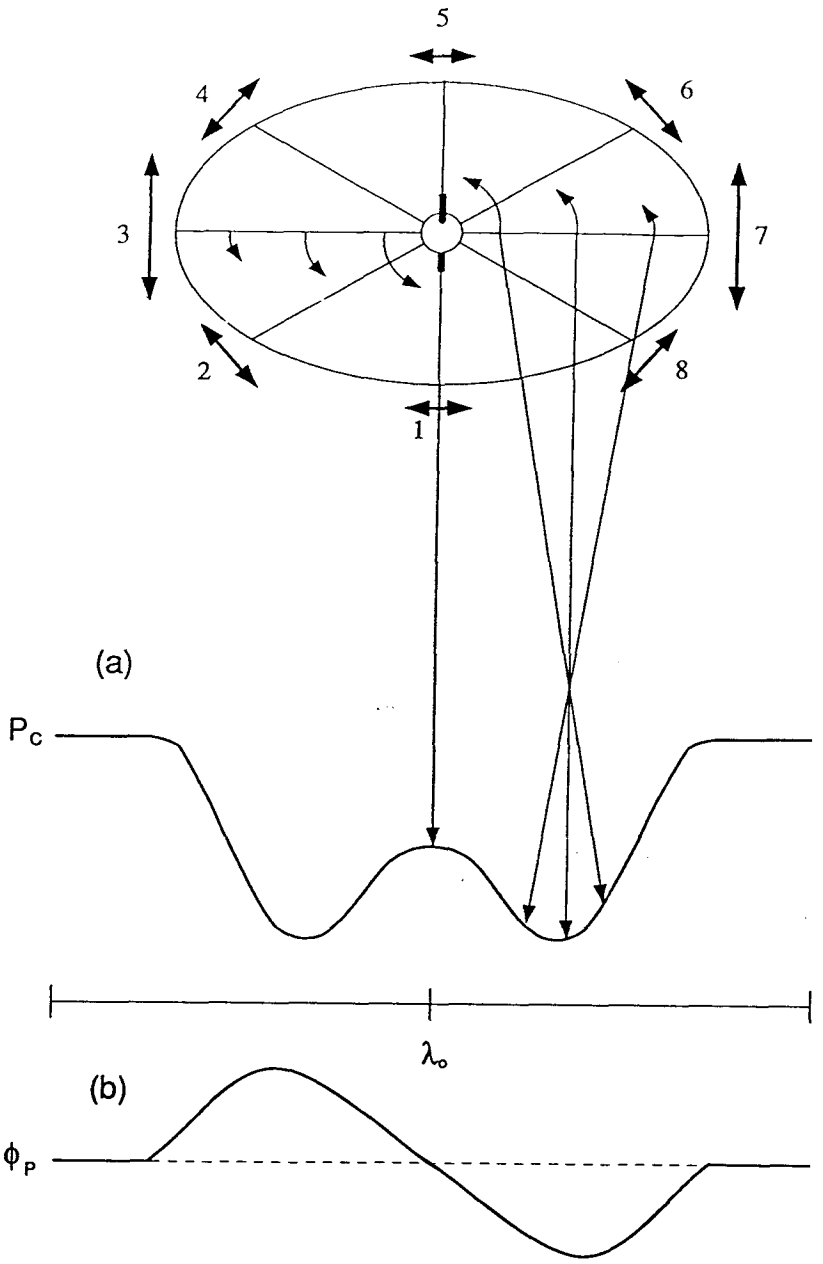

Figure 4.23: Schematic representation of the effects of absorption in a rotating axisymmetric circumstellar envelope on the degree and position angle of polarisation across a stellar line profile. The ellipse represents the envelope inclined at some arbitrary angle to the observer. The bold vectors represent the degree and direction of polarisation projected onto the sky. The rotational velocities of the envelope are indicated by the light arrows. The expected polarisation structure and position angle changes across the line profile are shown in (a) and (b), respectively.

shown in part (b) of Fig. 4.23).

In the case of an envelope undergoing pure rotation, these position-angle changes are antisymmetric with respect to the line center. That is, the variation in ϕ_p will have the same amplitude but opposite sense for both wings, as shown in part (b) of Fig. 4.23. Additional random motions, expansion or contraction will tend to produce more complicated position-angle changes.

The position-angle changes depend on the inclination of the disk, the magnitude of the changes decreasing with inclination (cf. Poeckert and Marlborough 1978b). For example, Poeckert and Marlborough (1978b; see their Fig. 3) show that at an inclination $i = 89°$ the position angle changes by less than 0.5°, while at $i = 30°$ the change can approach 30°. Thus, for a disk viewed edge-on, there is little rotation of the position angle. In contrast, the degree of line polarisation is highest for a disk viewed edge-on.

The principal effect of line emission is to dilute the polarisation in the profile. In the idealised case where the emission line flux is completely unpolarised, the line polarisation is given by (McLean and Clarke 1976)

$$P_L(\lambda) = \frac{P_C(\lambda)}{I_E(\lambda)} \tag{4.9}$$

where P_C is the continuum polarisation and I_E is the total intensity of the additional unpolarised emission flux (with the continuum normalised to unity). Note that here the degree of polarisation in the absorption line is assumed to be same as that in the adjacent continuum. In this (idealised) case, the line emission has no effect on ϕ_p. It should be pointed out, however, that there is no particular reason to believe the emission flux to be unpolarised. In fact, the line emission may itself be partially polarised either by further electron scattering, or by flourescence or resonance scattering[14] (McLean 1979). In this case, if the net plane of polarisation of the emission flux is not the same as that of the continuum flux, there is a rotation of ϕ_p through the line profile.

4.5.2.2 Individual Stars

ϕ Persei This bright (V = 4.07) Be star is a member of a double-lined spectroscopic binary (Abt and Cardona 1984); the underlying star has a spectral type of B2 Vep (Hoffleit

[14]For resonance scattering where an upward transition is followed by a downward transition, the re-emission of the photon is not isotropic, but follows a phase-angle distribution similar to that of Rayleigh scattering (Collins 1979; p. 467).

and Jaschek 1982) and a $v \sin i = 450$ km s^{-1} (Hutchings and Stoeckley 1977). Variations in the linear polarisation of the continuum light from ϕ Per have been reported by Coyne (1976), but were not found to correlate with either the radial-velocity or light curves of the binary orbit (Coyne 1975; Gies and McDavid 1987). Polarisation changes across the lower Balmer emission lines Hα and Hβ have been reported by McLean *et al.* (1979) and, at considerably lower resolution ($\sim$ 10 Å), by Coyne and McLean (1975), McLean and Clarke (1976) and Clarke and Brooks (1984). The general appearance of the ΔP profile of Fig. 4.19 agrees with that of McLean *et al.* (1979); however, the greater precision of our results allows us draw stronger conclusions.

As shown in Fig. 4.19, there is a strong ($\sim$0.85%) decrease[15] of the polarisation toward the center of the Hβ profile, accompanied by a smaller ($\sim$0.25%) increase at the line center. The ΔP profile is symmetric with respect to the line center which, according to the discussion in Section 4.5.2.1, suggests that the velocity field of the circumstellar envelope of ϕ Per is dominated by rotation. There is only slight evidence for a change in ϕ_p with wavelength. This is consistent with a circumstellar envelope of ϕ Per viewed equator-on (cf. Section 4.5.2.1). According to McLean and Clarke (1976), the equator-on aspect is also consistent with its high value of $v \sin i$.

We see no evidence in our data of the oscillatory behaviour of ΔP in the line wings reported by McLean *et al.* (1979). Given that the error level of our results is $\sim 4\times$ smaller than that of McLean *et al.* (1979), we believe it is unlikely that these variations are a genuine polarisation effect. However, it is not improbable that there has been a change in the line polarisation since their 1977 observations. (Changes in line polarisation are not uncommon in Be stars. We discuss a notable example in the next section.)

In Fig. 4.19, we have indicated (by the dashed line) the predicted ΔP if the reduced polarisation in Hβ is caused solely by unpolarised emission. The predicted effect was estimated from Eqn. 4.9. In order to obtain a good estimate of the total emission flux I_E, a synthetic (rotationally-broadened) absorption spectrum I_{ABS} was subtracted from the observed (normalised) intensity profile I_{OBS} (i.e., $I_E = I_{OBS} - I_{ABS}$). The synthetic spectrum was generated using the non-LTE model atmosphere program of Hubeny (1988). The model parameters used are those given by Poeckert and Marlborough (1979) and

[15] Recall that the ΔP plotted in Fig. 4.19 equal to $-\Delta P$ and that ΔP lies at the continuum polarisation.

listed in Table 4.4. We assumed a continuum polarisation of 2.0% near Hβ (Poeckert *et al.* 1979).

The predicted ΔP shows excellent agreement with the observed ΔP at the center of the line profile, as shown in Fig. 4.19. However, as apparent in the line wings, the observed ΔP profile is significantly broader than the ΔP profile predicted by Eqn. 4.9. This suggests that dilution by unpolarised line emission cannot completely account for the decrease in the line polarisation observed in ϕ Per. There is some indication in the lower panel of Fig. 4.19 that the width of ΔP profile is comparable to the width of the underlying absorption profile ($\sim$30 Å) of the star. (Better evidence for this is shown in the model absorption spectrum in Fig. 4.24.) The positive correlation between the width of ΔP and the absorption spectrum tends to favour the suggestion of Poeckert and Marlborough (1978a) that absorption in a rotating circumstellar envelope also contributes to the decrease of polarisation in the line profiles of Be stars.

Our results tend to reinforce the conclusions of Poeckert and Marlborough based on their model calculations (cf. Section 4.5.2.1) and should provide important additional constraints for their model.

γ Cassiopeiae This bright (V = 2.47) Be star was the first in which emission lines were discovered in its spectrum (Secchi 1867); the underlying star has a spectral type of B0 IVe (Hoffleit and Jaschek 1982) and a $v \sin i \simeq 300$ km s^{-1} (Hutchings and Stoeckley 1977). It is one of the most intensely studied of the emission-line stars for polarisation effects across its hydrogen Balmer lines (see Coyne 1976a; Coyne and McLean 1982; and references therein). Most of these studies have concentrated on the Hα and Hβ emission lines, where polarisation changes of $\simeq$ 0.2% and $\simeq$ 0.3 – 0.4% respectively from the continuum values have been measured. Reduced polarisation has also been detected in Hγ by Hayes and Illing (1974).

As shown in Figs. 4.20*a, b*, there is a steep drop in the polarisation in both wings of Hβ; the largest decrease occurred in the red wing. There is evidence for a small increase in the polarisation at the centre of the line. The total change in ΔP corresponded to about 0.3%. There also appears to be evidence for variations in ϕ_p across the line profile. The results for the second night Fig. 4.20*b* show changes of about 20°. This agrees reasonably well with the position-angle changes predicted by the model of Poeckert and Marlborough (1978a; see their Fig. 9). They assumed an inclination of 45° for the envelope of γ Cas.

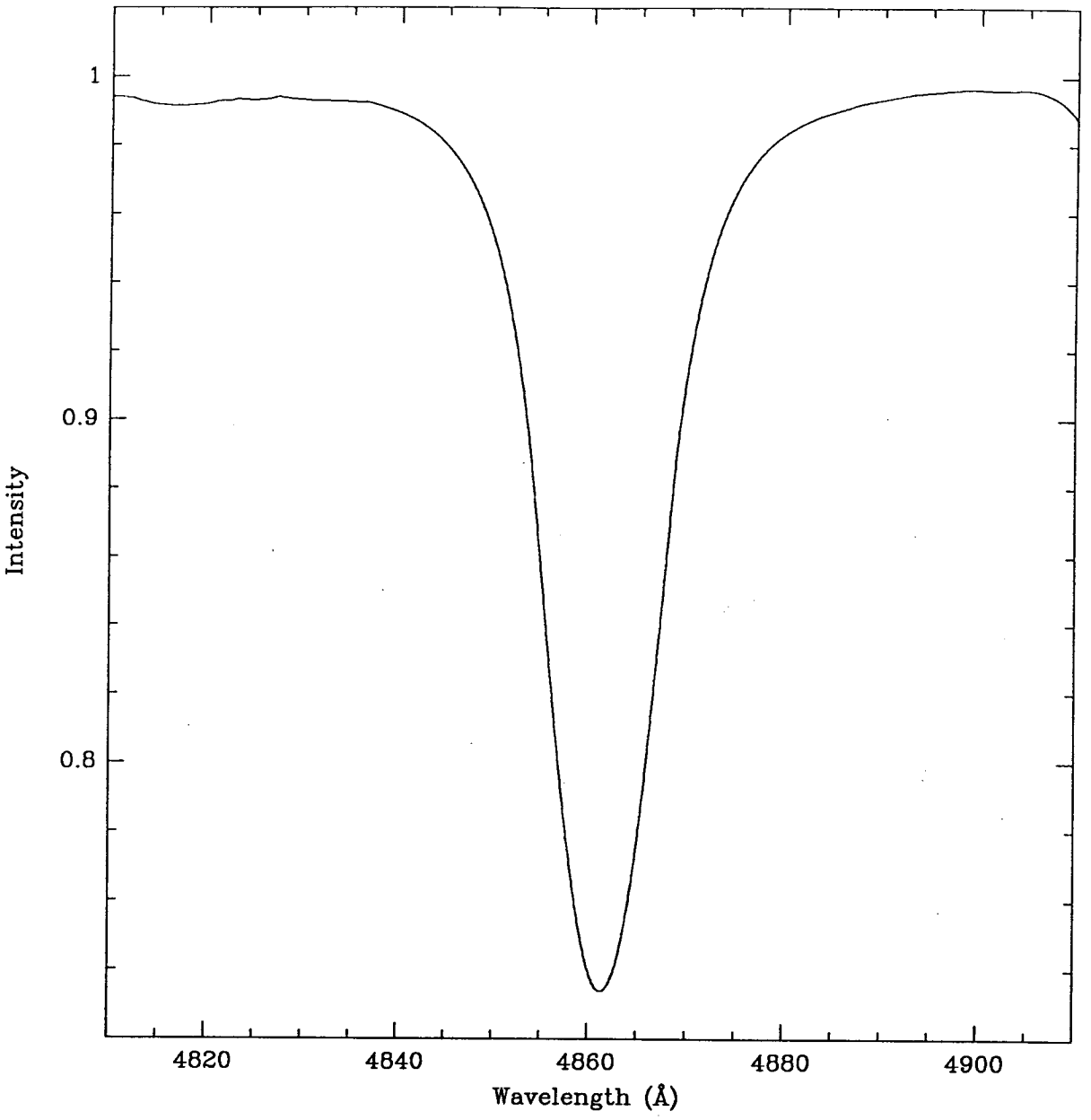

Figure 4.24: Synthetic spectrum of ϕ Per at Hβ. The spectrum was generated using the non-LTE model atmosphere program of Hubeny (1988) with $T_{eff} = 21,000K$, $\log g = 3.5$ and $v \sin i = 450$ km s^{-1}.

Table 4.4: Model Parameters for ϕ Per and γ Cas

Star	T_{eff} (K)	$\log g$	$v \sin i$ (km s^{-1})
ϕ Per.....	21,000	3.5	450
γ Cas.....	25,000	3.5	300

Our data do not show any evidence for the secondary polarisation minimum in the blue wing of Hβ near $\simeq$ 4850 Å reported by McLean *et al.* (1979). The data of McLean *et al.* suggest a decrease in the polarisation comparable to that in the line, i.e. $\Delta P \simeq 0.4\%$. The fact that we do not see this effect suggests that the polarisation profile may have changed since their observations.

We have computed the predicted ΔP for γ Cas in the same manner as for ϕ Per, using Eqn. 4.9. The synthetic (rotationally-broadened) absorption spectrum of γ Cas, shown in Fig. 4.25, was used in the calculations. We used the model parameters given by Poeckert and Marlborough (1978b) and listed in Table 4.4 to generate the synthetic spectrum.

Within the uncertainties of our measurements, the predicted ΔP profiles show good agreement with the observed ΔP profiles at the center of the Hβ line, as shown in Figs. 4.20. However, the observed ΔP profiles are significantly broader than the their corresponding predicted ΔP profiles. We interpret this in the same way as we did for ϕ Per; that is, at least part of the reduced polarisation in the line wings is caused by absorption processes in the circumstellar envelope of the star. This is supported by Fig. 4.25, which shows that the width of the absorption profile ($\sim$ 25 Å) is comparable to the width of the ΔP profile.

Comparing Figs. 4.20*a* and *b*, there is some suggestion that there has been a change in the ΔP profiles from the first night to the next. Although the general shape of the ΔP profiles is the same, there is slight evidence for an overall increase in the polarisation from the first night. However, it is possible that the difference is an artifact of the rectification of the residual spectra, although the rectification procedure would not be expected to affect the measurement of ΔP by more than $\pm 1\sigma$.

Assuming that the change in ΔP is in fact genuine, then some of it may be attributable to variable line emission. We found that the emission flux in the line decreased by about 1%, which according to Eqn. 4.9 corresponds to an increase in the line polarisation of about 0.005% assuming $P_C = 0.8\%$. Since the change in ΔP between nights appears to be an order of magnitude larger, $\sim$ 0.05%, it is possible that there may be an additional source contributing to the observed variations. Since the line emission arises from a much larger volume than the polarised flux, polarisation changes do not necessarily have to accompany changes in the emission lines (Piirola 1979). It has also been suggested by Poeckert *et al.* (1979) that polarimetric changes may precede spectroscopic changes on timescales of

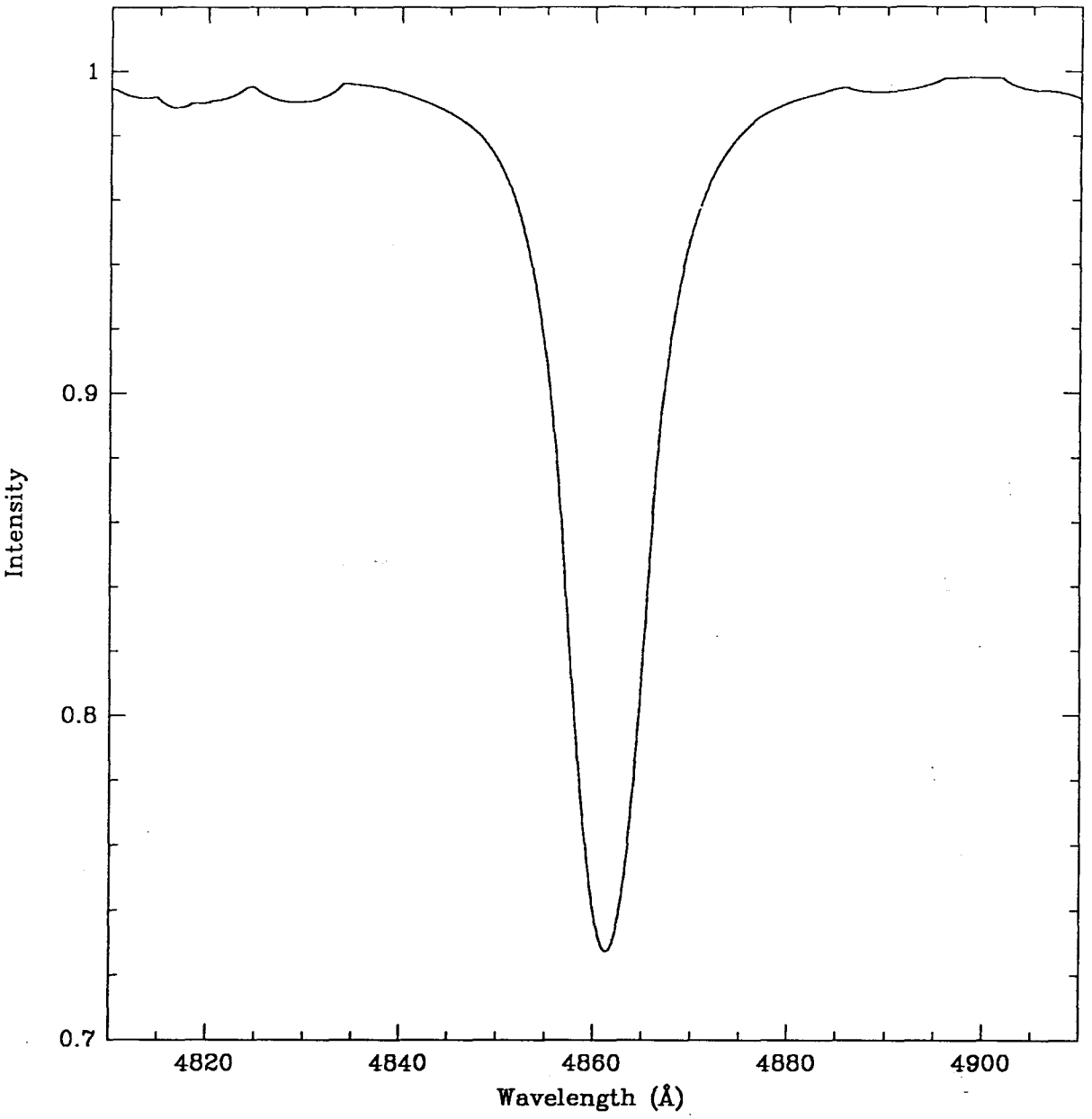

Figure 4.25: Synthetic spectrum of γ Cas at Hβ. The spectrum was generated using the non-LTE model atmosphere program of Hubeny (1988) with $T_{eff} = 21,000K$, $\log g = 3.5$ and $v \sin i = 300$ km s^{-1}.

the order of months. Alternatively, it not unlikely is that our measurement of the change in the intensity profile is in error because of problems in defining the continuum of the intensity profiles in a consistent way. Therefore, we do not feel that any firm conclusions can be drawn without further observations.

28 Cygni We found only one reference in the literature of polarisation measurements across the emission lines of this star. Coyne (1975) reported a decrease in the polarisation at Hβ of $\Delta P = 0.4\%$. At the time of our observations, no significant change in polarisation was apparent across the Hβ feature of this star despite the presence of appreciable emission in the line. We can place an upper limit to ΔP in 28 Cyg of 0.1% from our data.

Chapter 5

Summary and Conclusions

We have described in Chapter 2 the design and performance of the UBC/DAO polarisation analyser. The analyser was developed specifically for use at the DAO 1.83-m telescope; it is mounted before the Cassegrain spectrograph entrance slit, and is capable of providing polarisation data at the resolution of the spectrograph-detector system. The device incorporates a polarising beamsplitter for selecting a plane of polarisation, and a quarter-wave plate. We have shown that the quarter-wave plate is highly ($\sim 90\%$) effective in minimising effects of instrumental polarisation. Using observations of a standard unpolarised star, the overall efficiency of the analyser was estimated to be $\sim 40\%$. The analyser is microcomputer-controlled and may be rotated at a rate of $12.5^\circ\ s^{-1}$. Position angles of the analyser may be set to within $\pm 0.5^\circ$.

In Chapters 3 and 4, we have presented the results of three studies carried out with the polarisation analyser. Our results may be summarised as follows:

1. We have investigated differential polarisation in four of the strongest diffuse interstellar features in the spectra of HD 183143, 55 Cyg and ζ Per. No evidence for polarisation structure through any of the bands was found. From our results, we have established upper limits to the variation with wavelength of polarisation in the 5780, 5797, 6177 and 6284 Å DIBs of 0.01, 0.01, 0.02 and 0.03%, respectively. These limits are significantly lower than the predicted levels if the agent (agents) responsible for the DIBs resides (reside) in the same interstellar grains which produce the optical continuum polarisation. Thus, we concluded that the diffuse features are not associated with the grains responsible for the continuum polarisation. However, our

results do not allow us to eliminate *all* grains as possible carriers. Intermediate-sized grains ($0.02 < a < 0.1\mu m$) which are poorly aligned or spherical are consistent with our results as well as other observational properties of the DIBs. Our results are also consistent with (and would tend to favour) a molecular origin for the diffuse bands.

2. We have attempted to measure differential polarisation associated with the line profile variations of two OB stars. Analysis (by the methods described in Section 4.4) of the travelling subfeatures in the Hβ line of ζ Oph and the Hβ and He I λ4921 lines of ϵ Per failed to reveal polarisation structure related to the travelling subfeatures with upper limits of 0.08% and 0.1%, respectively. Theoretical estimates of the polarisation levels expected if the line profile variations arise from either NRP, spots or circumstellar spokes will be required before the limits placed by this study can be used to constrain the possible sources of the line profile variations.

3. We have presented differential polarisation measurements in the Hβ emission line of three intrinsically polarised Be stars: ϕ Per, γ Cas and 28 Cyg. No significant change of polarisation has been detected for 28 Cyg despite the presence of appreciable emission. However, ϕ Per and γ Cas exhibit significant polarisation changes across the Hβ line. These changes are characterised by a decrease of polarisation toward the center of the line and an increase at the line center itself. Our observations also show evidence for variations in the plane of polarisation across the line.

   We have argued that unpolarised line emission cannot completely account for the observed polarisation changes. The width of the polarisation structure is comparable to the width of the underlying rotationally-broadened absorption feature; it is significantly greater than the width of the expected polarisation structure if the effect is solely caused by dilution of the continuum polarisation by unpolarised line emission. This suggests that at least part of the polarisation structure, especially in the line wings, is due to absorption processes in a rotating circumstellar envelope. Our results are consistent with the stellar wind model of Poeckert and Marlborough (1978a).

Further observations are required in order to investigate temporal variations in the line polarisations of these stars. Recently, it has been suggested that NRP could provide

the additional force necessary to initiate localised mass loss. Consequently, the structure in the inner regions of the circumstellar envelopes may vary on timescales similar to those of nonradial oscillations, and such changes may be expected to produce variations in the polarisation. Therefore, time series of polarimetric observations could provide a means of establishing a possible link between NRP and the Be phenomenon.

References

Aannestad, P.A., and Purcell, E.M. 1973, *Ann. Rev. Astron. Ap.*, **11,** 309.

Abt, H.A., and Cardona, O. 1984, *Ap. J.*, **285,** 190.

A'Hearn, M.F. 1972, *A. J.*, **77,** 302.

Appenzeller, I. *Z. Astrophys.*, **64,** 19.

Baade, D. 1987, in *Proc. IAU Colloquium 92, Physics of Be Stars*, eds. A. Slettebak and T.P. Snow (Cambridge: Cambridge University Press), p. 361.

Behr, A. 1959, *Nach. Akad. Wiss. Cottingen 2, Math-Phys.*, **K1,** 7185.

Bless, R.C., and Savage, B.D. 1972 *Ap. J.*, **171,** 293.

Bromage, G.E. 1972, *Ap. and Space Sci.*, **15,** 426.

Capps, R.W., Coyne, G.V., and Dyck H.M. 1973, *Ap. J.*, **184,** 173.

Chandrasekhar, S. 1946a, *Ap. J.*, **103,** 351.

Chandrasekhar, S. 1946b, *Ap. J.*, **104,** 110.

Chlewicki, G., and Greenberg, J.M. 1990, *Ap. J.*, **365,** 230.

Chlewicki, G., van der Zwet, G.P., van Ijzendoorn, L.J, Greenberg, J.M., and Alvarez, P.P. 1986, *Ap. J.*, **305,** 455.

Clarke, D. 1974, in *Planets, Stars and Nebulae Studied with Polarimetry*, ed. T. Gehrels (Tucson: University of Tucson Press), p.45.

Clarke, D. 1986, *Astr. and Ap.*, **161,** 412.

Clarke, D., and McLean, I.S. 1974a, in *Planets, Stars and Nebulae Studied with Polarimetry*, ed. T. Gehrels (Tucson: University of Tucson Press), p.752.

Clarke, D., and McLean, I.S. 1974b, *M.N.R.A.S.*, **167,** 27.

Clarke, D., and McLean, I.S. 1975, *M.N.R.A.S.*, **172,** 545.

Clarke, D., and McLean, I.S. 1976, *M.N.R.A.S.*, **174,** 335.

Clarke, D., and Brooks, A. 1984, *M.N.R.A.S.*, **211,** 737.

Clayton, G.C., Anderson, C.M., Magalhães, A., Code, A.D., Nordsieck, K.H., Meade, M.R., Wolff, M.J., Babler, B., Bjorkman, K.S., Schulte-Ladbeck, R., Taylor, M., and Whitney, B.A. 1991, *preprint.*

Collins, G.W. 1970 *Ap. J.*, **159,** 583.

Collins, G.W. 1989 *The Fundamentals of Stellar Astrophysics*, (New York: W. H. Freeman and Company).

Coyne, G.V. 1974, *M.N.R.A.S.*, **169,** 7.

Coyne, G.V. 1975, *Spec. Vatican Ric. Astron.*, **8,** 533.

Coyne, G.V. 1976a, in *Proc. IAU Symp. 70 Be and Shell Stars*, ed. A. Slettebak (Dordrecht: Reidel), p. 233.

Coyne, G.V., 1976b, *Astron. Ap.*, **49,** 89.

Coyne, G.V., and Gehrels, T. 1967, *A. J.*, **72,** 887.

Coyne, G.V., and Kruszewski, A. 1969, *Astron. J.*, **74,** 528.

Coyne, G.V., and McLean, I.S. 1975, *A. J.*, **80,** 702.

Coyne, G.V. and McLean, I.S. 1982, in *Proc. IAU Symp. 98: Be stars*, eds. M. Jaschek and H-G. Groth (Dordrecht: Reidel), p. 77.

Coyne, G.V., and Vrba, F.J. 1976, *Ap. J.*, **207,** 790.

Crawford, M.K., Tielens, A.G.G.M., and Allamandola, L.J. 1985, *Ap. J.*, **293,** L45.

Dachs, J. 1987, in *Proc. IAU Colloquium 92, Physics of Be Stars*, eds. A. Slettebak and T.P. Snow (Cambridge: Cambridge University Press), p. 149.

Danks, A.C., and Lambert, D.L. 1976, *M.N.R.A.S.*, **174,** 571.

Davis, L., Jr. 1958, *Ap. J.*, **128,** 508.

Davis, L., Jr., and Greenstein, J.L. 1951, *Ap. J.*, **114,** 206.

Doazan, V. 1987, in *Proc. IAU Colloquium 92, Physics of Be Stars*, eds. A. Slettebak and T.P. Snow (Cambridge: Cambridge University Press), p. 384.

Draine, B.T. 1988, *Ap. J.*, **333,** 848.

Duke, D. 1951, *Ap. J.*, **113,** 100.

Fahlman, G.G., and Glaspey, J.W. 1973, in *Astronomical observations with television-type sensors*, eds. J.W. Glaspey and G.A.H. Walker (Vancouver: University of British Columbia), p. 347.

Fahlman, G.G., and Walker, G.A.H. 1975, *Ap. J.*, **200,** 22.

Gammelgaard, P., and Rudkjobing, M. 1973, *Astron. Ap.*, **27,** 261.

Gies, D.R., and Kullavanijaya, A. 1988, *Ap. J*, **326,** 813.

Gies, D.R., and McDavid, D. 1987, in *Proc. IAU Colloquium 92, Physics of Be Stars*, eds. A. Slettebak and T.P. Snow (Cambridge: Cambridge University Press), p. 84

Greenberg, J.M. 1978, in *Cosmic Dust*, ed. J.A.M. McDonnell (New York: Wiley), p. 187.

Greenberg, J.M., and Chlewicki, G. 1983, *Ap. J.*, **272,** 563.

Greenberg, J.M., and Hong, S.S. 1974, in *The Dusty Universe*, eds. G.B. Fields and A.G.W. Cameron (New York: Neale Watson), p. 131.

Greenberg, J.M., and Hong, S-S. 1976, *Ap. Space Sci.*, **39,** 31.

Greenberg, J. M., and Stoeckly, R. 1971, *Nature Phys. Sci.*, **230,** 15.

Greenstein, and Aller 1950, *Ap. J.*, **111,** 328.

Haisch, B.M., and Cassinelli, J.P. 1976, *Ap. J.*, **208,** 253.

Hall, J.S. 1949, *Science*, **109,** 166.

Hiltner, W.A. 1949, *Science*, **109,** 165.

Hiltner, W.A. 1956, *Ap. J. Suppl.*, **2,** 389.

Harmanec, P. 1982, in *Proc. IAU Symp. 98: Be stars*, eds. M. Jaschek and H-G. Groth (Dordrecht: Reidel), p. 413.

Harmanec, P. 1987, in *Proc. IAU Colloquium 92, Physics of Be Stars*, eds. A. Slettebak and T.P. Snow (Cambridge: Cambridge University Press), p. 339.

Hayes, D.P. 1975, *P.S.A.P.*, **87,** 609.

Hayes, D.P., and Illing, R.M.E. 1974, *A. J.*, **79,** 1430.

Herbig, G.H. 1975, *Ap. J.*, **196,** 129.

Herbig, G.H. 1988, *Ap. J.*, **331,** 999.

Herbig, G.H., and Soderblom, D.R. 1982, *Ap. J.*, **252,** 610.

Hoffleit, D., and Jaschek, C. 1982, *The Bright Star Catalogue*, (4th ed.; New Haven: Yale University Observatory).

Hubeny, I. 1988, *Computer Physics Communications*, **52,** 103.

Hutching, J.B., and Stoeckley, T.R. 1977, *P. A. S. P.*, **89,** 17.

Jaschek, M., and Groth H-G. (eds.) 1982, *Proc. IAU Symp. 98 Be stars*, (Dordrecht: Reidel).

Johnson, H.L. 1968, in *Stars and Stellar Systems, Volume 7 Nebulae and Interstellar Matter*, eds. B.M. Middlehurst and L.H. Aller (Chicago: University of Chicago Press),

p. 167.

Jones, T.J. 1979, *Ap. J.*, **228**, 787.

Jones, R.V. and Spitzer, L., Jr. 1967, *Ap. J.*, **147**, 943.

Josafatsson, K., and Snow, T.P. 1987, *Ap. J.*, **319**, 436.

Kahaner, D., Moler, C.B., and Nash, S. 1989, *Numerical Methods and Software* (Prentice-Hall: Englewood Cliffs).

Kelly, A. 1971, *Ap. Space Sci.*, **13**, 211.

Kennelly, E.J., Walker, G.A.H, and Hubeny, I. 1990, *preprint.*

Kitchin, C.R. 1982, *Early Emission-Line Stars* (Bristol: Adam Hilger Ltd.).

Krelowski, J. 1988, *P.A.S.P.*, **100**, 896.

Krelowski, J., and Walker, G.A.H. 1987, *Ap. J.*, **312**, 860.

Krelowski, J., Walker, G.A.H., Grieve, G.R., and Hill, G.M. 1987, *Ap. J.*, **316**, 449.

Kriz, S., and Harmanec, P. 1975, *Bull. Astron. Inst. Czechosl.*, **26**, 65.

Léger, A., and d'Hendecourt, L. 1985, *Astron. Ap.*, **146**, 81.

Lonsdale, C.J., Dyck, H.M., Capps, R.W., and Wolstencroft, R.D. 1980, *Ap. J. (Letters)*, **238**, L31.

Marlborough, J.M. 1969, *Ap. J.*, **156**, 135.

Marlborough, J.M. 1987, in *Proc. IAU Colloquium 92, Physics of Be Stars*, eds. A. Slettebak and T.P. Snow (Cambridge: Cambridge University Press).

Martin, P.G. 1975, *Cosmic Dust: Its Impact on Astronomy*, (Oxford, Oxford University Press), pp. 8–35.

Martin, P.G., and Angel, J.R.P. 1974, *Ap. J.*, **188**, 517.

Martin, P.G., and Angel, J.R.P. 1975, *Ap. J.*, **195**, 379.

McLean, I.S. 1979, *M.N.R.A.S.*, **186**, 265.

McLean, I.S. 1989, *Electronic and Computer-Aided Astronomy: From Eyes to Electronic Sensors*, (Toronto: Ellis Horwood Limited), p. 163.

McLean, I.S., and Clarke, D. 1976, in *Proc. IAU Symp. 70, Be and Shell Stars*, ed. A. Slettebak (Dordrecht: Reidel), p. 261.

McLean, I.S., and Clarke, D. 1979, *M.N.R.A.S.*, **186**, 245.

McLean, I.S., Coyne, G.V., Frecker, J.E., and Serkowski, K. 1979, *Ap. J.*, **228**, 802.

Merrill, P.W. 1934, *P. A. S. P.*, **46**, 206.

Merrill, P.W., and Wilson, O.C. 1938, *Ap. J.*, **87**, 9.

Mihalas, D., and Binney, J. 1981, *Galactic Astronomy, Structure and Kinematics*, (San Francisco: W. H. Freeman and Company).

Moore, C.E. 1959, *National Bureau of Standards Technical Note 36: A Multiplet Table of Astrophysical Interest*, (Washington: United States Department of Commerce, Office of Technical Services).

Nagirner, D.T. 1962, *Trudy Leningrad Astron. Obs.*, **19**, 79.

Nandy, K. and Seddon, H. 1970, *Nature Phys. Sci.*, **227**, 264.

Nandy, K., Morgan, D.H., and Houziaux, L. 1982, *Ap. Space Sci.*, **85**, 221.

Odell, A.P. 1979, *P.A.S.P.*, **91**, 326.

Odell, A.P. 1981, *Ap. J.*, **246**, L77.

Odell, A.P., and Tapia 1981, in *Proceedings of the Workshop on Pulsating B Stars*, (Nice Observatory) 329.

Osaki, Y. 1986, *P.A.S.P.*, **98**, 30.

Penrod, G.D. 1986, *P.S.A.P.*, **98**, 35.

Penrod, G.D. 1987, in *Proc. IAU Colloquium 92, Physics of Be Stars*, eds. A. Slettebak and T.P. Snow (Cambridge: Cambridge University Press), p. 463.

Percy, J.R. 1987, in *Proc. IAU Colloquium 92, Physics of Be Stars*, eds. A. Slettebak and T.P. Snow (Cambridge: Cambridge University Press), p. 49.

Piirola, V. 1979, *Astron. Ap. Suppl.*, **38**, 193.

Plavec, M.J. 1976, in *Proc. IAU Symposium 70, Be and Shell Stars*, ed. A. Slettebak (Dordrecht: Riedel), p. 1.

Poeckert, R. 1975, *Ap. J.*, **196**, 777.

Poeckert, R., Bastien, P. and Landstreet, J. D. 1979, *A. J.*, **84**, 812.

Poeckert, R. and Marlborough, J.M.. 1976, *Ap. J.*, **206**, 182.

Poeckert, R. and Marlborough, J.M.. 1977, *Ap. J.*, **218**, 220.

Poeckert, R. and Marlborough, J.M. 1978a, *Ap. J.*, **220**, 940.

Poeckert, R. and Marlborough, J.M.. 1978b, *Ap. J. Supp.*, **38**, 229.

Poeckert, R. and Marlborough, J.M.. 1979, *Ap. J.*, **233**, 259.

Press, W.H., Flannery, B.P., Teukolsky, S.A., and Vetterling, W.T. 1986, *Numerical Recipes*, (Cambridge: Cambridge University Press).

Pritchet, C.J., Mochnacki, S. and Yang, S. 1982, *P.A.S.P.*, **94**, 733.

Puget, J.L., and Léger, A., 1989, *Ann. Rev. Astron. Astrophys.*, **27**, 161.

Ruciński, S.M. 1966, *Astron. Obs. Warsaw Univ.*, reprint 208.

Ruciński, S.M. 1967, *Astron. Obs. Warsaw Univ.*, reprint 231.

Ruciński, S.M. 1970, *Acta Astron.*, **20,** 1.

Savage, B.D. 1976, *Ap. J.*, **205,** 122.

Seab, C.G., and Snow, T.P. 1984, *Ap. J.*, **277,** 200.

Secchi, A. 1867, *Astr. Nach.*, **68,** 63.

Serkowski, K. 1962, *Adv. Astron. Ap.*, **1,** 289.

Serkowski, K. 1968, *Ap. J.*, **154,** 115.

Serkowski, K. 1970, *Ap. J.*, **160,** 1083.

Serkowski, K. 1974, *Methods of Experimental Physics: Astrophysics, Part A Optical and Infrared*, ed. N. Carleton (New York: Academic Press) **12,** 361.

Serkowski, K. 1974, in *Planets, Stars and Nebulae Studied with Polarimetry*, ed. T.Gehrels (Tucson: University of Arizona Press), p.135.

Serkowski, K., Matthewson, D.S., and Ford, V.L. 1975, *Ap. J.*, **196,** 261.

Shakhovzkoj, N.M. 1962, *Astron. Circ. USSR*, 228.

Shakhovzkoj, N.M. 1964, *Soviet Astron.*, **8,** 83.

Slettebak, A. (ed.) 1976 *Proc. IAU Symp. 70 Be and Shell Stars*, (Dordrecht: Reidel).

Slettebak, A., and Snow, T.P. (eds.) 1987, *Proc. IAU Colloquium 92, Physics of Be Stars*, (Cambridge: Cambridge University Press).

Smith, W.H., Snow, T.P., and York, D.G. 1977, *Ap. J*, **218,** 124.

Sneden, C., Gehrz, R.D. Hackell, J.A., York, D.G., and Snow, T.P. 1978, it Ap. J., **223,** 168.

Snell, R.L., and Vanden Bout, P.A. 1981, *Ap. J.*, **244,** 844.

Stamford, P.A., and Watson, R.D. 1980, *Acta Astron.*, **30,** 193.

Struve, O. 1931, *Ap. J.*, **73,** 94.

Underhill, A.B. 1955, *Pub. DAO*, **10,** 201.

Underhill, A.B. 1987, in *Proc. IAU Colloquium 92, Physics of Be Stars*, eds. A. Slettebak and T.P. Snow (Cambridge: Cambridge University Press), p. 412.

Underhill, A.B., and Doazan, V. 1982, *B Stars with and without emission lines*, (NASA SP 456; Washington, D.C.: GPO), pp. 279–451.

Underhill, A.B. and Fahey, R. 1984, *Ap. J.*, **280,** 712.

Unno, W., Osaki, Y., Ando, H., Saio, H., and Shibahashi, H. 1989, *Nonradial Oscillations*

of Stars, (Tokyo: University of Tokyo Press).

van de Hulst, H.C. 1949, *Rech. Obs. Utrecht*, **11**, Pt. 2.

van der Zwet, G.P. 1986, in *Polycyclic Aromatic Hydrocarbons in Astrophysics*, (Dordrecht: Reidel), p.351.

van der Zwet, G.P., and Allamandola, L.J. 1985, *Astron. Ap.*, **146**, 76.

Vogt, S.S., and Penrod G.D. 1983, *Ap. J.*, **275**, 661.

Walker, G.A.H. 1963, *M.N.R.A.S.*, **125**, 141.

Walker, G.A.H. 1987, *Astronomical Observations, an optical perspective*, (Cambridge: Cambridge University Press).

Walker, G.A.H. 1991, private communication.

Walker, G.A.H., Yang, S., and Fahlman, G.G. 1979, *Ap. J.*, **233**,199.

Walker, G.A.H., Johnson, R., and Yang, S. 1985, in *Adv. in Electronics and Electron Physics*, ed. B.L. Morgan (London: Academic Press), **64A**, p. 213.

Walker, G.A.H., Yang, S., and Fahlman, G.G. 1987, *Ap. J.*, **320**, L139.

Wampler, E.J. 1966, *Ap. J.*, **144**, 921.

Welter, G.L., and Savage, B.D. 1977, *Ap. J.*, **215**, 788.

Wilking, B.A., Lebofsky, M.J., and Rieke, G.H. 1982, *A.J.*, **87**, 695.

Wilson, L. A. 1986, *P.A.S.P.*, **98**, 37.

Witt, A.N., Bohlin, R.C., and Stecher, T.P. 1983, *Ap. J. (Letters)*, **267**, L47.

Wu, C-C. 1972, *Ap. J*, **178**, 681.

Wu, C-C., York, D.G., and Snow, T.P. 1981, *A.J.*, **86**, 755.

Yang, S., Ninkov, Z., and Walker, G.A.H. 1988, *P.A.S.P.*, **100**, 233.

Zellner, B., and Serkowski, K. 1972, *P.A.S.P.*, **84**, 619.

Appendix A

Component Specifications for the UBC/DAO Polarisation Analyser

Table A.1: Optical Component Specifications

Product Number	Manufacturer	Dimensions (mm)	λ_c (nm)	λ_{eff}^{a} (nm)
Polarising Beamsplitter Cubes				
03 PBS 017.....	Melles Griot	25.4	488	430 – 500
03 PBS 047.....	Melles Griot	25.4	633	575 – 665
Quarter-wave Plate (Mica Retarder)				
02 WRM 005.....	Melles Griot	30.0	550	400 – 700

a) Effective wavelength range for maximum transmittance.

Table A.2: Mount Components[a]

Product Number	Description	Manufacturer
2615.....	Beamsplitter-cube cell	Oriel Corporation
25059.....	Mounting flange	Oriel Corporation

a) Includes only the purchased components.